Technische Universität München
TUM School of Engineering and Design

Evaluation of the short-term and long-term behaviour of vehicle-track-system at track transitions based on numerical simulations

Kangle Chen

Vollständiger Abdruck der von der TUM School of Engineering and Design der Technischen Universität München zur Erlangung eines

Doktors der Ingenieurwissenschaften (Dr.-Ing.)

genehmigten Dissertation.

Vorsitz: Prof. Dr.-Ing. Rolf Moeckel

Prüfer*innen der Dissertation:

1. Prof. Dr.-Ing. Stephan Freudenstein
2. Prof. Dr.-Ing. Jia Liu

Die Dissertation wurde am 21.06.2022 bei der Technischen Universität München eingereicht und durch die TUM School of Engineering and Design am 26.10.2022 angenommen.

Table of contents

List of abbreviations

Abbreviation	Explanation
IM	infrastructure manager
DB	DB Netz AG
HMA	Hot mix asphalt
USP	Under-sleeper pad
UBM	Under-ballast mat
CAE	Computer aided engineering
FEM	Finite-Element method
MBS	Multi-body-simulation
DoF	Degree of freedom
WRC	Wheel-rail contact
FPL	Frost protection layer
MGT	Million gross tons

Glossary

Railway engineering is a multi-disciplinary field. Several definitions have been provided according to the different contexts they are used in. To avoid confusion, the meaning of several definitions in this research is clarified here.

- Track transition:

Here in this research, track transition refers to the position where the track design changes. Instances of track transition include the boundary between a ballasted track and a ballastless track, the boundary between an earthwork and a bridge, the boundary between the subsections with/without under-ballast mat (UBM), etc. The investigation here focuses on the first type. According to the context, the term “track transition” can also refer to those specially designed sections that aim to smooth the discontinuities in the track design.

- Track irregularity:

Without an explicit declaration, the term “track irregularity” that appears in this investigation refers only to longitudinal level. Longitudinal level deviation with a wavelength significantly smaller than rail seat spacing (e.g., rail corrugation) is outside the scope of this investigation. Here only the deviation of longitudinal level caused by the variation of rail seat stiffness and uneven ballast settlement is considered.

In this research, the variance of longitudinal level between the left and right rail is ignored, because the investigation is restricted to straight track without superelevation, and no variation in lateral direction is considered. Consequently, rail longitudinal level equals to track longitudinal level here.

Depending on the measurement conditions, track longitudinal level can be further divided into unloaded longitudinal level, which is measured under the self-weight of the track, and loaded longitudinal level, which is measured under the axle-load of the measurement wagon. They are explicitly distinguished from one another in this research.

- Stiffness:

In this research, following three terms related with stiffness are distinguished:

- Track stiffness [kN/mm]

Track stiffness is defined as the ratio between the static point load on rails (e.g., axle load) and the rails deflection caused by it. It describes the resist of the total track structure to deformation.

- Rail seat stiffness [kN/mm]

The stiffness of rail pad and fastening system is designated as rail seat stiffness.

- Bedding modulus of subgrade [N/mm^3]

In this research, all layers below the ballast layer in a ballasted track, which possibly include sub-ballast layer, frost protection layer (FPL) and base layer, are simplified as one layer designated as “subgrade”. Its resistance to deformation is described by its linear bedding modulus. In ballasted track, the bedding modulus of subgrade is also designated as ballast supporting stiffness.

There are different types of ballastless track system. Here it is focused on the ballastless track, whose rails are installed onto concrete supporting layers, which consists of concrete slab, HBL, FPL and base layers. Similarly, FPL and base layers are simplified as one layer, which is described by its bedding modulus.

It should also be pointed out that stiffness can be further divided into static stiffness and dynamic stiffness according to the load condition. In this research, static stiffness of track components has been employed in the investigations. The reason is that it is the difference of track stiffness between adjacent sections that has decisive influence on the performance of track transition, rather than the absolute value of track stiffness in each section. Moreover, the stiffness of rail pads, which is the dominate part of track stiffness (Eisenmann, 1981), increases under dynamic loading condition. Therefore, the difference of track stiffness under dynamic loading condition will decrease compared to under static loading condition. Therefore, investigation with static stiffness lies on the safe side.

- Short-term behaviour and long-term behaviour:

Behaviour of track transition can be investigated in two scales of time: long-term and short-term. Its short-term behaviour is described by the vehicle-track-interaction of a single train run, whereas its long-term behaviour additionally takes the deterioration of track geometry caused by short-term interaction during a specified period into consideration. Essentially, investigation of long-term behaviour requires investigation of the short-term interaction, prediction of ballast settlement and determination of track irregularity with given ballast settlement.

Abstract

Track transition is known for potentially critical track quality deterioration due to the track stiffness discontinuity and especially due to the uneven degradation of rail longitudinal level caused by the variance of track design. At such locations, increase in maintenance costs and decrease in passenger comfort can be observed. To overcome these problems, infrastructure managers (IMs) have issued requirements for track transition designs. In Germany for example, required countermeasures at a transition between a ballasted track and a ballastless track in standards and regulations include glued ballast, auxiliary rail, extension of the Hydraulically Bonded Layer (HBL) and adjustment of rail seat stiffness. However, those requirements are mainly proposed based on practical experience. The aim of this research is to investigate the effect of these countermeasures using numerical simulation. An optimized design plan for the ballastless-ballasted track transition is proposed.

For this purpose, a simulation tool was developed first, which enabled the simulation of short-term vehicle-track interaction, the prediction of long-term ballast settlement and the evaluation of the performance of vehicle-track-system with consideration given to dynamic wheel-rail contact force and maintenance interval. The amplitude of track longitudinal level defects increased with the increase of load cycles due to the uneven settlement along the track transition section. At critical positions, under sleeper gap might appear. Therefore, in the numerical simulation, special focus was paid to considering the non-linearity characteristics. The vehicle-track interaction tool was validated by comparing the calculation results with field measurement results and with calculation results from commercial software. The ballast settlement law was validated by laboratory test and field measurement results provided by literature.

With this simulation tool, the current design plan for ballastless track – ballasted track transition proposed in standards and regulations has been investigated in both short-term view and long-term view. The calculation results in short-term view demonstrated that the current design plan has successfully smoothed the stiffness discontinuity between the ballasted track and the ballastless track, which is mainly achieved by the implementation of rail pads with adjusted stiffness. Short-term vehicle-track interaction due to the discontinuity at track transitions has been reduced to an insignificant level at transitions following the standard design plan.

In the investigation in long-term view, an alternative design plan without gluing the ballast has been proposed. Compared with the standard design plan with 3 subsections, following modifications are suggested based on numerical simulation:

- The length of the extended HBL/flexible pavement layer should be the same as the length of one subsection to avoid extra stiffness discontinuity.
- Increase the initial tension stiffness of the rail fastening system of auxiliary rail.
- Extension the length of auxiliary rail from only covering the 1st subsection to covering all the 3 subsections of the track transition
- Adjust rail seat stiffness, so that the change of designed static deflection between each two adjacent subsections is constant.
- Implementation of USP with adjusted bedding modulus along the 1st and 2nd subsection (the 1st subsection refers to the subsection near the ballastless track)

To evaluate effect of the new design plan, the SR-value (see Ril 821.2001 (DB Netz AG, 2010)) and the dynamic factor of wheel-rail contact force are calculated after 4.1 million repeated load cycles, which corresponds to 80 million gross tons (MGT) with the static wheel load of 95.6 kN. Significant improvement of both parameters has been demonstrated by numerical simulation. Finally, the required minimal length of the track transition has been determined based on the operation speed and settlement difference between the ballasted track and the ballastless track. The simulation results fit the requirement in current standard well.

1. Introduction

1.1 Track transition and its influence on vehicle-track interaction

Railway track transitions refer to the locations where tracks with different designs meet each other. Typical examples of track transitions include the boundary between a track on earthwork and a track on bridge /culvert, between a ballasted track and a ballastless track, between track subsections with and without under-ballast mat (UBM), etc. Accelerated track quality degradation can be observed at such locations, causing problems including appearance of under-sleeper gap, decrease of passenger comfort and track component life (Banimahd, Woodward, Kennedy, & Medero, 2012; Coelho & Hicks, 2016; Kerr & Moroney, 1993; D. Li & Davis, 2005; D. Li, Otter, & Carr, 2010; Pita, Teixeira, & Robuste, 2004). Consequently, maintenance costs and operation costs due to traffic speed limitation and eventually track closure along track transition sections are generally high. Experience gained in previous years indicates that the maintenance incidences at track transitions can be eight times higher than those that occur on normal track sections (Varandas, 2013). In Europe, the expenditure associated with geometric deterioration at track transition zones amounts to approximately 110 million dollars, and the number climbs to 200 million dollars in the United States (Hyslip, Li, & McDaniel, 2009; Sasaoka & Davis, 2005; Erol Tutumluer, Timothy D Stark, Debakanta Mishra, & James P Hyslip, 2012). Experts estimate that 26 million dollars are spent on maintenance at open track-bridge transitions annually (Nicks, 2009).

In past decades, plenty of research has been performed on track quality degradation at track transition zones. Based on previous research, the mechanics of this issue can be concluded as in Figure 1-1.

First, change in track design causes local variation of track stiffness, which can lead to spatially elastic track deflection discontinuity under train runs. Second, differently designed track sections settle differently inherently (e.g., a ballastless track shall be settlement free, but a ballasted track not), which can lead to track irregularity in unloaded state. Besides, strong variance of local track settlement along the track might also lead to under-sleeper gaps. These three factors attribute to the loaded track irregularity during train runs, which induces strong vehicle-track interactions, accelerated track component deterioration and unequally distributed

track settlement (Banimahd et al., 2012; Choi, 2013; Dahlberg, 2010; Frohling, Scheffel, & Ebersöhn, 1996; Huang & Brennecke, 2013; Hunt, 1997; Kerr & Moroney, 1993; D. Li & Davis, 2005). Self-accelerating track quality deterioration can consequently be expected if no appropriate intervention is taken. The severity of the problem is influenced by various parameters that include traffic density, vehicle speed, vehicle type, train run direction, the gradient of stiffness and track geometry changes with respect to track length, etc. (Banimahd et al., 2012).

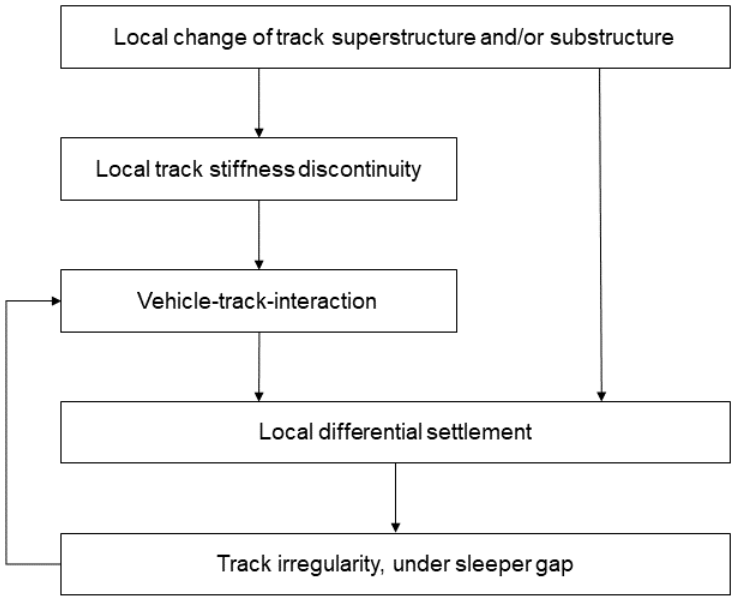

Figure 1-1: Track deterioration process at track transition zones

1.2 State of art – remedies in standards

Requirements for track transition designs have been issued according to several standards and regulations that have been developed by different infrastructure managers (IMs).

For example, in Germany, the requirement on a track transition between a ballasted track and a ballastless track is addressed by BetonKalender 2015 (Freudenstein, Geisler, Mölter, Mißler, & Stolz, 2015), the standard DIN EN 16432-2:2017-10 (Deutsches Institut für Normung e. V., 2017), and the guideline Ril. 820.2020 (DB Netz AG, 2018).

In Ril. 820.2020 (DB Netz AG, 2018), it is suggested that the ballast should be glued for 45 meters in three steps, if the travel speed is greater than 160 km/h. Along the first 15 meters directly next to the ballastless track, the ballast under the sleeper, the ballast at the ballast shoulder and the ballast between the sleepers should be glued. Along the following 15 meters, the ballast under the sleeper and the ballast at the ballast shoulder should be glued. Along the next 15 meters, only the ballast under the sleeper should be glued. The length of the glued ballast could be adjusted according to the traffic density and line geometry if the speed is lower. A twenty-meter-long auxiliary rail is another suggested remedy. Fifteen meters of the auxiliary rail should be fixed in the ballasted track, and five meters should be fixed in the ballastless track. Finally, the Hydraulically Bonded Layer (HBL) in the ballastless track can be extended 10 m to the ballasted track. Besides, in BetonKalender 2015 (Freudenstein et al., 2015), it is also required that the rail seat stiffness along the transition should be adjusted in at least three steps (60 kN/mm, 40 kN/mm, 27 kN/mm).

According to DIN EN 16432-2:2017-10 (Deutsches Institut für Normung e. V., 2017), the minimal length of each subsection of the transition section is determined by the formula (1):

$$\mathrm{L} = 0.5 * \mathrm{V} \tag{1}$$

with

$L = \text{minimal length of the track transition section } [\mathrm{m}]$

$V = \text{maximal train speed on the line } [\mathrm{m/s}]$

In Spain, suggestions for using four-step superstructures or transition wedges between a ballastless track and a ballasted track are provided (Sañudo, dell'Olio, Casado, Carrascal, & Diego, 2016). Recommendations for materials (stiffness, Young modulus, type of soils, etc.) and geometry (slopes and distribution of track layers) used in transition wedges from open track to bridge can be found in (Paixão, Fortunato, & Calçada, 2015) and (Giner, Pita, Chaves, & Álvarez, 2012).

A common disadvantage of these recommendations in standards is that they are usually proposed based on practical experience without sufficient theoretical investigation and justification. Therefore, it is uncertain whether the dimensions and physical parameters of the suggested transition design are the most optimal choice.

1.3 State of art – remedies in research projects

In past decades, copious scientific research has been conducted on the optimization of track transition design (Indraratna, Sajjad, Ngo, Correia, & Kelly, 2019; Read & Li, 2006; Sañudo et al., 2016).

In (D. Li & Davis, 2005), the effect of hot-mix asphalt (HMA) underlayment, geocell-confined sub-ballast layers and cement-stabilized backfill between well-compacted subgrade surface and ballast layer were studied in three bridge transitions. Although the settlement of subgrade was controlled, the track geometry quality over time was not optimized in any of the three sections. Track stiffness measurements have revealed significant variation between the approach section and the bridge. The result emphasises the importance of continuous stiffness distribution in track transition zones.

In (Paixão et al., 2015), an earthwork-bridge transition comprising well-graded crushed aggregates in the abutment backfill was studied in detail. In situ measurements revealed that gradually increasing E_{v2} values were obtained as expected. After opening the line to traffic, no significant settlements were reported at the transition zone in three years, and no specific maintenance operations were needed. The author concluded that track substructure with sufficient bearing capacity and meticulously designed stiffness could mitigate the problems at bridge-earthwork transition zones.

Additional rails often exist when bridge guardrails extend past the abutment onto the approach track (Namura & Suzuki, 2007). In (Heydari-Noghabi, Varandas, Esmaeili, & Zakeri, 2017), influence of auxiliary rail on track displacement has been investigated by field measurement, which has only demonstrated insignificant influence. Long-term effect was not investigated.

In (Kennedy, Woodward, Medero, & Banimahd, 2013), laboratory tests and field measurements were conducted to study the effects of glued ballast. The results suggested that this approach could reduce long-term track settlement by up to 99% for 10 years, which would significantly improve track geometry and reduce the need for track maintenance. Mattner & Eisenmann have also performed field measurement along a ballasted-ballastless track transition with glued ballast (Mattner & Eisenmann, 1990). The measurement result showed that although glued ballast has resolved the settlement difference between the ballastless track and the ballasted track, it has also led to new discontinuity between the

ballasted track section with glued ballast and the ballasted track section without glued ballast. Further measurement data would be helpful to understand the effect of glued ballast.

Besides the research on the countermeasures mentioned in the standard, several other countermeasures have also been proposed and studied.

A reinforced concrete slab is a structural element that acts as a local track-supporting structure between ballast layer and earthwork to increase track stiffness. It can be used at ballastless track-ballasted track transition and at earthwork-bridge transition. The slab is placed in the ballasted track section or the earthwork section, with one end lying on the HBL of the ballastless track or on the abutment of bridge. It is either designed with a taper or is uniform in thickness but placed at an angle with a tapering of the ballast depth to achieve a gradual increase in stiffness (Read & Li, 2006). With the help of numerical calculation, Read & Li believed that placing a concrete approach slab between the ballast and sub-ballast layers was the most effective technique for increasing ballasted track stiffness. However, field measurement results have proven that the long-term effects of implementing an approach slab are still controversial. In (Fara, 2014) , measurements were taken before and after the installation of approach slabs in a bridge transition zone. The results demonstrated that the solution has brought nearly no long-term improvement. In (Coelho, Hölscher, Priest, Powrie, & Barends, 2011), a section with a transition slab in a culvert transition was monitored. This revealed that the approach slab exacerbated rather than mitigated the problem. The inclination of the approach slab increased from 3% to 13% due to the large settlement of the underlying soft soil, as well as the rotation about the fixed point on the edge of the culvert. As a result, unsupported sleepers above the slab and the amplification of slab movement were observed. Coelho et al. concluded therefore that successful implementation of this method required meticulous design.

The company Rhomberg Sersa Rail Holding GmbH has developed a solution for the ballastless-ballasted track transitions designated as “V-TRAS”. One end of the steel frame hinges on the ballastless track while the other end rests freely on the ballast. Gradually reducing stiffness was achieved by the ladder form of the steel frame. Its performance was numerically studied in (Hawksbee, Bezin, & Neves, 2018), which revealed that V-TRAS solution could significantly reduce ballast pressure but only slightly contributed to smoothing stiffness gradients between the ballastless track and the ballasted track. Although this solution

has already been constructed at several sites, no measurement result has been published to the author's knowledge. Therefore, this solution was not studied in this research.

Another category of remedies is to introduce resilient components into track structures.

In (Kerr & Bathurst, 2001), the authors proposed the adjustment of rail pad stiffness on bridges as the most suitable approach to smooth track stiffness distribution, both technologically and economically. This is especially true for high-speed tracks. Implementation in pilot projects demonstrated that the installation of adjusted pads could significantly reduce the deflection difference and vehicle vertical acceleration.

In (Iliev, 2012; Loy & Augustin, 2013), laboratory tests and field measurements were performed to prove that the installation of under-sleeper pads (USP) could increase the contact area between sleepers and ballast by up to 33%, which would decrease the stress on the ballast layer and reduce ballast settlement by up to 40%. In another research (Schneider, Bolmsvik, & Nielsen, 2011), the degradation of track geometry also appeared to slow down when USPs were installed.

Under-ballast mat (UBM) is another kind of elastomer that could protection ballast from abrasion. But implementation of UBM would reduce the stiffness of ballast supporting layer, which could cause a dramatic increase in ballast settlement (Baeßler, 2008; Raymond & Richard, 1987; Sol-Sánchez, Pirozzolo, Moreno-Navarro, & Rubio-Gámez, 2016). Therefore, the prerequisite of UBM installation is the ballast supporting layer must be stiff enough, such as bridge decks, tunnels, etc. (Fendrich & Fengler, 2014).

Based on the preceding literature review, following conclusions can be drawn:

- A low-settlement subgrade with proper stiffness is the precondition for track transition optimization. It is assumed in this research that subgrade always has sufficient stiffness, and its settlement can be neglected. This is validated by (Shenton, 1985), in which it is stated that the main contribution to ballasted track settlement normally comes from the ballast, while the subgrade only contributes to the permanent movement of the track during its early life, provided it was adequately specified and dimensioned.
- Auxiliary rail can be an effective countermeasure at track transition.

- More field measurement data are required for clarify the long-term effect of glued ballast. The implementation of glued ballast is therefore excluded in the long-term research.
- Approach slab could theoretically provide gradually changed track stiffness, but its successful implementation requires meticulous design.
- Proper adjustment of rail seat stiffness can help improve track transition behaviour.
- USP could reduce the pressure on ballast layer and ballast settlement.
- The implementation of UBM can protect ballast particles, but it should only be used on stiff subgrade.

In this research, countermeasures including auxiliary rail, rail seat stiffness and USP are investigated using numerical simulation.

1.4 State of art – theoretical research

Computer-aided engineering (CAE) is a powerful tool for structural evaluation and optimization. Over the last few decades, several approaches have been proposed to study the vehicle-track interaction at track transitions.

- **Short-term vehicle-track interaction**

In (Lei & Mao, 2004), the influence of track geometry and track stiffness on track transition quality was studied. Lei & Mao had assumed the rail longitudinal level changed continuously from open track to bridge. Consequently, the transition can be described by its length and the irregularity angle. The computation results revealed that permanent settlement had stronger influence on longitudinal rail levels than the alteration of track stiffness did. Based on the simulation results, the maximum irregularity angle of rail longitudinal level changes and the minimum length of transition section are suggested for Chinese conventional high-speed railways in (Lei & Mao, 2004).

Similar studies focusing on short-term vehicle-track interaction can be found in (Alves Ribeiro, Calçada, & Delgado, 2018; Banimahd et al., 2012; Bronsert, 2017; Nicks, 2009; Shan, Shu, & Zhou, 2017; Steger, 2017; Erol Tutumluer, Timothy D. Stark, Debakanta Mishra, & James P. Hyslip, 2012; Varandas, Hölscher, & Silva, 2011; Wang, Markine, Shevtsov, & Dollevoet, 2015), to list a few. Despite the different tools used, all these studies have focused on short-term

vehicle-track interaction. Researchers have studied the influence of vehicle-track parameters such as train speed, traffic direction, track component stiffness, etc. on the magnitude of dynamic force, rail deflection or other equivalent results. However, the development of permanent track settlement and its influence on vehicle-track interaction have not been considered. Therefore, the significance of such research is compromised.

- **Ballast settlement law**

To understand and predict long-term track performance, it is essential to describe the development of track settlement. In this study, the settlement of subgrade is disregarded, while according to (Shenton, 1985), settlement of adequately designed subgrade can be omitted. The settlement of track equals to the settlement of ballast in this context.

The settlement process of ballast can be divided into two phases: the relatively fast phase that occurs directly after tamping due to ballast consolidation and the relatively slow phase that comes afterwards due to ballast particle movement, sub-ballast penetration, particle breakdown, abrasive wear and the inelastic behaviour of ballast (Dahlberg, 2001). Until now, those mechanisms have seldom been incorporated into widely used ballast settlement models. In contrast, the settlement models are mostly descriptive and empirical, such as in (Alva-Hurtado & Selig, 1981; Demharter, 1982; Dietrich, 1978; Fröhling, 1997; Guerin, 1996; Hecke, 1998; Henn, 1978; Hettler, 1984; Holzlöhner, 1978; Mauer, 1995; Sato, 1995; Shenton, 1985; van As & Kearsley, 1995; Y. Zhang, 2000; Y. Zhang, Murray, & Ferreira, 1999). In these models, ballast settlement is modelled by a linear function, power function or logarithmic function of load amplitudes and load cycles.

In (Varandas, Hölscher, & Silva, 2010) a new settlement model is presented. The advantage of this model lies in the integration of the influence of load history. Its output aligns with the observed fact that the maximum applied load is the dominant factor in ballast settlement independent of load sequence (Diyaljee, 1987; Shenton, 1985).

It should be mentioned that some of the influencing factors, including minimum stress levels (Augustin, Gudehus, Huber, & Schünemann, 2003; Baeßler & Ruecker, 2003), load frequency (X. Zhang, Zhao, & Zhai, 2019) and confinement stress (Sun, Indraratna, & Nimbalkar, 2016) could hardly be integrated into current settlement models. As stated in (Baeßler & Ruecker, 2003), discrete element method (DEM) that accounts for single ballast particles might be the

best option for further numerical investigations. However, integration of discrete element model into a full-scale track model is still ineffective currently due to the restriction of computational resources.

- **Long-term vehicle-track interaction**

Over the last three decades, several researchers have attempted to extend the research on vehicle-track interaction from short-term to long-term.

Research in (Mauer, 1995) was one of the first attempts to derive the relationship between the ballast settlement, inhomogeneous track stiffness and rail irregularity growth. The utilized model encompasses the following three components: the dynamic vehicle model, the discrete non-linear static track model and the track settlement law proposed by Hettler (Hettler, 1984). With the development of research and the increase in computation power today, investigation with more detailed and more complex vehicle-track interaction models and ballast settlement laws becomes possible.

In (Varandas, Hölscher, & Silva, 2013), the settlement of track transitions was studied using algorithms proposed in (Zhai, 1996) and ballast settlement law proposed in (Varandas et al., 2010). The disadvantage of this research is that the track model is relatively simple, which has modelled the contact between rail and sleepers as bonded and modelled all layers below sleepers together as one layer. As demonstrated in later investigation, more detailed track model is needed to investigate the possibility of optimizing track design at transition zone.

In (X. Li, Nielsen, & Palsson, 2014), track settlement in the entrance to railway turnouts has been studied and predicted. The procedure was performed following an iteration schema containing four steps: (I) the simulation of dynamic vehicle-track interaction, (II) the calculation of load distribution and sleeper-ballast contact pressure, (III) the prediction of track settlement and (IV) the calculation of the resulting vertical track irregularity as input for the next step of the iteration. A noteworthy limitation of the employed model is that under sleeper gap was not considered.

In (Vale & Calçada, 2014), a quarter-bogie model and a 2D track model were applied to parameter studies. Ballast settlement is assumed the function of total tonnage and dynamic load on the track. The results have demonstrated that vehicle characteristics influences the

evolution of the track profile. The conclusion is in accordance with the study (Steenbergen & de Jong, 2016), in which vehicle type plays an especially important role in geometrical track deterioration. As mentioned in the previous studies, a more elaborate vehicle model is needed if vehicle vibration is to be evaluated.

In (Wang & Markine, 2018), a comprehensive analysis of earthwork-bridge transition zones was performed. Short-term vehicle-track interaction was simulated using the commercial simulation program LS-DYNA. The ballast settlement law developed in (Dahlberg, 2001) was used. The influence of design variations on ballast stress and wheel-rail contact force were investigated. However, the employed ballast settlement law is not suitable to describe the settlement of new track, which is discussed in detail in Chapter 4.1.

- **Evaluation of vehicle-track-system performance**

Another limitation of previous research lies in the evaluation of the vehicle-track system. In previous research, the performance of vehicle-track system is usually evaluated by the dynamic vehicle-track interaction along track transition zone, e.g., calculating dynamic wheel-rail contact (WRC) force. In this research, the maintenance interval is employed as another parameter to evaluate the performance of track transition, so that the calculation results can be integrated with praxis better. As it is known, IMs regulate maintenance activities based on track geometry measured using track recording car. For example, DB Netz AG (DB) has proposed the monitoring interval and thresholds of track geometry defects SR values in the regulation Ril 821.2001 (DB Netz AG, 2010). Based on that, the maintenance interval can be determined.

1.5 Conclusion

In conclusion, comprehensive analysis of vehicle-track system behaviour at track transition zones requires the consideration of short-term non-linear vehicle-track interaction, long-term ballast settlement and comprehensive evaluation of vehicle-track-system performance. Although some publications have partially accomplished such a systematic investigation process, a complete study that considers all these aspects is not available. From this perspective, further research is meaningful and needed.

2. Research aim and methodology

2.1 Aim of the research

The first aim of this study is to create a numerical analysis tool for the systematic evaluation of track transitions that includes the following functionalities:

- Calculation of the short-term vehicle-track interaction with consideration of non-linear effects such as under-sleeper gaps.
- Prediction of long-term track settlement development employing proper ballast settlement law.
- Evaluation of vehicle-track system concerning dynamic factor and maintenance interval.

With the help of the analysis tool developed in MATLAB, the current design of ballastless-ballasted track transition has been evaluated. Besides, potential improvements have been investigated.

2.2 Structure of this investigation

The next chapters of this investigation are structured in the following manner.

In Chapter 3, the methodology that is used to set up the short-term vehicle-track interaction model and to solve it in time domain has been proposed based on the literature review. The primary focus of this chapter is to develop an accurate and efficient numerical method that could simulate vehicle-track interaction under consideration of the non-linear characteristic of track structure due to the possible existence of under sleeper gaps.

The first approach succeeded by using co-simulation of a Finite-Element (FE) software and a Multi-Body-Simulation (MBS) software as illustrated in (Chen, 2014). After substructure analysis and modal analysis on the FE model of the track structure, the simplified track model was imported into the MBS environment to realise the co-simulation. The disadvantage of this

method using commercial tools was that it could not consider the non-linearity of the track structure.

To overcome this disadvantage, a new method to simulate vehicle-track interaction was proposed by author in the European research project DESTination RAIL (Chen & Lechner, 2018). In this approach, track components were modelled in the MBS environment directly as flexible or rigid bodies. The interaction between track components was simulated by using non-linear force elements and dampers (Figure 2-1). To improve the simulation's efficiency, a script based on SIMPACK QtScript was written, which realized the automation of model building, calculation, and evaluation.

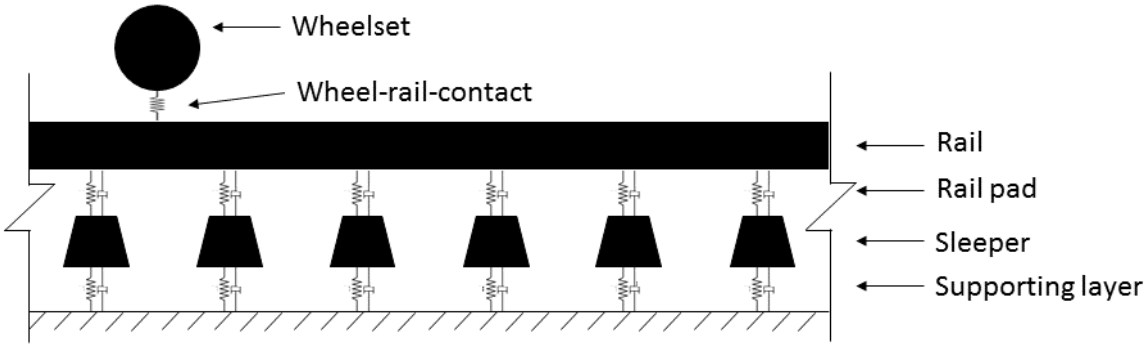

Figure 2-1: Sketch of the MBS model proposed by the author (Chen & Lechner, 2018)

The disadvantage of this method was that the calculation speed was too low, which made the study of long-term track behaviour under repeated loads ineffective.

To overcome these problems, in this research, a new numerical calculation model is created using MATLAB. To validate the model, comparison with results from commercial software and field measurement has been performed.

In Chapter 4, a suitable ballast settlement law is selected based on literature review, which is integrated into the newly developed numerical simulation tool. Its parameters are also verified through an examination of documented laboratory tests and field measurement results.

With the established theoretical base, the short-term and long-term behaviour of a typical ballastless-ballasted track transition zone are investigated in Chapter 5 and in Chapter 6, respectively. In chapter 5, the influence of vehicle type, travel direction and speed on the short-

term behaviour of track transition is evaluated. In chapter 6, the possibility to optimise the standard design with respect to long-term performance is investigated. Finally, a new design plan with adjusted rail seat stiffness, extended auxiliary rail, HBL/flexible pavement and implementation of USP has been proposed.

In Chapter 7, conclusions drawn in this researched are summarised.

In Chapter 8, suggestions on further research are provided.

2.3 Workflow

The workflow of the developed MATLAB calculation program is graphically illustrated in Figure 2-2, which can be divided into the following four modules.

Module I: Track equilibrium

In this module, the track is brought to static equilibrium under its self-weight. The aim is to determine the unloaded track geometry and the potential under-sleeper gaps with given ballast settlement. Afterwards, the track is brought to equilibrium under the vehicle load. The aim is to eliminate the transient oscillation at the beginning of the following dynamic calculation.

The FE model of the track is established and solved using MATLAB. The main difficulty lies in solving the FE equation with the non-linear sleeper-ballast contact, which is caused by the uneven settlement of the ballast layer. To solve this problem, the Newton-Raphson method with line search is employed, which is illustrated in Chapter 3.1 in detail.

Module II: Dynamic vehicle-track interaction

In this module, the short-term dynamic interaction between vehicle and track is calculated. The dynamic interaction is solved in the time domain by using an explicit algorithm, which is illustrated in Chapter 3 in detail. The output of this module includes the dynamic load on the vehicle, load on track components and change in vertical wheel position (which equals to the loaded track longitudinal level). Loaded track longitudinal level are exported to Module IV for evaluation of the necessity of maintenance. Pressure on the ballast layer is exported to Module III to predict the caused ballast settlement.

Module III: Track settlement

In this module, the ballast settlement caused in the current load cycle is determined by using the ballast pressure that is determined in Module II and the settlement law that is proposed in Chapter 4. The determined ballast settlement is then introduced into Module I as the input for the next load cycle.

A closed loop between Modules I, II and III is thereby formed.

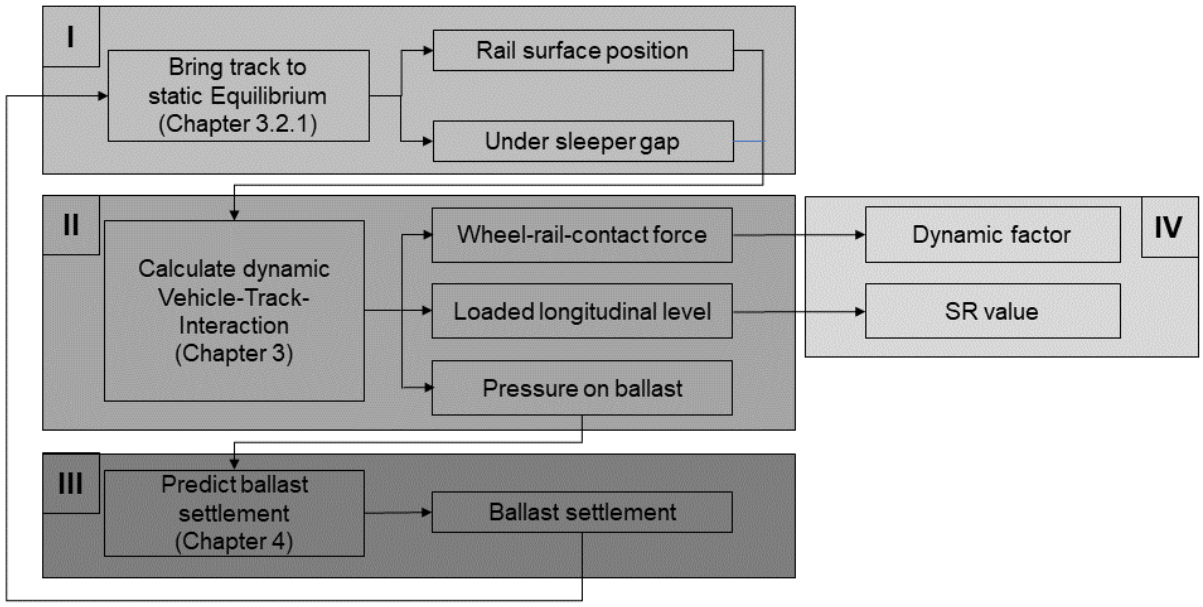

Figure 2-2: Workflow of track transition evaluation tool developed in MATLAB

Module IV: Evaluation

This module evaluates the output from Module II. Besides the maximal dynamic WRC force, the determined actual loaded track longitudinal level is also used for evaluation. It is converted to SR-value, corresponding to the measured longitudinal track level defect using chord-based measurement method proposed in DB regulation Ril 821.2001 (DB Netz AG, 2010), and is compared with the threshold proposed in the same regulation. The amplitude of SR-value is employed as an indicator to evaluate the performance of transition design.

2.4 Assumptions

The following assumptions are supposed to be necessary, but do not harm the validity of this research:

- The subgrade in all cases is supposed to be settlement-free as discussed in chapter 1.4. Consequently, the effect of subgrade is integrated following the Winkler spring model approach.
- Initial track stiffness discontinuity along the track is given due to changes in track design. Track stiffness within each track subsection is assumed constant. This is needed to clearly identify the effect of the designed track stiffness change for design evaluation, which is not affected by track quality defects dependent on construction and maintenance work.
- In long-term simulation, the track irregularity caused by track stiffness discontinuity and uneven ballast settlement is considered.
- The study is focusing on vehicle-track interaction in vertical direction. All investigated tracks are supposed to be straight and horizontal.

3. Numerical investigation of short-term vehicle-track interaction

3.1 Set up the numerical model of vehicle-track interaction

The conventional coordinate system of vehicle-track system is defined as follows: the x-axis of the coordinate system is defined as the longitudinal direction of track, the y-axis as the lateral direction of track, and the z-axis as the vertical direction of track. The positive direction of x-axis points to the direction of train speed. The positive direction of z-axis points downwards, corresponding to the direction of gravity.

The vehicle-track coupled dynamic model concept described in (Zhai & Sun, 1994; Zhai, Wang, & Cai, 2009) is employed here. The vehicle-track interaction model in x-z plane is demonstrated in Figure 3-1.

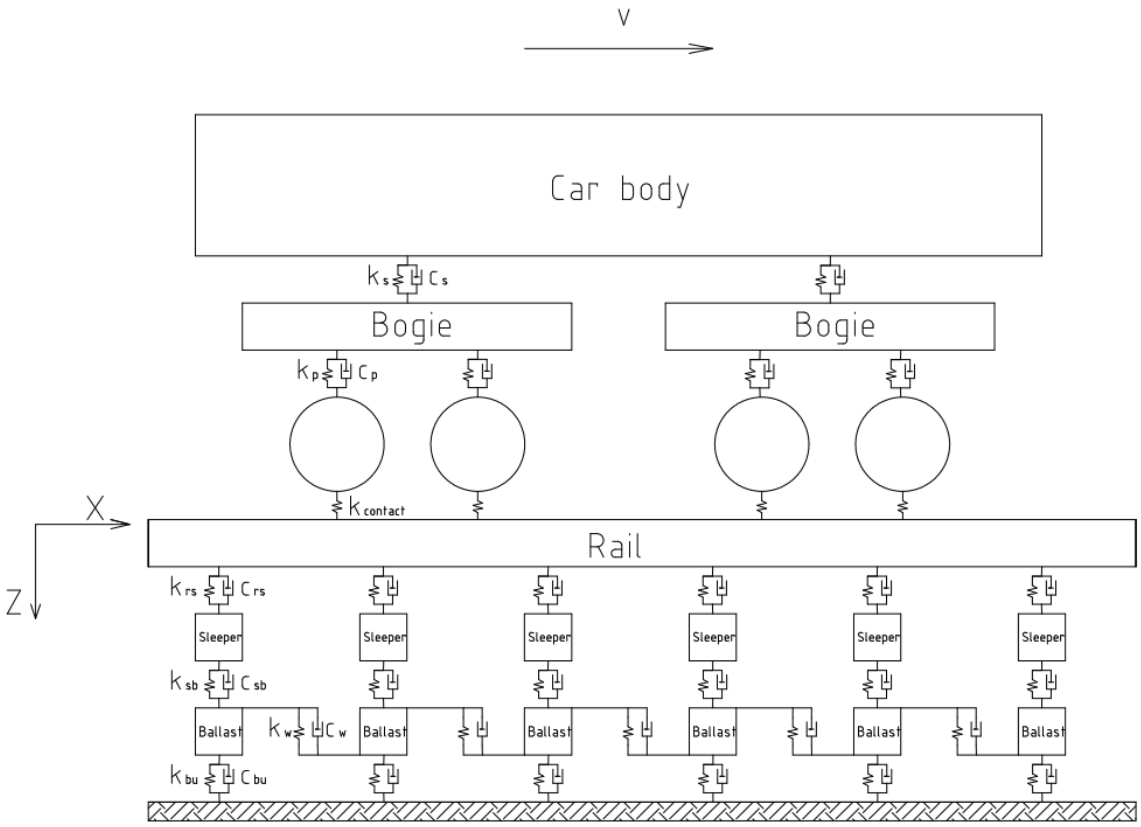

Figure 3-1: The detailed vehicle/track interaction model proposed in (W. Zhai & Sun, 1994)

In this model, the vehicle model consists of a rigid car body, two rigid bogies and four rigid wheelsets, which are connected by linear spring in parallel with viscous dampers representing the primary and secondary suspension. The vehicle has 10 degree-of-freedoms (DoF), i.e., the bounce motion along z axis of the car body, 2 bogies and 4 wheels, as well as the pitch motion about the y axis of the car body and 2 bogies.

Rail is modelled as Euler- Bernoulli Beam. Each node has three DoF consisting of translational motion along the x axis and the z axis as well as the rotational motion about the y axis. Sleepers and the mass of ballast are modelled as rigid bodies. They have only one DoF of translational motion along the z axis. Rail fastening system, stiffness of ballast layer, bedding modulus of subgrade are modelled with parallel linear spring and viscous dampers. See Appendix 1 for more detail.

Here in this research, several modifications to the original model are essential.

Firstly, since under-sleeper gap is a common phenomenon at track transitions, the linear spring/damper elements between sleeper and ballast are replaced by bi-linear force element as in (2):

$$F_{sb} = \begin{cases} k_{sb}(u_s - u_b - \delta_{sb}) + c_{sb}(\dot{u}_s - \dot{u}_b), & if\ (u_s - u_b) \geq \delta_{sb}, \\ 0, & otherwiese \end{cases} \quad (2)$$

with

k_{sb}, c_{sb} : stiffness and damping of the ballast layer

$u_s, \dot{u}_s$: deflection and deflection velocity of the sleeper

$u_b, \dot{u}_b$: deflection and deflection velocity of the ballast

δ_{sb} : gap between sleeper and ballast under track self-weight

F_{sb} : interaction force between sleeper and ballast

Secondly, stiffness of subgrade is described by its bedding modulus according to (Freudenstein, 2020b; Iliev, 2012; Klotzinger, 2008a; Rapp, 2017).

Table 3-1: Bedding modulus of subgrade in different conditions (Freudenstein, 2020b; Rapp, 2017)

Subgrade condition	Bedding modulus [MN/m³]
subgrade in poor condition	50 - 100
subgrade in good condition	100 - 150
subgrade in particularly good condition	150 - 300
intensively tampered subgrade, concrete, bridge, tunnel	300 - 435

3.2 Determination of the dynamic response in time-domain

The first step of the dynamic calculation is to bring the vehicle-track-system into static equilibrium under self-weight. Considering the non-linearity in the system, e.g., under sleeper gap, iteration process is needed. For this purpose, Newton-Raphson method with line search (Belytschko, Liu, Moran, & Elkhodary, 2013) is adopted here. Detailed illustration can be found in Appendix 2. One feature of this algorithm compared to the basic Newton-Raphson method is that it can be accelerated using parallel computation.

The next step is to solve the vehicle-track interaction in time domain. Corresponding numerical methods can generally be divided into two families: explicit methods and implicit methods. In an explicit approach, all constitutive variables are available from the computation of previous time steps. On the other hand, in an implicit approach, the constitutive variables are not expressed explicitly, but provided as functions of the current time step of analysis. They are illustrated below by solving the generalized equation of motions for dynamic systems:

$$[M]\,\ddot{u} + [C]\,\dot{u} + [K]\,u = p \tag{3}$$

with

$[M], [C], [K]$: Mass, Damping and Stiffness Matrix of the system

$u, \dot{u}, \ddot{u}$: Vector of Displacements, velocities, and accelerations

p : Vector of externally applied forces

One widely used implicit method is the Newmark-beta method (Newmark, 1959). The basic idea is to predict the velocity and displacement of the next integration step using the acceleration, velocity, and displacement of the current step.

$$\begin{aligned} \dot{u}_{t+\Delta t} &= \dot{u}_t + [(1-\beta)\Delta t]\ddot{u}_t + (\beta\Delta t)\ddot{u}_{t+\Delta t} \\ u_{t+\Delta t} &= u_t + (\Delta t)\dot{u}_t + \left[\left(\frac{1}{2}-\alpha\right)(\Delta t)^2\right]\ddot{u}_t + [\alpha(\Delta t)^2]\ddot{u}_{t+\Delta t} \end{aligned} \tag{4}$$

with

$u_t, \dot{u}_t, \ddot{u}_t$: Vector of Displacements, Velocities and Accelerations at step t

$u_{t+\Delta t}, \dot{u}_{t+\Delta t}, \ddot{u}_{t+\Delta t}$: Vector of Displacements, Velocities and Accelerations at step $t + \Delta t$

α, β : constant coefficients

In (4), α and β influence the stability and accuracy of the method.

Substituting (4) into (3) yields:

$$u_{t+\Delta t} = \hat{K}^{-1}\hat{p} \tag{5}$$

with

$$\hat{K} = \left[K + \frac{\gamma}{\beta\Delta t}C + \frac{1}{\beta(\Delta t)^2}M\right]$$

and

$$\hat{p} = p_{t+\Delta t} + \left[\frac{\gamma}{\beta\Delta t}C + \frac{1}{\beta(\Delta t)^2}M\right]u_t + \left[\frac{1}{\beta\Delta t}M + \left(\frac{\gamma}{\beta}-1\right)C\right]\dot{u}_t + \left[\left(\frac{1}{2\beta}-1\right)M + \Delta t\left(\frac{\gamma}{2\beta}-1\right)C\right]\ddot{u}_t$$

By solving (5), the displacement in the next integration step can be determined. Afterwards, acceleration and velocity can be calculated based on (4).

In (Lei & Noda, 2002), the Newmark-beta method has been employed to solve vehicle-track interaction problem (Figure 3-2).

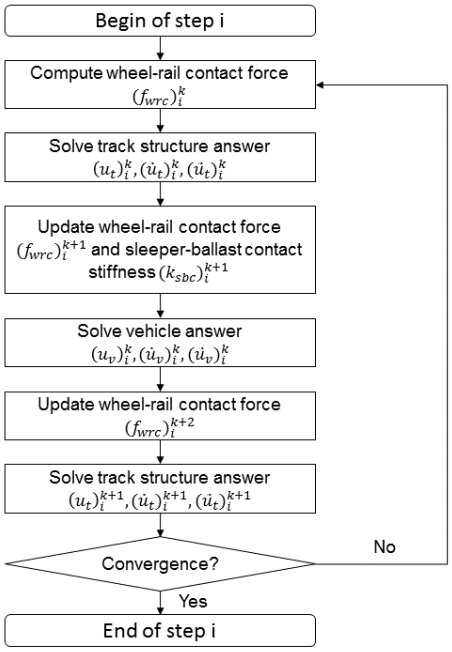

Figure 3-2: Workflow based on (Lei & Noda, 2002)

One widely used explicit algorithm in vehicle-track-dynamics is the “Zhai-method” proposed in (Zhai, 1996):

$$\begin{aligned} u_{t+\Delta t} &= u_t + (\Delta t)\dot{u}_t + \left[\left(\frac{1}{2}+\psi\right)(\Delta t)^2\right]\ddot{u}_t - [\psi(\Delta t)^2]\ddot{u}_{t-\Delta t} \\ \dot{u}_{t+\Delta t} &= \dot{u}_t + [(1+\varphi)\Delta t]\ddot{u}_t - (\varphi\Delta t)\ddot{u}_{t-\Delta t} \end{aligned} \tag{6}$$

with

$u_t, \dot{u}_t, \ddot{u}_t$: Vector of Displacements, Velocities and Accelerations at step t

$u_{t+\Delta t}, \dot{u}_{t+\Delta t}$: Vector of Displacements and Velocities at step $t + \Delta t$

$\ddot{u}_{t-\Delta t}$: Vector of Accelerations at step $t - \Delta t$

ψ, φ : constant coefficients

Substituting (6) into (3) yields:

$$\ddot{u}_{t+\Delta t} = M^{-1}\hat{p} \tag{7}$$

with

$$\hat{p} = p_{t+\Delta t} - Ku_t - (C + K\Delta t)\dot{u}_t - \left[(1+\varphi)C + \left(\frac{1}{2}+\psi\right)K\Delta t\right]\ddot{u}_t\Delta t + (\varphi C + \psi K\Delta t)\ddot{u}_{t-\Delta t}\Delta t$$

The workflow is shown in Figure 3-3.

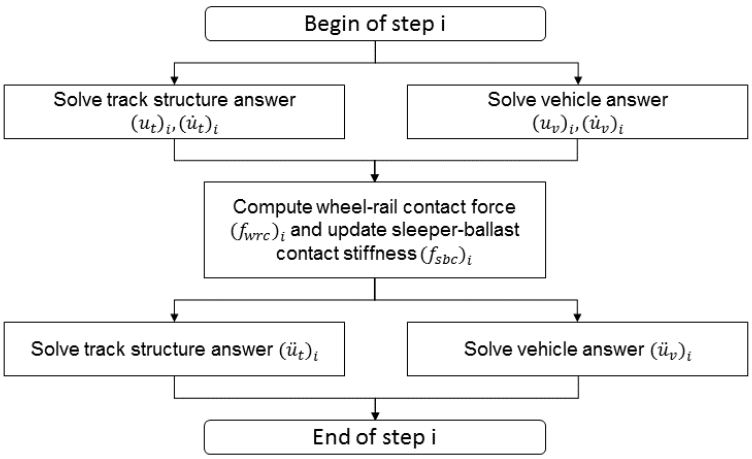

Figure 3-3: Workflow based on (Zhai, 1996)

Both implicit and explicit methods have its advantages and disadvantages. For linear system, implicit methods allow larger integration step size than explicit methods, because implicit methods are unconditionally stable, when parameters of the method meet certain conditions. For example, Newmark-beta method is unconditionally stable for linear system, when $\beta \geq 0.5$ and $\alpha \geq 0.25*(0.5+ \beta)^2$. In contrast, the integration step size in explicit methods must be small enough to assure its stability and adequate accuracy. Therefore, implicit methods tend to require less computation resources when solving linear problems.

However, in this research, influence of under-sleeper gap could not be ignored, which brings non-linearity into the system. The unconditional stability of implicit method is thus violated. When using implicit method, additional iteration within each time step is required. Consequently, the computational cost of an implicit analysis may significantly exceed than that of an explicit solution (Soares, 2018).

In a vehicle-track-system, the mass matrix is always a constant diagonal matrix, whereas the stiffness matrix and damping matrix in most cases are not. A special benefit of Zhai-method is that there is no need to compute the inverse of stiffness matrix in each time step, which greatly improves the computation efficiency, compared to solving equation (7) and solving equation (5).

In the following calculation, the algorithm from (Zhai, 1996) and the Newmark-beta with iteration method from (Lei & Noda, 2002) are compared to each other. For simplicity, they are designated as algorithm 1 and algorithm 2 in the following chapters, respectively.

3.3 Comparison of the two algorithms with commercial software

Due to the restriction of computation power, the comparison is performed with a simplified version of the standard vehicle-track interaction model proposed in chapter 3.1. Firstly, a bogie model with 4 DoF instead of the 10 DoF vehicle model is employed. Secondly, the elasticity and damping of ballast layer and subgrade are modelled together as one supporting layer beneath the sleeper, using a parallel set-up of spring and damper. Sketch of the model is shown in Figure 3-4.

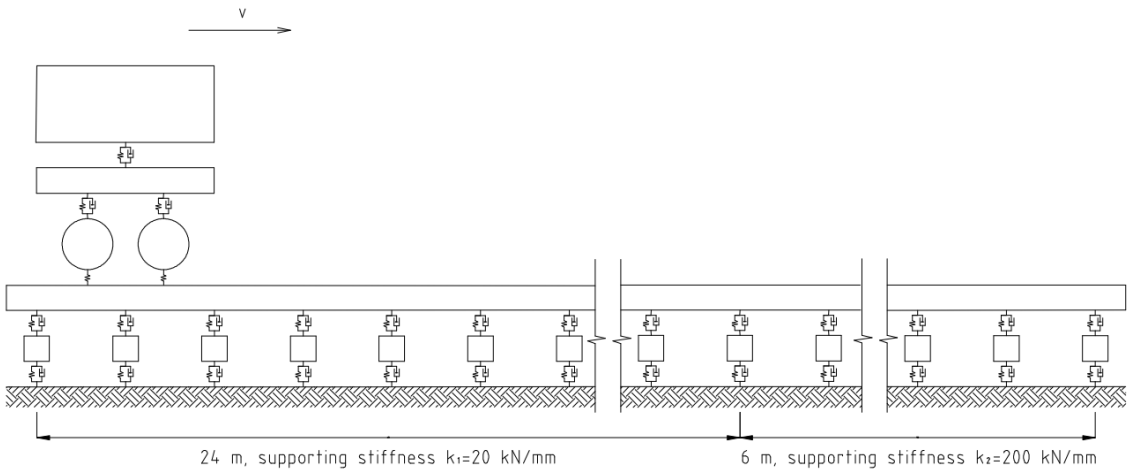

Figure 3-4: Sketch of the model with track stiffness discontinuity, not to scale

The track parameters are listed in Table 3-2, which represents a standard ballasted track design. As shown in Figure 3-4, track stiffness discontinuity is introduced at the 41st rail seat, where the stiffness of the sleeper supporting layer increases from 20 kN/mm to 200 kN/mm. Damping of the sleeper supporting layer in both subsections is however set as the same. To demonstrate the effect of track stiffness discontinuity neither other track irregularity nor rail roughness is introduced.

Table 3-2: Summary of parameters of the ballasted track (Zhai, 2014)

Notation	Parameter [unit]	Value
E	Young's modulus of rail material [N/m^2]	2.0×10^{11}
ρ	Density of rail material [kg/m^3]	7850
A	Area of rail cross section [m^2]	7.67×10^{-3}
I_z	Rail second moment of area about z axis [m^4]	3.04×10^{-5}
M_r	Rail mass per unit length [kg/m]	60.21
K_{rs}	Static stiffness of fastening system in vertical direction [kN/mm]	6.5×10^7
C_{rs}	Damping of fastening system in vertical direction [N·s/m]	7.5×10^4
M_s	Half sleeper mass [kg]	140
l_s	Sleeper spacing [m]	0.60
l_e	Effective support length of half sleeper [m]	1.04
l_b	Sleeper width [m]	0.285
K_y	Static stiffness of the supporting layer [N/m]	2×10^7 / 2×10^8
C_y	Supporting layer damping [N·s/m]	3.115×10^4

The parameters for vehicle are cited from SIMPACK Rail Training (see Table 3-3), which corresponds to a standard passenger coach. The axle distance is 3.0 m, corresponding to 5 times of the sleeper spacing. The static axle load is 95.0 kN. Calculation was performed with a vehicle speed of 180 km/h (50 m/s).

Table 3-3: Summary of vehicle parameters (source: SIMPACK Rail Training)

Notation	Parameter [unit]	Value
M_c	Car body mass [kg]	16868
M_b	Bogie mass [kg]	1500
M_w	Wheelset mass [kg]	500
I_{cy}	Mass moment of inertia of car body about y axis [kgm^2]	45993
I_{by}	Mass moment of inertia of bogie about y axis [kgm^2]	2500
K_{ps}	Stiffness coefficient of primary suspension along z axis [N/m]	1.2×10^7
C_{ps}	Damping coefficient of primary suspension along z axis [N·s/m]	4.0×10^3
K_{ss}	Stiffness coefficient of secondary suspension along z axis [N/m]	4.5×10^5
C_{ss}	Damping coefficient of secondary suspension along z axis [N·s/m]	2.0×10^4
l_t	Semi-longitudinal distance between wheelsets in bogie [m]	1.5

By calculation using algorithm 1, the first 133 normal modes of rail were selected, corresponding to the upper frequency of 1000 Hz.

As comparison, the same model is also built in the commercial software SIMPACK. Detail about setting up the model can be found in (Chen & Lechner, 2018). The built model in static equilibrium state is demonstrated in Figure 3-5.

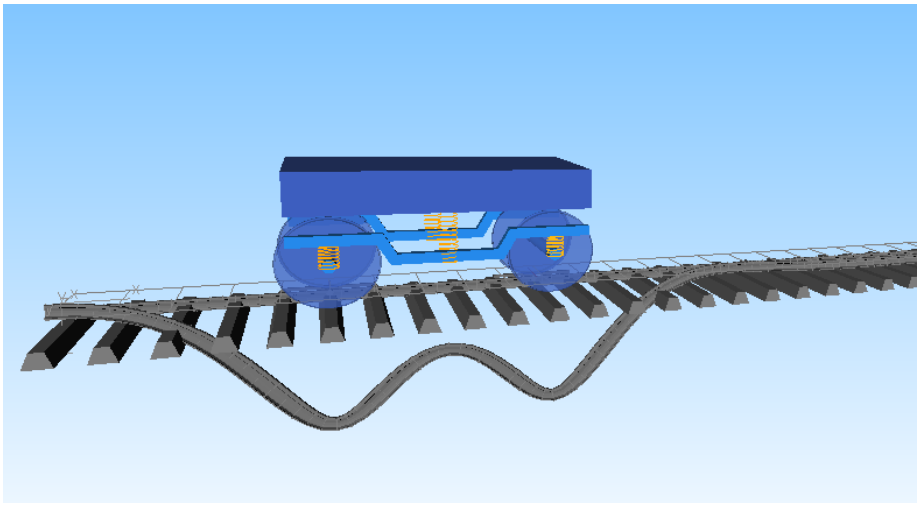

Figure 3-5: SIMPACK model in static equilibrium state (Rail deflection is 1000 times amplified).

Figure 3-6 demonstrates the change of the vertical position of the front wheel during the train run, calculated using three different methods. In Figure 3-6, the x-axis shows the longitudinal position of the front wheel with respect to rail seat sequence, and the y-axis shows the change of the vertical position with respect to its start position. The positive vertical direction is defined as the gravity direction.

The abrupt increase of sleeper support stiffness from the 41st rail seat on leads to the increase of track stiffness already from the 38th rail seat on due to the load transfer effect brought by rail. The increase of track stiffness consequently leads to the reduction of rail deflection and the upwards movement of the front wheel when it passes the 38th rail seat. As could be observed in Figure 3-9, the amplitude of the wheel movement corresponds to the difference of rail deflection at both sections. All three approaches show nearly the same results, with a variation within 3%.

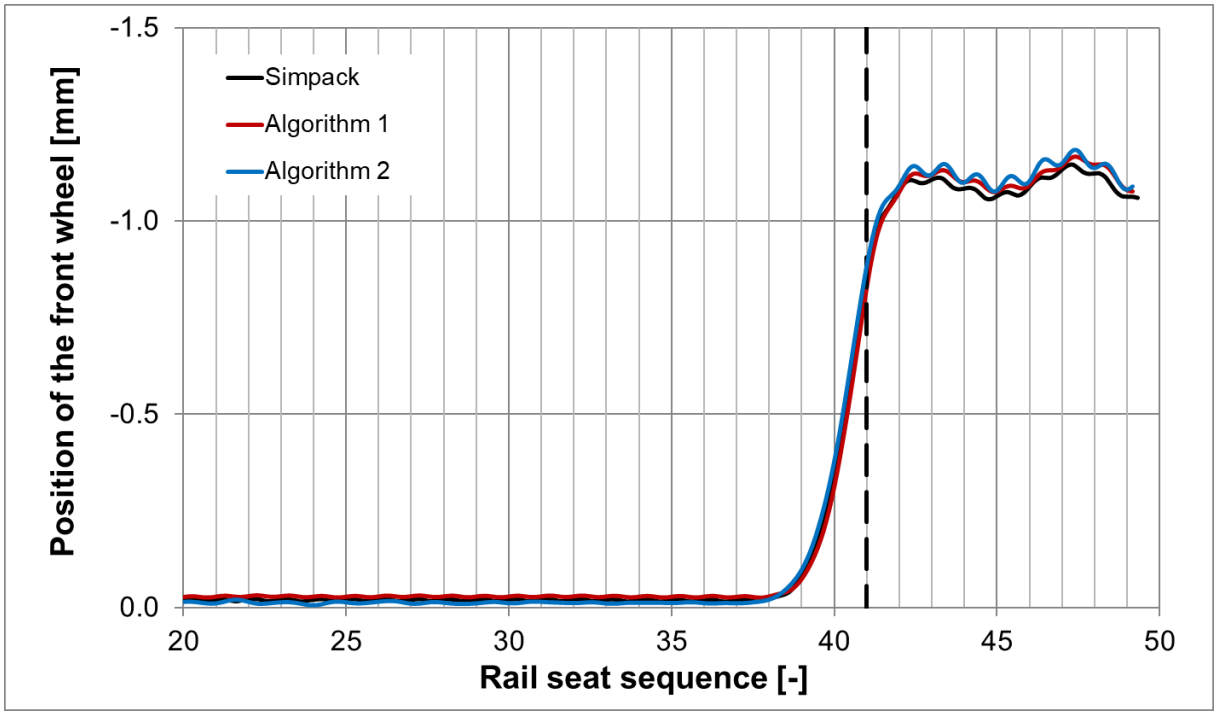

Figure 3-6: Change of the vertical position of the front wheel, dash line indicates the position of sleeper support stiffness discontinuity

Comparison of the dynamic wheel-rail contact (WRC) force between the front wheel and the rail calculated using three methods is presented in Figure 3-7, in which the x-axis shows the position of the front wheel with respect to the rail seat sequence. Because of the upwards movement of the front wheel, the dynamic WRC force increases from the 38th rail seat on. The WRC force increases to 100.9 kN due to the stiffness discontinuity, corresponding to a dynamic factor of 1.06 compared to the static wheel load 95.0 kN. The maximal WRC force in Figure 3-7 is nevertheless observed at around 45th rail seat, when the back wheel is entering the sleeper support stiffness discontinuity boundary (see Figure 3-8).

Besides, short-wave variation in WRC force (see Figure 3-7 and Figure 3-8) and wheel vertical position (see Figure 3-6) could be observed. The wavelength of the variation equals to the rail seat distance, which implies that it is caused by the secondary rail deflection between two adjacent rail supports.

Despite of the good correlation, variation between the results from algorithm 2 and the results from the other two calculations, especially in the second track subsection (after the 42nd rail

seat) can be observed. The difference between the three approaches/calculations is nevertheless minor, not exceeding 2%.

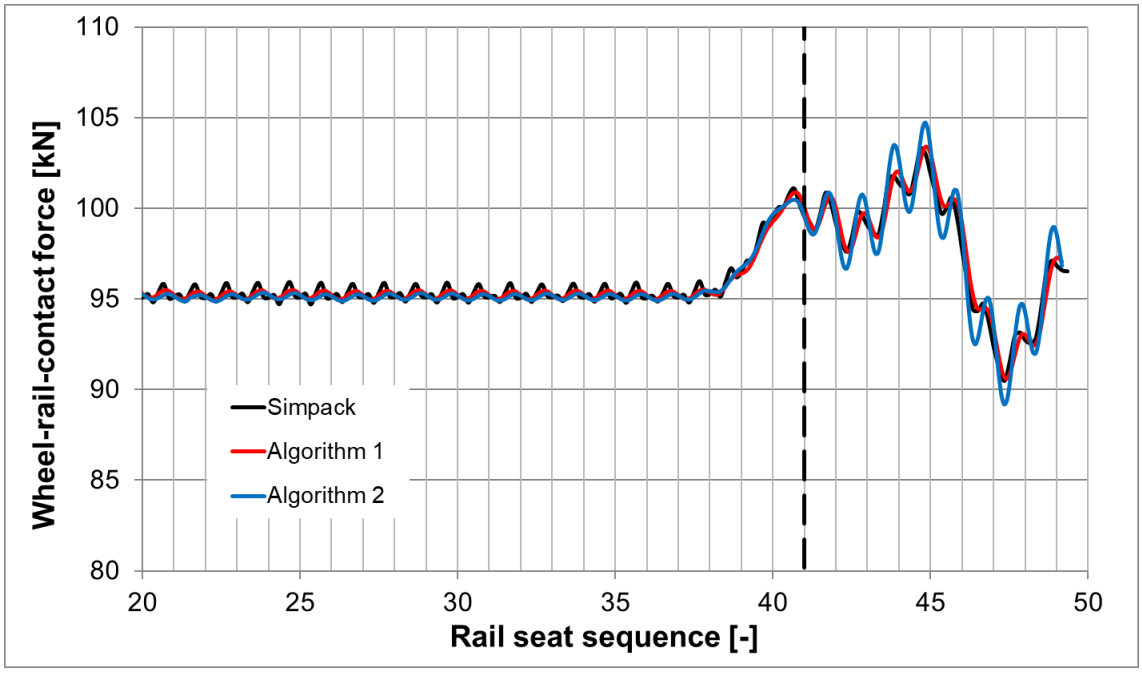

Figure 3-7: Dynamic WRC force of the front wheel, dash line indicates the position of sleeper support stiffness discontinuity

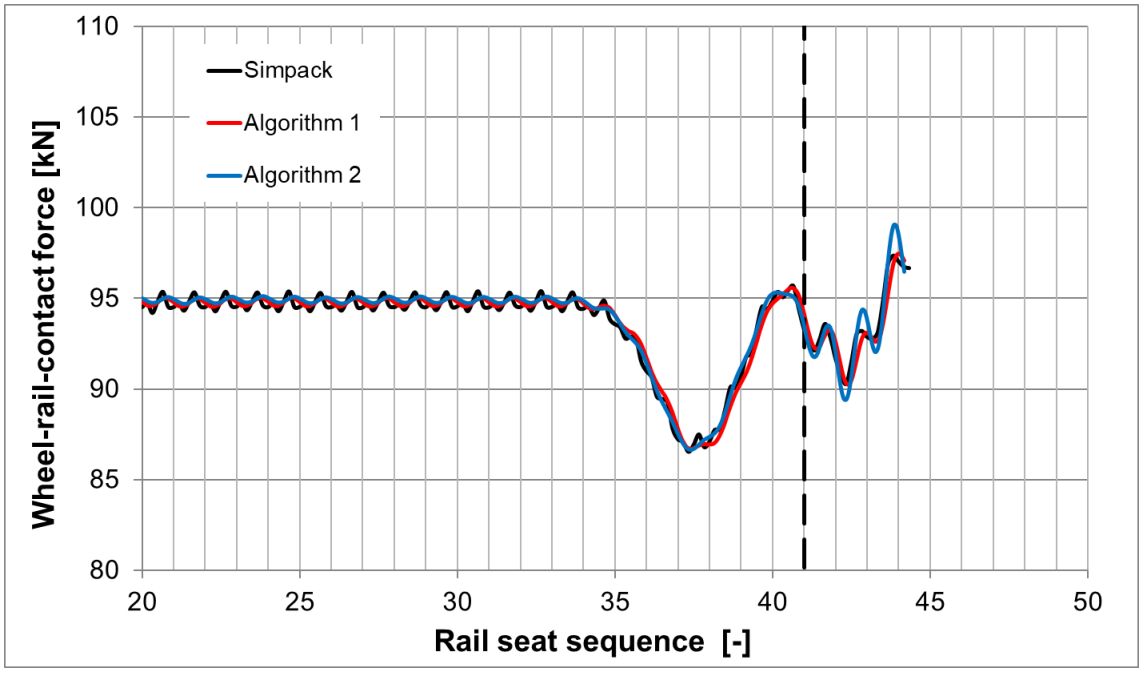

Figure 3-8: Dynamic WRC force of the back wheel, dash line indicates the position of sleeper support stiffness discontinuity

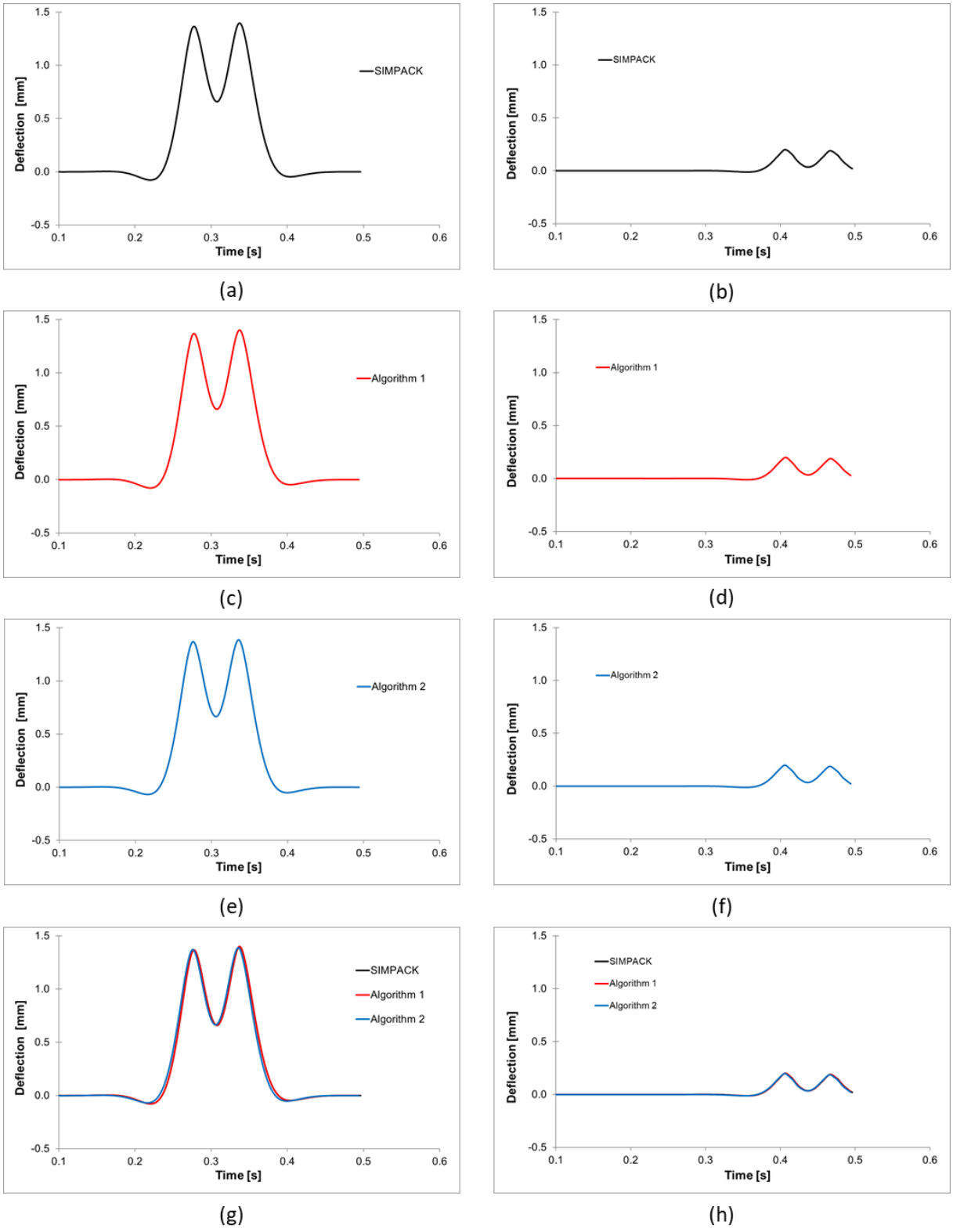

Figure 3-9: Comparison of calculated sleeper deflection using SIMPACK, algorithm1 and algorithm 2, figure (a), (c), (e) and (g): deflection of the sleeper at the 31st rail seat (k_1 = 20 kN/mm), figure (b), (d), (f) and (h): at the 42nd rail seat (k_2 = 200 kN/mm)

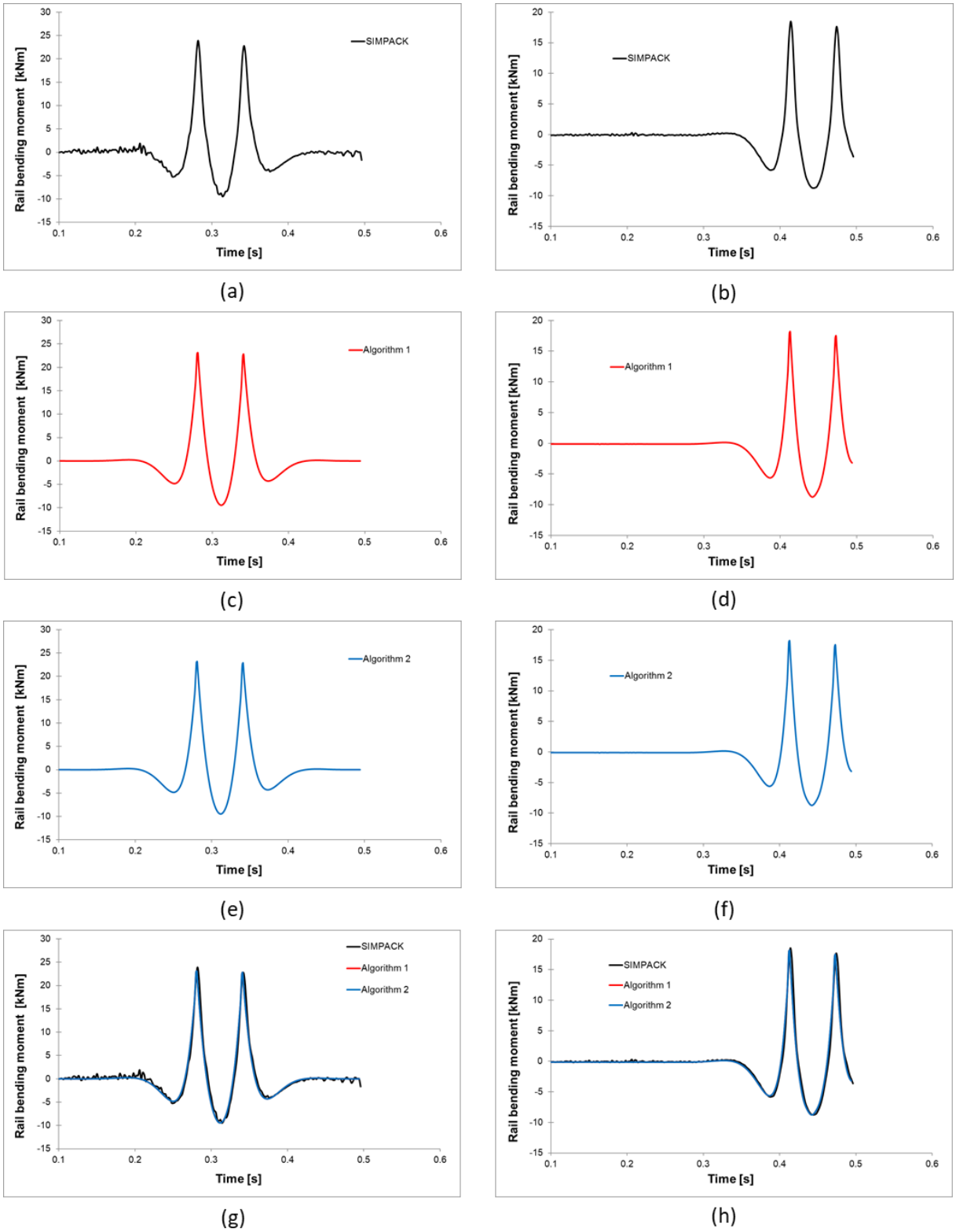

Figure 3-10: Comparison of calculated rail bending moment using SIMPACK, algorithm1 and algorithm 2, figure (a), (c) ,(e) and (g): rail bending moment between the 31st and 32nd rail seat, figure (b), (d), (f) and (h): rail bending moment between the 42nd and 43rd rail seat

The determined sleeper deflection at 31st rail seat (where the supporting stiffness is lower) and the sleeper deflection at 42nd rail seat (where the supporting stiffness is higher) are plotted in Figure 3-9. In Figure 3-10, calculated rail bending moment at both subsections from the three approaches are compared. Good agreement can also be concluded (see Figure 3-9 (g) (h) and Figure 3-10 (g) (h)). In Figure 3-10, high-frequent variation of rail bending moment can be observed in the calculation result from SIMPACK, which is not considered in the other two methods. Nevertheless, this variation vanishes in the sleeper deflection curves in Figure 3-9, since high-frequent oscillation (greater than 50 Hz) is decoupled from track components below the rail by the mass of rail (Fendrich & Fengler, 2014).

The calculation time using algorithm 2 is half so long as that using algorithm 1, and nearly 100 times shorter than that using the SIMPACK software tool. The comparison of calculation results proves that in this case the accuracy of interested results is not negatively affected.

At next step, the algorithms 1 and 2 are compared in case of track structure with non-linearity. For this purpose, stiffness of supporting layer is set as 20 [kN/mm] uniformly along the whole track section. But under the 25th, 26th and 27th rail seat, under-sleeper gaps are introduced as demonstrated in Figure 3-11. The amplitude of the gap under each sleeper amounts to 1 mm, 2 mm and 1mm, respectively.

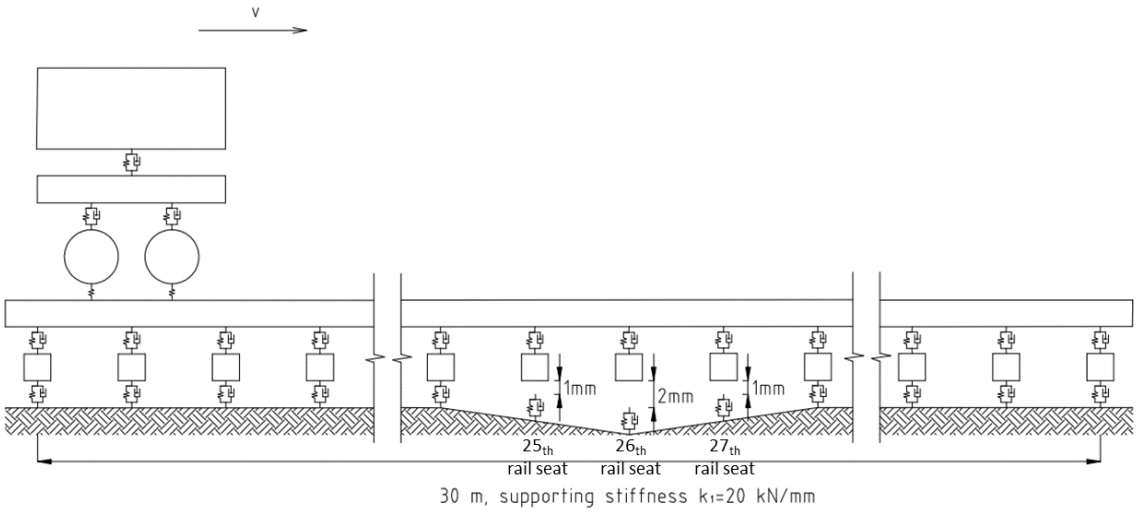

Figure 3-11: Sketch of the model with under-sleeper gaps, not to scale

As mentioned in formula (2), bilinear characteristic curves are used to model the contact between sleeper and ballast in case of under-sleeper gap. It is assumed that the contact stiffness and damping are zero if the gap is not filled. Otherwise, the stiffness and damping are assumed as constant. The determined WRC forces of both wheels against rail seat sequence are presented in Figure 3-12.

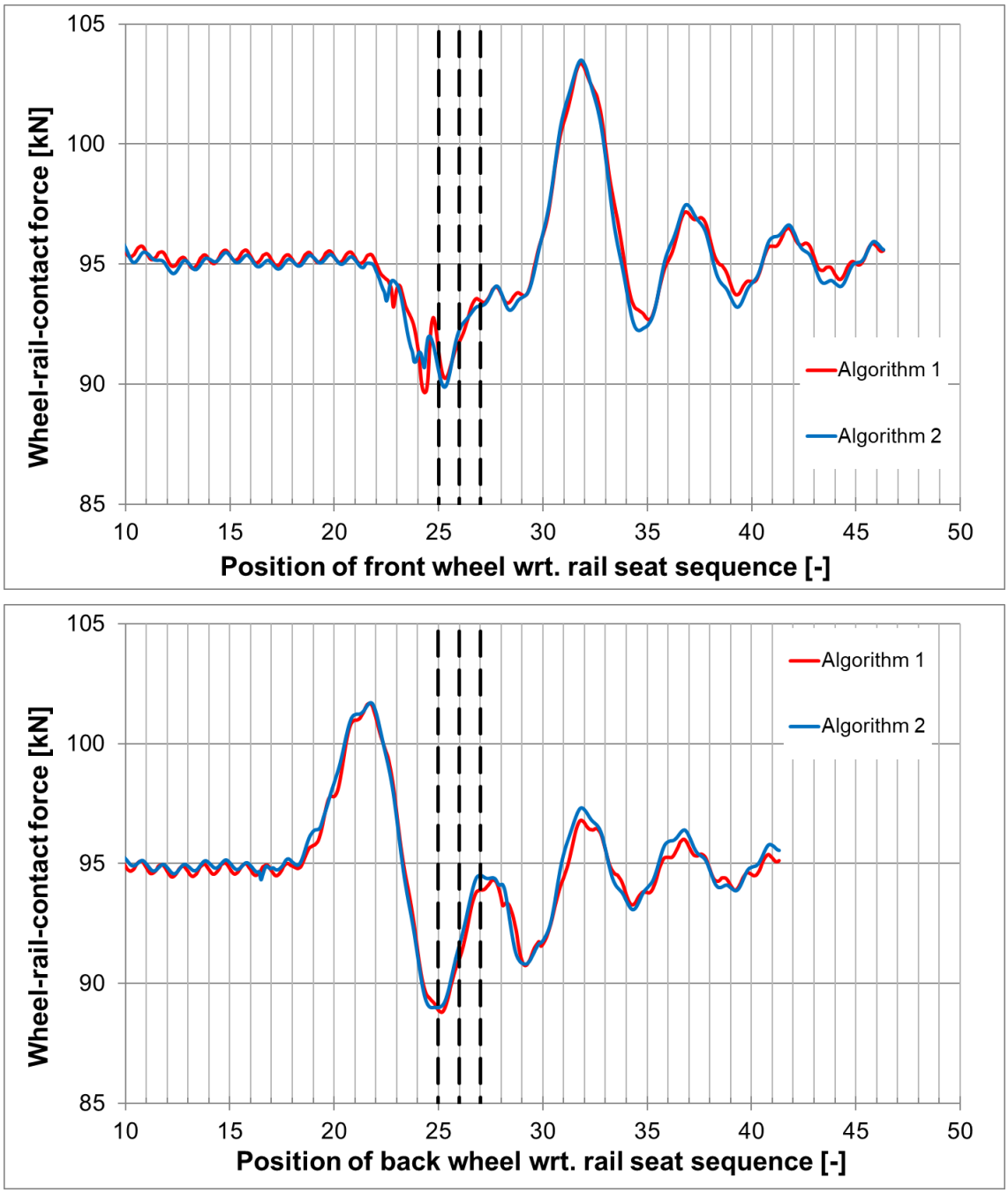

Figure 3-12: Wheel-rail contact force, top: front wheel, bottom: back wheel, dash lines indicate the position of the three rail seats with under sleeper gap

The existence of under-sleeper gap reduces the track stiffness at the affected rail seats and at several adjacent rail seats. As demonstrated in Figure 3-12, the front wheel moves downwards when it reaches the 23rd rail seat, which leads to a decrease of contact force between the front wheel and the rail. Besides, a similar coupling effect between the two wheels as in Figure 3-7 and in Figure 3-8 can also be observed. For example, when WRC force at the front wheel decreases at the rail seats with under sleeper gap, the WRC force at the back wheel increases due to the redistribution of the vehicle self-weight. Maximal dynamic factor during the whole train run is determined as 1.08.

Sleeper deflection at three selected rail seats, 25th, 26th and 31st rail seat, are compared with each other in Figure 3-13. The amplitude of the under-sleeper gap at the three selected rail seats is 1 mm, 2 mm, and 0 mm, respectively, as indicated by the horizontal dash lines in Figure 3-13. The influence of under-sleeper gap on the deflection behaviour of sleepers can be observed. Compared to the rail deflection at the 31st rail seat, the increase of the total deflection of sleepers due to under-sleeper gap at the 25th and 26th rail seat can be noticed. For those sleepers that are not fully supported, the total sleeper deflection has two components: the component due to the under-sleeper gap and the component due to the stiffness of sleeper supporting layer. This can be observed in Figure 3-13, when the sleeper deflection exceeds the amplitude of the under-sleeper gap, the gradient of sleeper deflection decreases, because the sleeper is then in contact with the supporting layer and the resistance to deflection increases consequently. The elastic part of sleeper deflection at the 31st rail seat, corresponding to the total sleeper deflection is 1.44 mm. The elastic part of sleeper deflection at the 25th and 26th rail seat is determined as 1.31 mm and 0.70 mm, respectively. The decrease of elastic part of sleeper deflection indicates the reduction of local stiffness and increased load on adjacent rail seats.

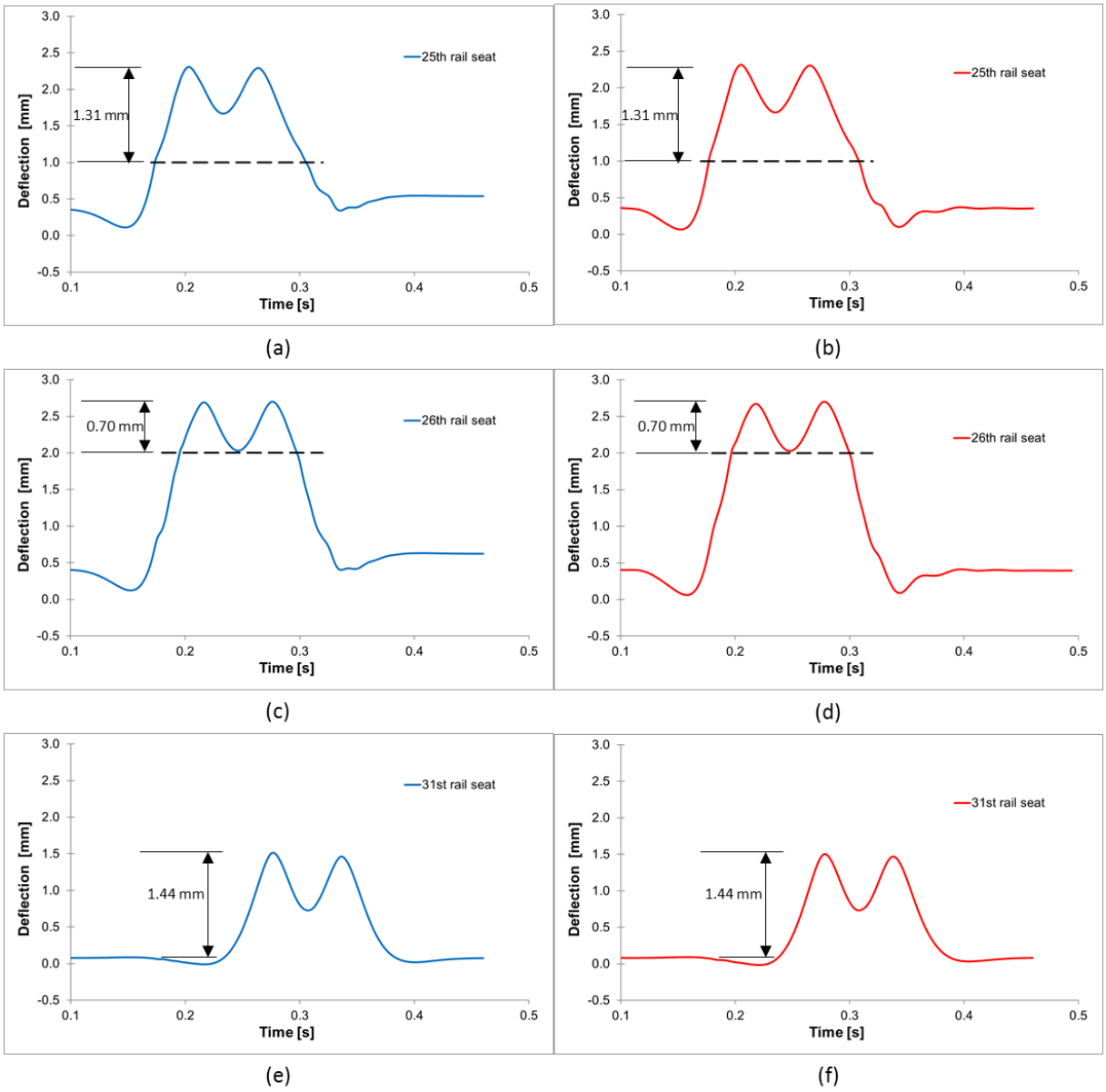

Figure 3-13: Determined sleeper deflection at 25th, 26th and 31st rail seat, left: using algorithm 1, right: using algorithm 2. Dash line indicates the amplitude of under-sleeper gap.

In this case, results from both the algorithms also fit well together. Moreover, the calculation time using algorithm1 is around one third of that using algorithm 2. No comparison calculation with the SIMPACK software is performed, since the huge demand on computation resource made it unfeasible.

3.4 Model validation using field measurement results

As next step, the numerical model is validated using field measurement results from two previous research projects documented in (D. Liu, Lechner, & Freudenstein, 2014). These two measurement activities have been performed following nearly identical measurement plans. To avoid repetitions the model calibration procedure is illustrated using one measurement series. For model validation using the second measurement series, only the results are presented.

3.4.1 Model validation using measurement results at bridge transition

The first field measurement has been performed along an earthwork-bridge transition. The field measurement has been performed in 2014 as a part of the European research project “SMART rail” (D. Liu et al., 2014). Static rail deflection under given wheel load has been measured along the section. More detailed description of the measurement section, measurement plan and measurement equipment can be found in (D. Liu et al., 2014).

Since the results are measured under quasi-static vehicle load, the vehicle in the model is simplified as a moving, constant load, corresponding to static wheel force of 95 kN. The sketch of the employed model is demonstrated in Figure 3-14.

Total length of the track model is 40.2 m, corresponding to 68 rail seats. The first 3.6 m is employed to eliminate the influence of the boundary effect, followed by a 24.6-meter-long track section on subgrade. The support distance of the one-span bridge deck is 12 m. The rail seat at 3.6 m is designated as the 1st rail seat. The bridge deck support is at the 42nd rail seat.
Along the whole section, the track superstructure remained unchanged. It was therefore assumed that the track stiffness variation was only caused by the variation of the subgrade/substructure bedding modulus, since no variation of superstructure elements were observed along the whole section. Besides, the subgrade/substructure was modelled as linear springs. The potential existence of under sleeper gap was not considered. The parameter of track superstructure along the measurement section is concluded in Table 3-4. Other unlisted track parameters are cited from Appendix 3-3.

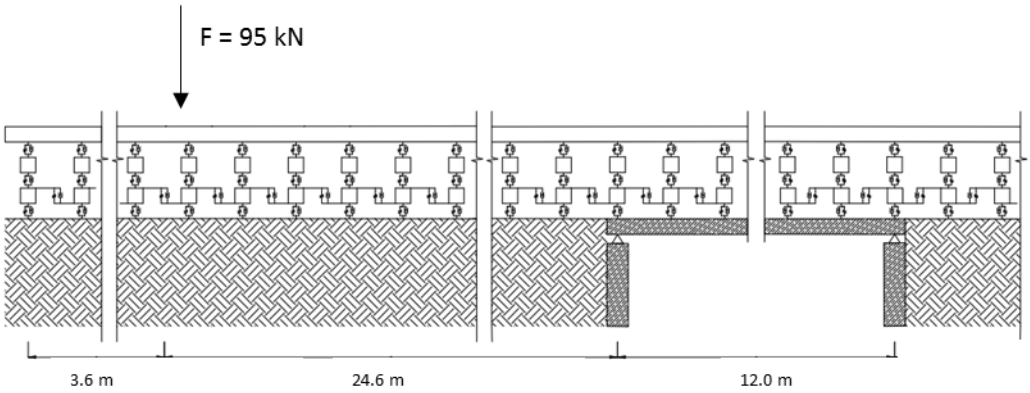

Figure 3-14: Overview of the model for calibration, not to scale

Table 3-4: Component of track superstructure, cited from (D. Liu et al., 2014)

Item	Value
Rail	
Profile	60E1
Fastening system	
Pad stiffness [kN/mm]	200
Sleeper	
Type	B 70
Length [mm]	2600
Weight [kg]	300
Sleeper spacing [mm]	600
Ballast	
E-modulus [N/mm²]	150
Thickness [mm]	300

Since rail deflection at one rail seat is not only influenced by its own supporting stiffness, but also influenced by the stiffness of adjacent rail seats, iteration is needed to determine the subgrade bedding modulus based on the measured static rail deflection. The iteration process is graphically illustrated in Figure 3-15, which was firstly proposed by (D. Liu, 2015).

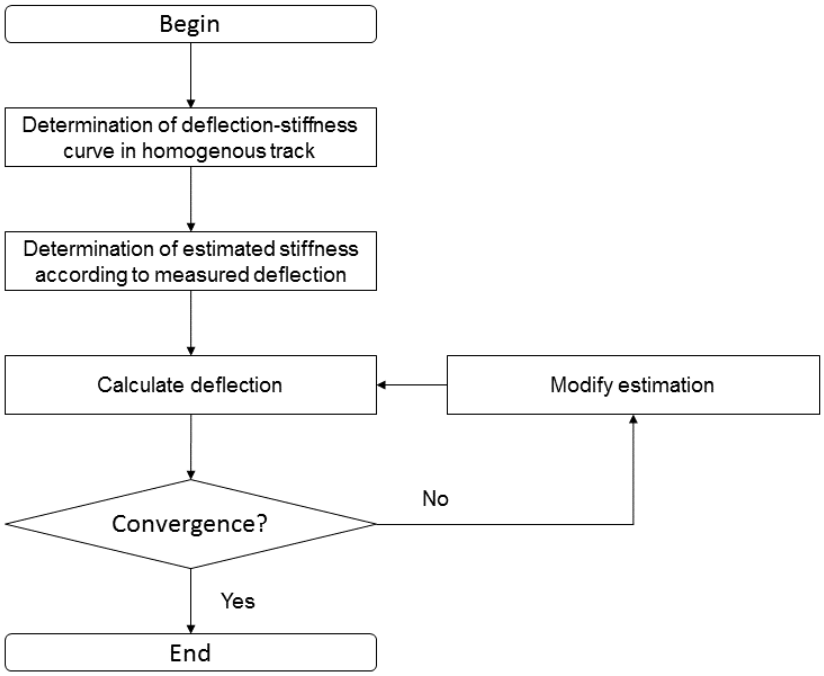

Figure 3-15: Work flow of the iteration process based on (D. Liu, 2015)

The key step of the iteration process is how to modify the estimated subgrade bedding modulus for each rail seat support based on the variance between the calculated and the measured rail deflection. Here in this research, the subgrade bedding modulus for individual rail seat support is determined based on the algorithm proposed in (Chen & Lechner, 2018) as follows:

The subgrade bedding modulus at position i at iteration step $t+1$, designated as $k_{i,t+1}$, is predicted based on the value of iteration step t and the difference between the calculated rail deflection at iteration step t, designated as $s_{i,t}$, and the target rail deflection from measurement $s_{i,tar}$ as:

$$\mathrm{k_{i,t+1}} = \mathrm{k_{i,t}} * (\frac{\mathrm{s_{i,t}} - \mathrm{s_{i,tar}}}{\mathrm{s_{i,t}}})^2 \qquad (8)$$

with

i : rail seat sequence

t : iteration step

$\mathrm{k_{i,t}}$: subgrade bedding modulus of rail seat i determined at iteration step t, $[\mathrm{N/m^3}]$

$\mathrm{k_{i,t+1}}$: subgrade bedding modulus of rail seat i predicted at iteration step $\mathrm{t}+1$, $[\mathrm{N/m^3}]$

$\mathrm{s_{i,t}}$: calculated rail deflection of rail seat i at iteration step t, $[\mathrm{mm}]$

$s_{i,tar}$: target rail deflection from measurement results, [mm]

Compared to (D. Liu, 2015), the calculation speed here is increased significantly. The main reason contributing to the reduction of calculation time is that the track in this research is modelled as combination of 1-D beam elements, rigid bodies and springs instead of 3-D volume elements in (D. Liu, 2015). As proved by the calculation results below, the accuracy is not harmed.

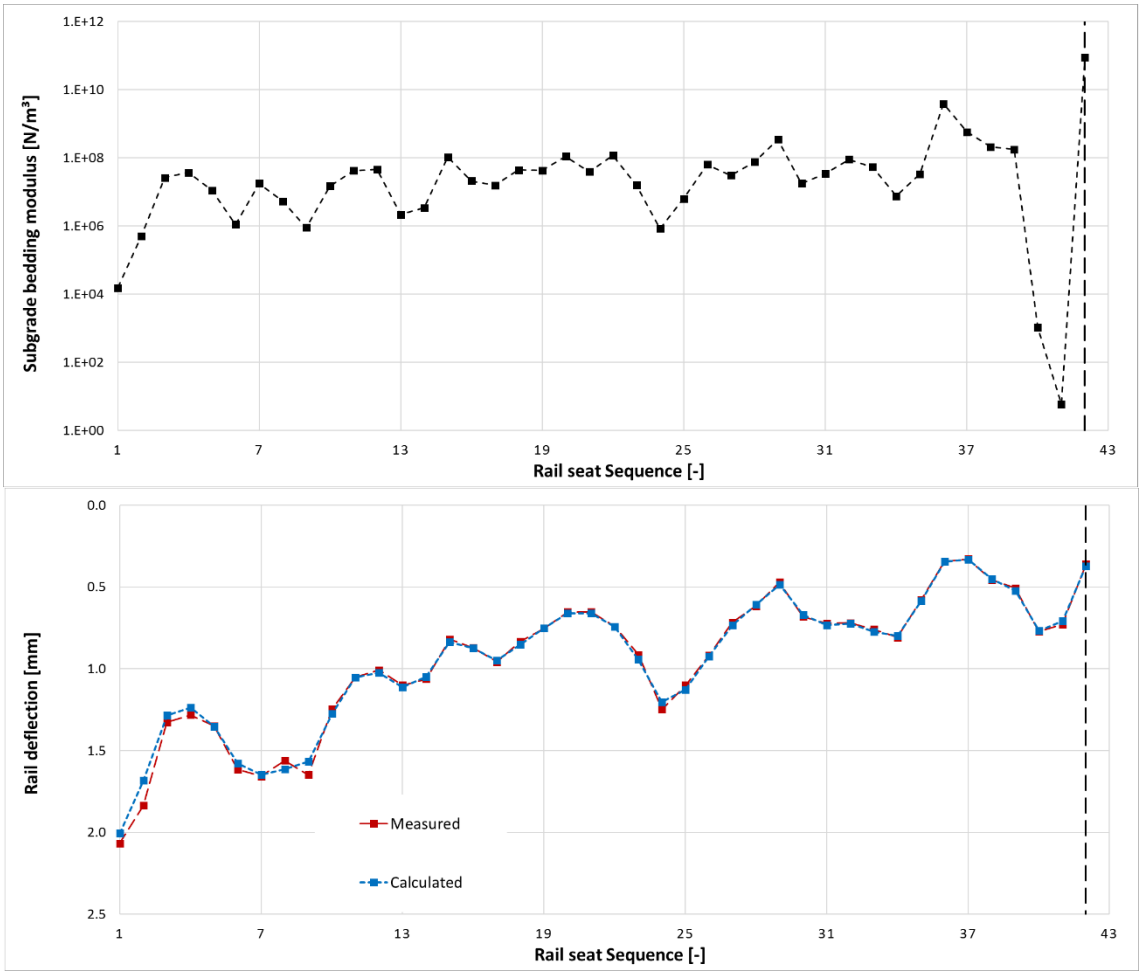

Figure 3-16: Results of model validation case 1, top: inhomogeneous track support stiffness determined using proposed iteration method, bottom: comparison of measured and calculated rail deflection. The dash line indicates the position of bridge abutment

The iteration converges after 50 iteration steps. The inhomogeneous track support stiffness determined using the proposed iteration method is shown in Figure 3-16. The vertical dash line at the 42nd rail seat indicates the position of bridge abutment. As could be expected, the determined bedding modulus there is also much higher than the rail seat in open track. In

contrast, determined subgrade bedding modulus at 40th and 41st rail seat are extremely low compared to other rail seats, which indicates the existence of under-sleeper gap there at the entrance of bridge, which has been observed in previous research (Nicks, 2009).

The calculated static rail deflection using the determined track support stiffness is compared with the measured rail deflection in Figure 3-16, which shows good accordance.

3.4.2 Model validation using measurement results at Under-Ballast-Mat-subgrade transition

The second field measurement has been performed at an Under-Ballast-Mat (UBM)-subgrade transition. More detailed description of the measurement section, measurement plan as well as the measurement results can be found in (D. Liu, Lechner, & Freudenstein, 2012).

As in previous case, constant wheel load is used for calculation. UBM is modelled as springs connected with the springs modelling the subgrade in serial.

The model is validated following a similar process as described in Chapter 3.4.1. Determined subgrade bedding modulus and comparison of the measured and calculated static rail deflection are demonstrated in Figure 3-17. Determined bedding modulus in section with UBM is lower as in section without UBM as expected. Directly near the boundary between two sections, from 39th rail seat to 41st rail seat, gradually changing bedding modulus is observed due to the influence of adjacent rail seats.

The lower bedding modulus determined at 41st, 42nd and 43rd rail seat indicates the sleepers are not fully supported.

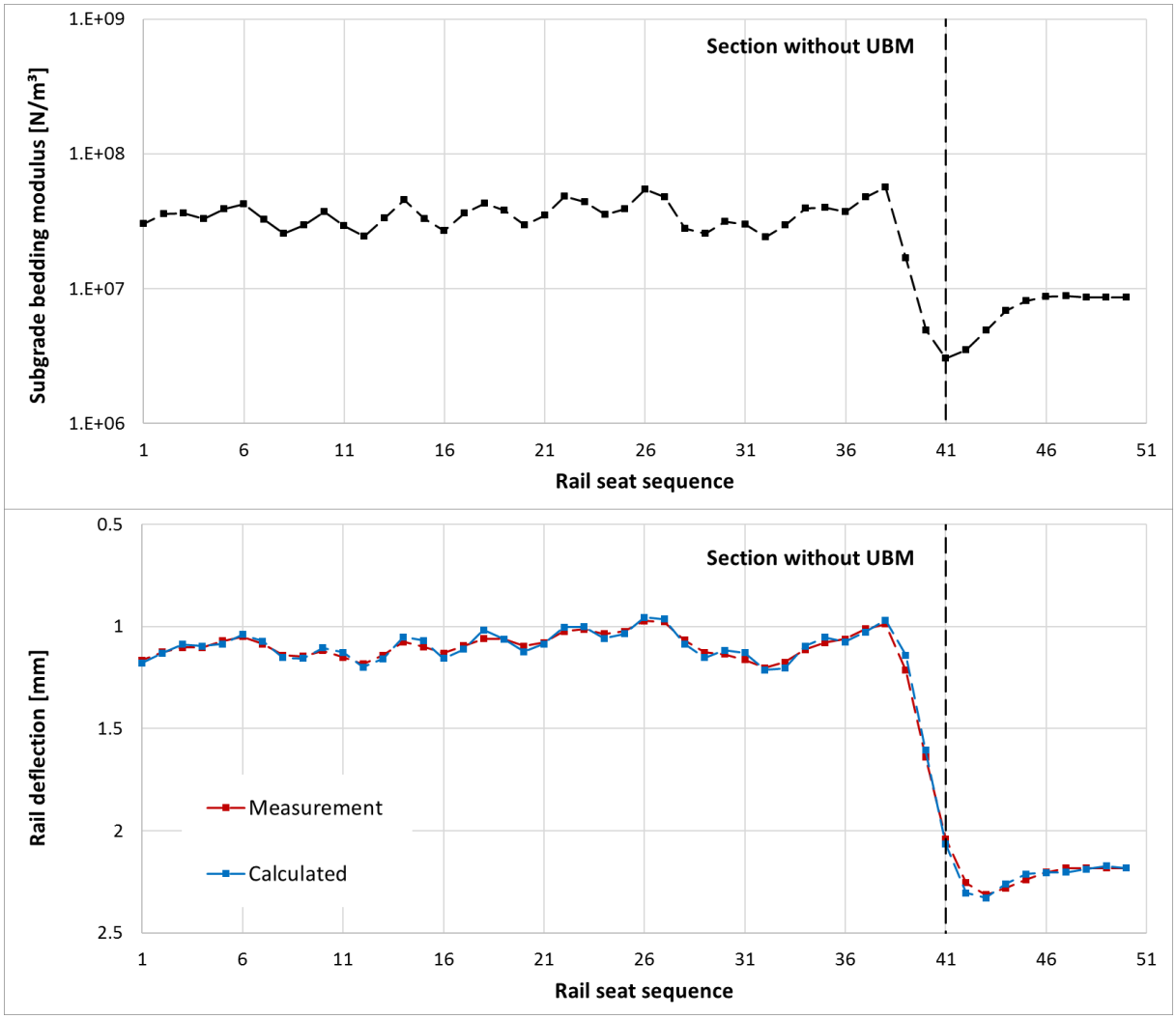

Figure 3-17: Results of model validation case 2, top: track support stiffness determined using the proposed iteration method, bottom: comparison of the measured and calculated rail deflection. The dash line indicates the position of the transition.

In this case, the numerical model is also well validated.

4. Ballast settlement law

In this chapter, existing settlement laws are reviewed and compared to select a proper way to describe ballast settlement.

4.1 Selection of ballast settlement model

In (Dietrich, 1978; Hettler, 1984), ballast settlement is supposed to be a function of the settlement after the first load cycle and number of load cycles, as illustrated in formula (9):

$$u_N = u_1(1 + c \times ln(N)) \qquad (9)$$

with

u_1 : settlement after the first load cycle [mm]

c : constant parameter [-]

N : load cycle [-]

u_N : total settlement after load cycle N [mm]

The disadvantage of this method is that it cannot describe the ballast settlement under the load cycles with varying load amplitude. Therefore, it could not be used to describe ballast settlement accurately, considering the interaction between ballast settlement (which leads to a change in track geometry) and vehicle-track interaction.

A better approach is to model ballast settlement with respect to ballast pressure. Typically, a power function relation between the pressure on ballast and ballast settlement is assumed. As for the relationship between the ballast settlement and the number of load cycles, three typical approaches are listed in the next few pages that use the linear function (Sato, 1995), logarithm function (Demharter, 1982) and cumulative histogram (Varandas et al., 2010), respectively.

In (Dahlberg, 2001), the following formula has been proposed based on linear regression of the measurement data in (Sato, 1995):

$$y = 4.365 \times 10^{-12} P^{5.276} \tag{10}$$

with

P : force on ballast surface [kN]

y : track settlement increment per load cycle [mm/10,000 cycles]

In (Demharter, 1982), based on the laboratory tests and the field measurement results, ballast settlement is determined as the function of load cycles and ballast pressure as follows:

$$\begin{aligned}
N < 10^4 \quad & \text{optimal case:} && \Delta s_{opt} = 1.57 \cdot p \cdot ln\frac{N_1}{N_2} \\
& \text{pessimistic case:} && \Delta s_{pess} = 2.33 \cdot p \cdot ln\frac{N_1}{N_2} \\
& \text{neutral case:} && \Delta s_{mittel} = 1.89 \cdot p \cdot ln\frac{N_1}{N_2} \\
N \geq 10^4 \quad & \text{optimal case:} && \Delta s_{opt} = 3.04 \cdot p^{1.21} \cdot ln\frac{N_1}{N_2} \\
& \text{pessimistic case:} && \Delta s_{pess} = 15.2 \cdot p^{1.21} \cdot ln\frac{N_1}{N_2} \\
& \text{neutral case:} && \Delta s_{mittel} = 5.15 \cdot p^{1.21} \cdot ln\frac{N_1}{N_2}
\end{aligned} \tag{11}$$

with

N_1, N_2 : number of load cycles [-]

Δs : settlement increment between load cycle N_1 and N_2, [mm]

p : pressure on ballast layer [N/mm^2]

The reason why a series of settlement laws instead of one formula has been proposed is due to the diversity of ballast settlement observed in repeated tests. Even though the test conditions at beginning of the test and during the test procedures have been carefully controlled to make them as identical as possible, Demharter has found that ballast settlement behaviour is not the same when performing test repetitions.

In (Varandas et al., 2010), a settlement model is presented as in (12):

$$u_{p.N} = \frac{\gamma}{M_{\alpha\beta}} \int_0^{\overline{F}_N} F^{\alpha} \left(\frac{1}{h(F,N)+1}\right)^{\beta} dF \tag{12}$$

with

$u_{p.N}$: The settlement produced during load cycle N, [mm]

α: 1st parameter of the settlement law, see the explanation below [-]

β: 2nd parameter of the settlement law, see the explanation below [-]

γ: 3rd parameter of the settlement law, see the explanation below [mm]

$\overline{F}_N$: Amplitude of load acting on ballast layer surface [kN]

$h(F,N)$: Inverted cumulative histogram of load [-]

$M_{\alpha\beta}$: Normalizing parameter [-], determined as in (13)

$$M_{\alpha\beta} = \frac{{F_0}^{(\alpha+1)}}{\alpha+1} \sum_{n=1}^{N_0} \left(\frac{1}{n}\right)^{\beta} \tag{13}$$

with

F_0 : Reference loading amplitude [kN]

N_0: Reference number of load cycles [-]

The parameter α is the coefficient of the power function between the amplitude of load and settlement. The parameter β describes the relationship between the number of load cycles and settlement. The parameter γ describes the intrinsic settlement ability of the ballast, which is influenced by the mechanical properties of the ballast, foundation type, sleeper type and so on. The normalizing parameter $M_{\alpha\beta}$ is derived so that the parameter γ equals the total settlement after N_0 load cycles, assuming a constant loading amplitude of F_0 with a given α and β.

By introducing the concept of the cumulative histogram, this model could reflect the influence of load history on ballast settlement. To illustrate the difference among these three settlement models, they are compared with one another below based on laboratory measurement results documented in (Varandas et al., 2010)).

For this purpose, two load paths, Load Path 1 and Load Path 4 described in (Varandas et al., 2010) Fig. 5 as shown in Figure 4-1 (a) and (b), are employed. When comparing Load Path 1 and Load Path 4, it can be observed that only the load sequence changes. Curve (c), (d) and

(e) in Figure 4-1 demonstrates the calculation results following the three settlement models. Curve (c) was already validated with laboratory measurement results (see (Varandas et al., 2010)).

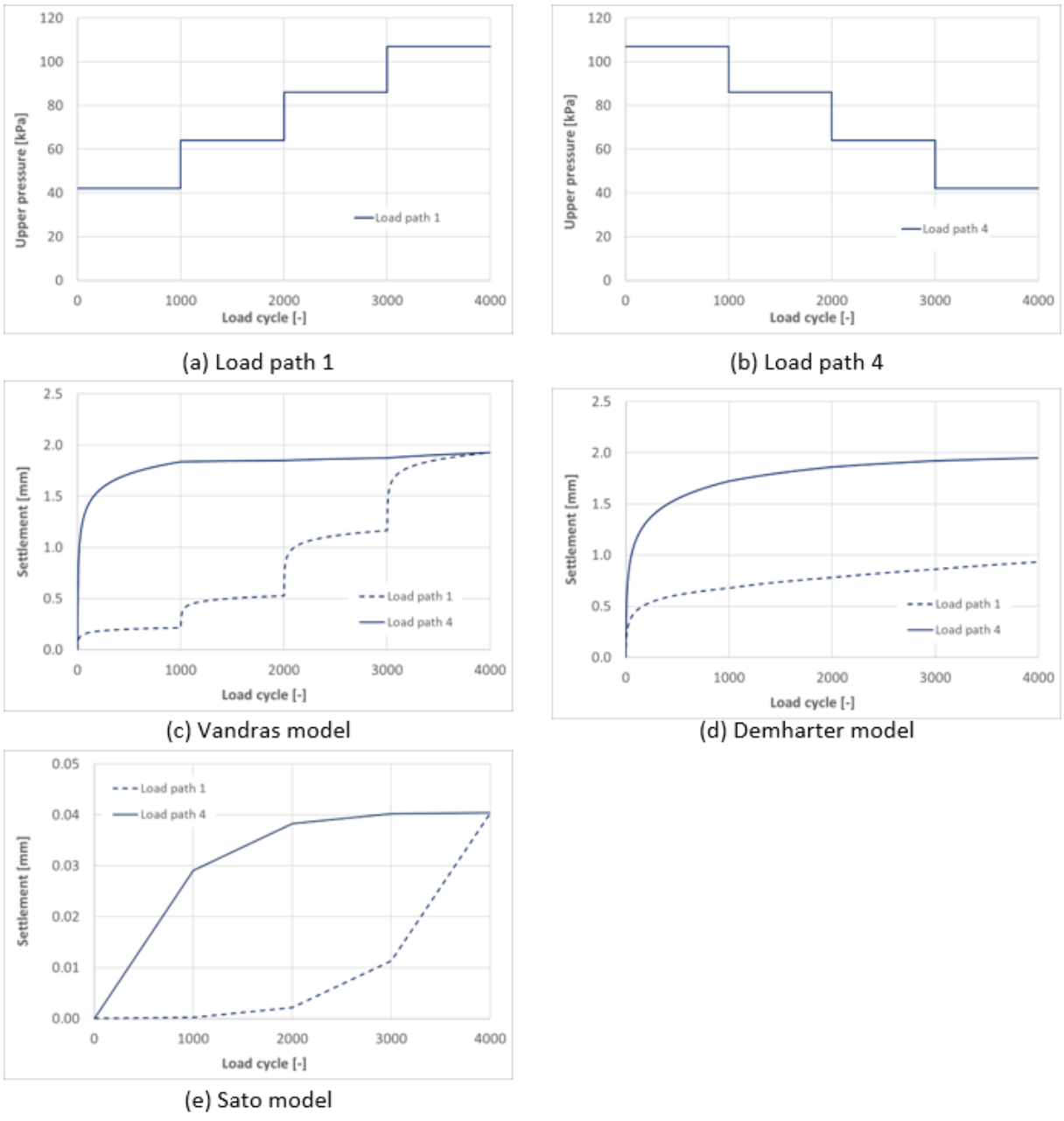

Figure 4-1: Comparison of results from three settlement models: I: Demharter Model; II: Sato model; III: Varandas model

First, one can observe that the finale settlement in Curve (e) is much smaller than in Curves (c) and (d). This can be explained by the employed settlement law, which maintains that a

sleeper-ballast pressure of below approximately 125 kPa causes nearly no settlement. Therefore, it is not suitable to describe the ballast settlement in this laboratory test. Since the data have been collected from old operation lines in Japan, one could infer that this law might be aimed to describe track that has experienced a long load history. It therefore underestimates the settlement of a new line.

The second observation is that in both curve (c) and (e), the final amplitude of settlement is not influenced by the load sequence, but the total settlement in (d) after Load Path 1 is smaller than in Load Path 4. The reason is that the item $\ln(N_1/N_2)$ in formular (11) decreases with the increase of load cycles numbers. Consequently, load with large amplitude introduced earlier leads to a greater settlement than when it is introduced later. This contradicts the experimental results in (Varandas et al., 2010).

When load increases, the settlement also increases rapidly. The introduction of a load cycle with an amplitude that is lower than the previous load leads to nearly no settlement. This has also been confirmed in (Shenton, 1985) and in (Diyaljee, 1987). Curve (c) and curve (d) can both simulate this effect.

Based on above comparison, the Varandas model ((12) and (13)) is used in further study.

4.2 Verification of the settlement law

In (Varandas et al., 2013), the model parameters were determined based on measurement results that were collected in the Netherlands, which are recorded in (Coelho et al., 2011) and summarised in Table 4-1.

Table 4-1: The parameters of the settlement law determined in (Varandas et al., 2013)

Section	Fitted parameters of the settlement law (12)				
	F_0 [kN]	N_0 [−]	α [−]	β [−]	γ [mm]
Embankment before and after the culvert	50	1x10^5	0.6	0.82	12.5 ~ 20.0
On top of the Culvert					4.5 ~ 6.0

As illustrated in Chapter 4.1, the parameters α and β were not influenced by the stiffness of the ballast support layer, so they remain the same in all sections. In contrast, the fitted γ value on the culvert was lower in comparison to the value on the earthwork. This corresponds to the conclusion drawn by several previous researchers: weaker ballast support leads to larger ballast settlement (Holtzendorff, 2003; Kumar et al., 2019; Raymond & Richard, 1987; Sol-Sánchez et al., 2016; Sol-Sánchez, Thom, Moreno-Navarro, Rubio-Gámez, & Airey, 2015), and, therefore, a higher γ value in this case. A possible reason for greater ballast settlement is that the low support stiffness allows more movement of ballast particles. As stated in (Coelho et al., 2011), the earthwork of the measured section lies on soft peat soil. One could infer that γ for ballast on normal subgrade will be lower than the determined values for earthwork in table 4-1.

The γ value for ballast on normal subgrade is determined based on measurement results documented in other literature. In (Henn, 1978) and (Demharter, 1982), field measurements along in-service track and laboratory measurements were taken. Demharter has conducted the laboratory test as follows: a 30 cm ballast bed was built above a 30 cm frost protection layer (FPL), providing a high deformation modulus of 250 MPa. 0.5 million load cycles with an upper pressure of 0.2 N/mm² were firstly introduced, followed by another 0.3 million load cycles with an upper pressure of 0.3 N/mm². The contact area was designed as 2826 cm², which equals half of the contact area of a B70 sleeper. The max. sleeper-ballast force in the two phases, which could be calculated from the pressure on the ballast and the contact area, amounted to 56.5 kN and 84.8 kN, respectively. Significance variance was observed among parallel tests. As mentioned in Chapter 4.1, Demharter has concluded that the variance could not be eliminated even though all starting conditions were controlled carefully. The range of measurement results from the six repetition is demonstrated in Figure 4-2.

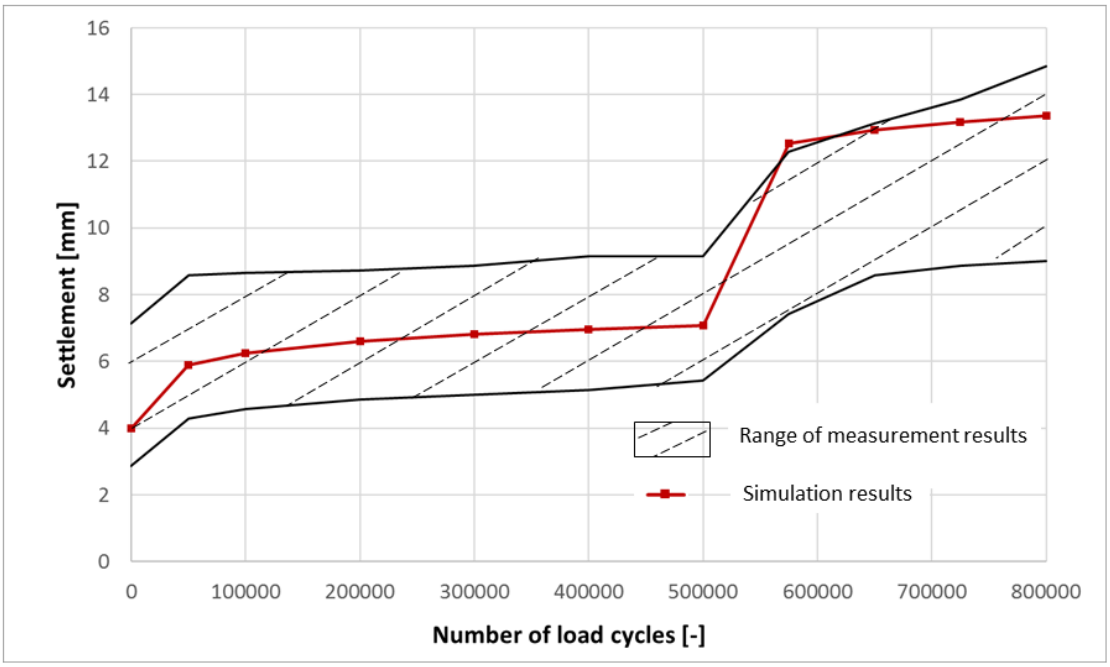

Figure 4-2: Comparison of laboratory measurement result in (Demharter, 1982) and simulated results.

The parameters listed in Table 4-2 are determined by fitting the curve using the Varandas model. The simulated settlement curve is also demonstrated in Figure 4-2, which lies in the range of the measurement result.

Table 4-2: Determined parameters of Varandas model acc. to measurement result in Figure 4-2

F_0 $[kN]$	N_0 $[-]$	α $[-]$	β $[-]$	γ $[mm]$
50	1x10^5	0.6	0.82	5

In (Demharter, 1982), Demharter has also compared the measurement results in laboratory with in in-situ track lines. He has found that settlement in a mixed traffic line is nearly two times higher than that in the laboratory test. Demharter explained the cause of this phenomenon as the excitations that could not be considered in laboratory tests, such as flat wheel and so on.

Consequently, γ used for in-service track is set as 10 [mm] in calculations in following chapters. This also fits the suggested value in (Varandas et al., 2010).

4.3 Conclusion

In conclusion, track settlement under the influence of load amplitude, load history and number of load cycles can be modelled using Formula (12). Moreover, the parameter γ in this formula is strongly influenced by the ballast-supporting stiffness. Based on measurement results, the parameters listed in Table 4-3 are determined and used for further calculation.

Table 4-3: Parameters of the settlement law (12) depending on ballast supporting stiffness

Ballast supporting stiffness	$F_0\ [kN]$	$N_0\ [-]$	$\alpha\ [-]$	$\beta\ [-]$	$\gamma\ [mm]$
Stiff supporting					5
Normal supporting	50	$1x10^5$	0.6	0.82	10
Soft supporting					15

5. Investigation of the ballastless-ballasted-track-transition in short-term view

5.1 Standard transition design

According to BetonKalender 2015 (Freudenstein et al., 2015), DB regulation Ril. 820.2020 (DB Netz AG, 2018) and the standard DIN EN 16432-2:2017-10 (Deutsches Institut für Normung e. V., 2017), following countermeasures should be taken at the transition between a ballastless track and a ballasted track:

- Hydraulically bonded layer (HBL) should be extended for 10 meters to the ballasted track.
- Auxiliary rails with a total length of 20 meters should be implemented. 5 meters of the auxiliary rails should be in the ballastless track, and 15 meters of it should be in the ballasted track.
- Ballast should be glued for 45 meters. In the first 15 meters directly after the ballastless track, the ballast under sleepers, the ballast at sleeper shoulder and the ballast between sleepers should all be glued. In the following 15 meters, the ballast under sleepers and the ballast at sleeper shoulder should be glued. In the last 15 meters, only the ballast under sleepers should be glued.
- The rail seat stiffness should increase gradually in at least three steps from ballastless track to ballasted track. One common design plan is to synchronize the change of rail seat stiffness with glued ballast. It is suggested in BetonKalender 2015 (Freudenstein et al., 2015) as following: in the first 15 meters next to ballastless track, the rail seat stiffness is 27 kN/mm. In the next 15 meters, the rail seat stiffness is 40 kN/mm. In the last 15 meters, the rail seat stiffness is 60 kN/mm.

Besides, in DIN EN 16432-2:2017-10 (Deutsches Institut für Normung e. V., 2017), it is required that the difference of design track deflection between each two subsections of the transition should not exceed 0.5 mm for high-speed lines. It also requires that the length of the transition should be determined based on design speed (see formular (1)).

Standard transition design is graphically demonstrated in Figure 5-1.

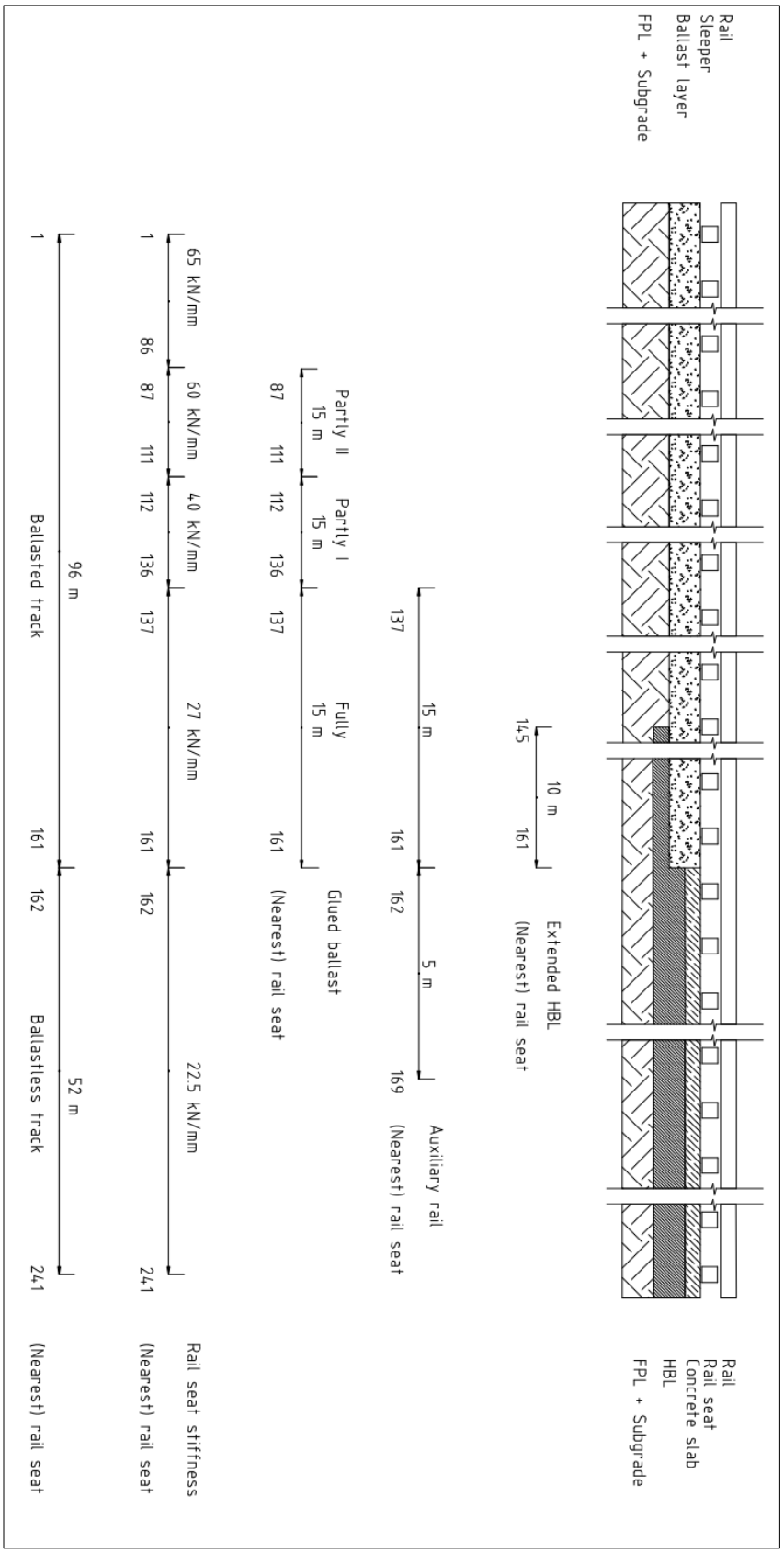

Figure 5-1: Standard design of a ballasted-track-ballastless-track-transition based on BetonKalender 2015 (Freudenstein et al., 2015), not to scale

The static rail seat stiffness of the ballastless track is set as 22.5 kN/mm as required in DB regulation Ril. 820.2020 (DB Netz AG, 2018). The stiffness of rail pad used in the open track section of the ballasted track is set as 65 kN/mm as in typical design of modern high-speed lines (Esveld, 2001). In this chapter, the short-term effect of this standard design is investigated.

5.2 Set up of the numerical model

The vehicle-track interaction model is built as proposed in chapter 3.1. Total length of the track is 148 m, corresponding to 241 rail seats. The first subsection of the track is 96-meter-long ballasted track that consists of 161 rail seats with rail seat distance of 0.6 m. The second subsection is 52-meter-long ballastless track consists of 80 rail seats with rail seat distance of 0.65 m. Track transition locates between the 161st and the 162nd rail seat.

All layers below the ballast layer in the ballasted track are modelled as one layer with an equivalent bedding modulus. The equivalent bedding modulus in open track is read from Table 3-1 as 0.10 N/mm³ (subgrade in good condition). The equivalent bedding modulus of the section with the extended HBL can be determined according to multi-layer theory proposed in the lecture note of Concrete Pavement System (Freudenstein, 2020a) as follows:

$$k = \frac{E_2}{0.9 \cdot h_1 \cdot \sqrt[3]{\frac{E_1}{E_2}}} \tag{14}$$

With

k: equivalent bedding modulus of the section with the extended HBL $[\mathrm{N/mm^3}]$

E_1: E-module of HBL $[\mathrm{N/mm^2}]$, empirical value: $10000\ \mathrm{N/mm^2}$

E_2: E-module of frost protection layer and subgrade $[\mathrm{N/mm^2}]$, empirical value: $100\ \mathrm{N/mm^2}$

h_1: Thickness of the extended HBL, empirical value: 150 mm.

It can be determined accordingly that the equivalent bedding modulus of the section with extended HBL increases from 0.10 N/mm³ to 0.16 N/mm³.

The profile of the auxiliary rails is 60 E1, which is the same as the main rails. Based on practical experience, the rail tension clamp SKL 14 is chosen for main rails in the ballasted track, SKL 15 for main rails in the ballastless track, while SKL 24 together with rail pad 687 (static stiffness of 400 kN/mm (Gramowski, 2013)) are used for auxiliary rails. The rail pad stiffness is shown in Figure 5-1. The load-deformation-curve of these three rail tension clamps under tension are plotted below in Figure 5-2. In the praxis, rail tension clamp is usually so installed that a 2 mm gap remains between the rail foot and the middle ring of the rail tension clamp.

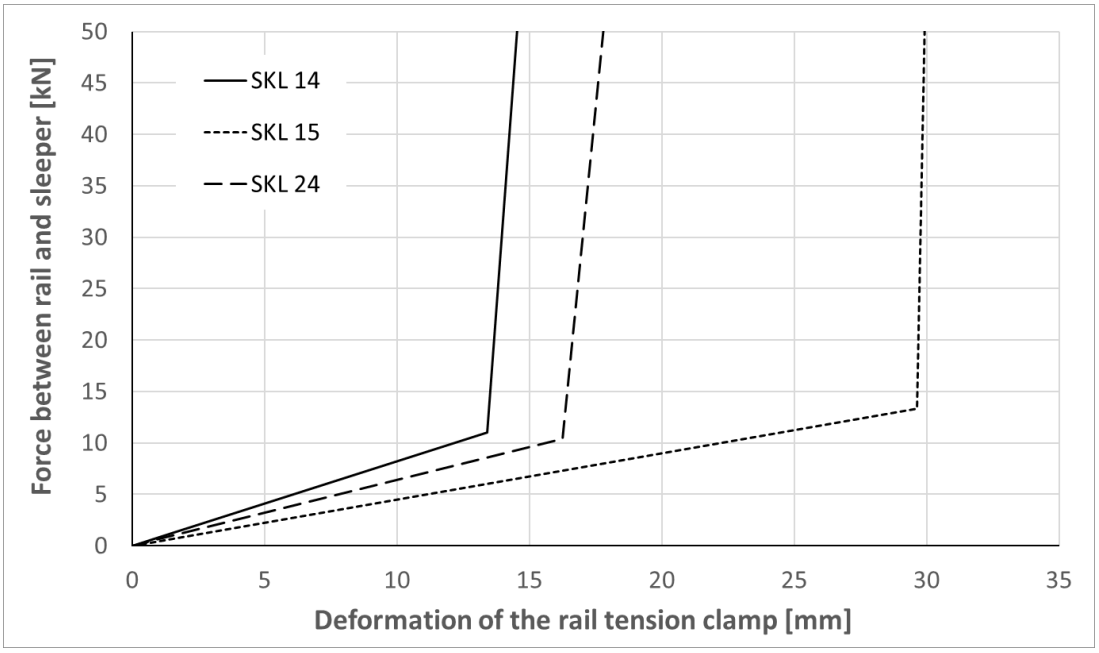

Figure 5-2: Force-deformation curves of SKL 14, SKL 15 and SKL 24

If the research focuses on the rail seat deflection under traffic load, it is sufficient to only consider rail pad stiffness according to Zimmermann's theory (Freudenstein, 2020b). When a rail seat is under compression, the influence of rail tension clamp can be neglected, and the stiffness of rail pad plays the dominant role. Therefore, in following calculation, instead of using the non-linear model, the stiffness of rail fastening systems for main rails is set as constant and equals to the corresponding rail pad stiffness. In this way, the calculation time can be significantly reduced.

Nevertheless, the working mechanism of auxiliary rail is different from main rail. It is not directly subjected to the traffic load. Instead, the auxiliary rail is pulled down by the rail tension clamp when sleepers move downwards under traffic load. Therefore, the non-linear characteristic of its rail tension clamp should be considered.

In (Keene, Edil, Fratta, & Tinjum, 2013), Keene et al. has studied the influence of polyurethane stabilized ballast on track modulus. They reported that after polyurethane stabilized the track modulus has only increased insignificantly. Similar conclusion has also been drawn in (Gundavaram & Hussaini, 2019). Therefore, it is assumed in this investigation that the stiffness of ballast layer does not change after polyurethane stabilization.

The ballastless track is modelled in the way that the rail seats lie directly on a stiff supporting layer. The bedding modulus of the supporting layer is read from Table 3-1 as 0.30 N/mm³ (concrete).

Parameters for other track components are listed in Appendix 3.

5.3 Determination of static track stiffness

First, the static track stiffness following the standard design is determined as the quotient of the amplitude of static wheel load by the caused elastic rail deflection:

$$k_{track} = \frac{F}{s_F - s_0} \tag{15}$$

with

k_{track}: static track stiffness [kN/mm]

F: amplitude of static wheel load [kN]

s_F: rail deflection under wheel load and self-weight [mm]

s_0: rail deflection under track self-weight [mm]

In this calculation, a point load is used instead of the vehicle model as the external force on track for simplicity. The amplitude of the point load is set as 95.6 kN, corresponding to the wheel load of the passenger power car in Appendix 3-1. The calculation is performed in two steps: first, the track is brought to equilibrium under self-weight using the Module I of the MATLAB program proposed in chapter 2 to determine s_0. Then the track is brought to equilibrium under static wheel load and self-weight to determine s_F using the same Module of the MATLAB program. The determined elastic rail deflection and the calculated track stiffness are shown in Figure 5-3 and Figure 5-4 respectively. According to formula (15), static track stiffness is inversely proportional to track elastic deflection.

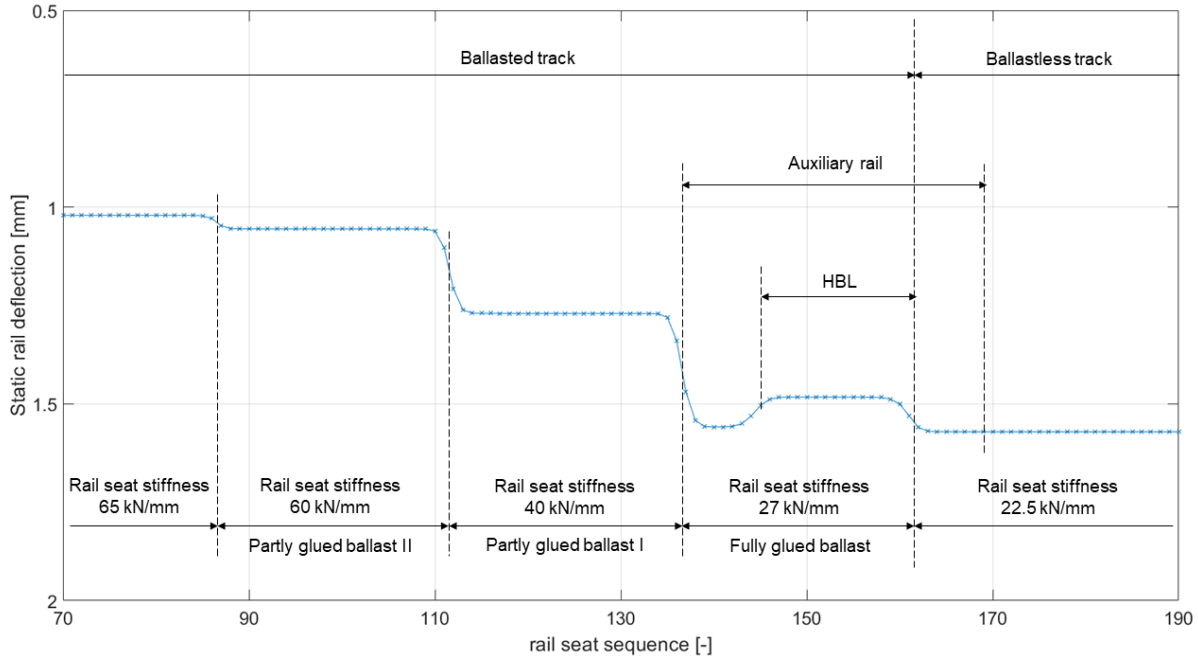

Figure 5-3: Determined static rail deflection of the track transition following standard design

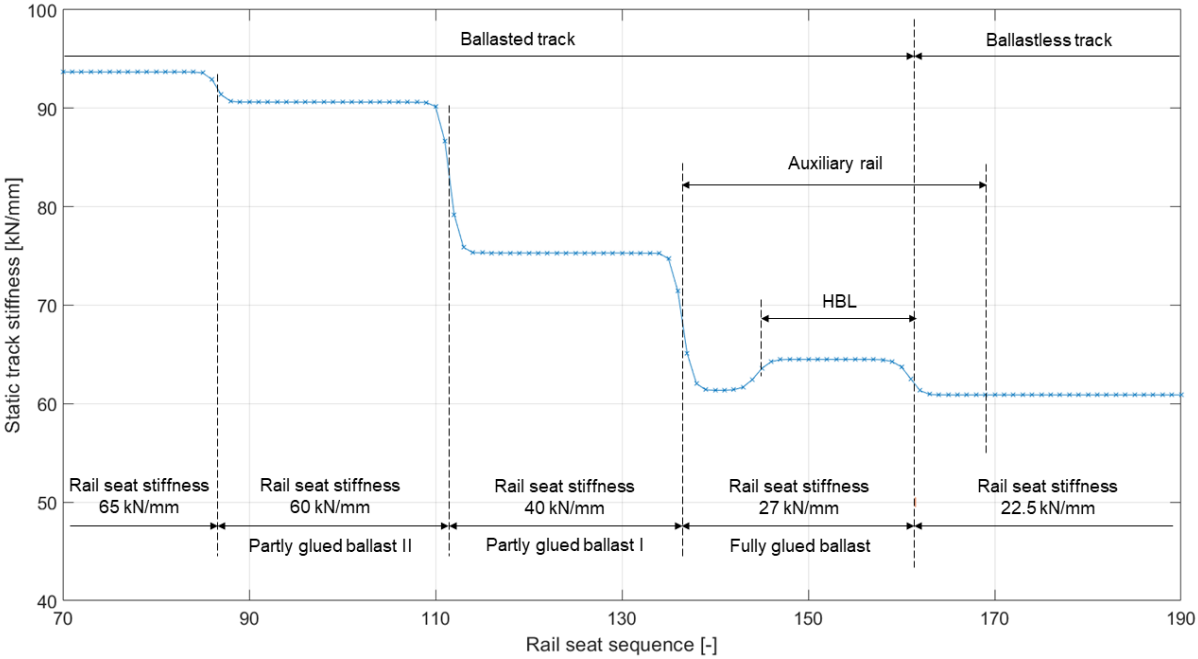

Figure 5-4: Calculated static track stiffness of the track transition following standard design

The designed static rail deflection at the ballastless track is 1.57 mm, while the designed static rail deflection at the ballasted track is 1.02 mm, corresponding to track stiffness of 60.9 kN/mm and 93.7 kN/mm, respectively. A quasi-continuous three-step change of track stiffness at the

transition is achieved: from 90.6 kN/mm to 75.3 kN/mm and finally to 61.7 kN/mm. It can also be observed that the extension of HBL causes an additional track stiffness discontinuity within the 1st subsection.

The requirement in DIN EN 16432-2:2017-10 (Deutsches Institut für Normung e. V., 2017) that the difference of track deflection between every two adjacent subsections does not exceed 0.5 mm is also met.

5.4 Investigation of dynamic effect

To evaluate the dynamic effect of the design proposed in Figure 5-1, the dynamic vehicle-track interaction along this section is calculated in this chapter. The investigation focuses on the influence of designed track stiffness on track transition behaviour, so the track irregularity not relevant with rail seat stiffness and uneven ballast settlement is excluded from the calculation.

First, dynamic vehicle-track interaction with following conditions is investigated:

- Vehicle type: passenger power car with nominal wheel load of 95.6 kN (see Appendix 3-1)
- Speed level: 300 km/h
- Travel direction: from the ballasted track to the ballastless track.

For simplicity, this calculation case is designated as ‘P-300-B-S’ following the name rule illustrated in Table 5-1.

Table 5-1: Name rule of calculation cases

Position 1: vehicle type	Position 2: speed	Position 3: travel direction	Position 4: Intervention
‘P’ for passenger power car, ‘G’ for freight wagon	Speed [km/h]	‘B’ for vehicle starting from ballasted track, ‘S’ for vehicle starting from ballastless track	‘S’ for standard design ‘N’ for no intervention

After setup of the model, the vehicle-track interaction model is firstly brought to static equilibrium using Modul I of the MATLAB program, before the dynamic calculation is performed using Modul II of the program. This step is essential to eliminate the oscillation at the beginning

of the dynamic calculation. To eliminate the influence of the boundary conditions, the starting position of the last wheelset of vehicle at the beginning of the calculation is 3.6 m ahead of the first rail seat, and the ending position of the first wheelset is 3.6 m beyond the last rail seat.

Figure 5-5 demonstrates the calculated dynamic wheel-rail contact (WRC) force between the four wheelsets and rail, which is plotted against the position of each wheelset with respect to rail seat sequence. In this case, the vehicle travels from the track with higher stiffness to lower stiffness (except for at the entrance of the HBL extension section). It can be observed that at the position of stiffness decrease, the dynamic WRC force firstly decreases and then increases. This tendency applies generally for all the four wheelsets. The maximal dynamic WRC force is determined as 98.1 kN, corresponding to a dynamic factor of 2.6%. The minimal dynamic wheel-rail contact force is determined as 93.1 kN, corresponding to a dynamic loss factor of 2.6%. Both the maximal and minimal values are observed near the stiffness discontinuity at the 137th rail seat.

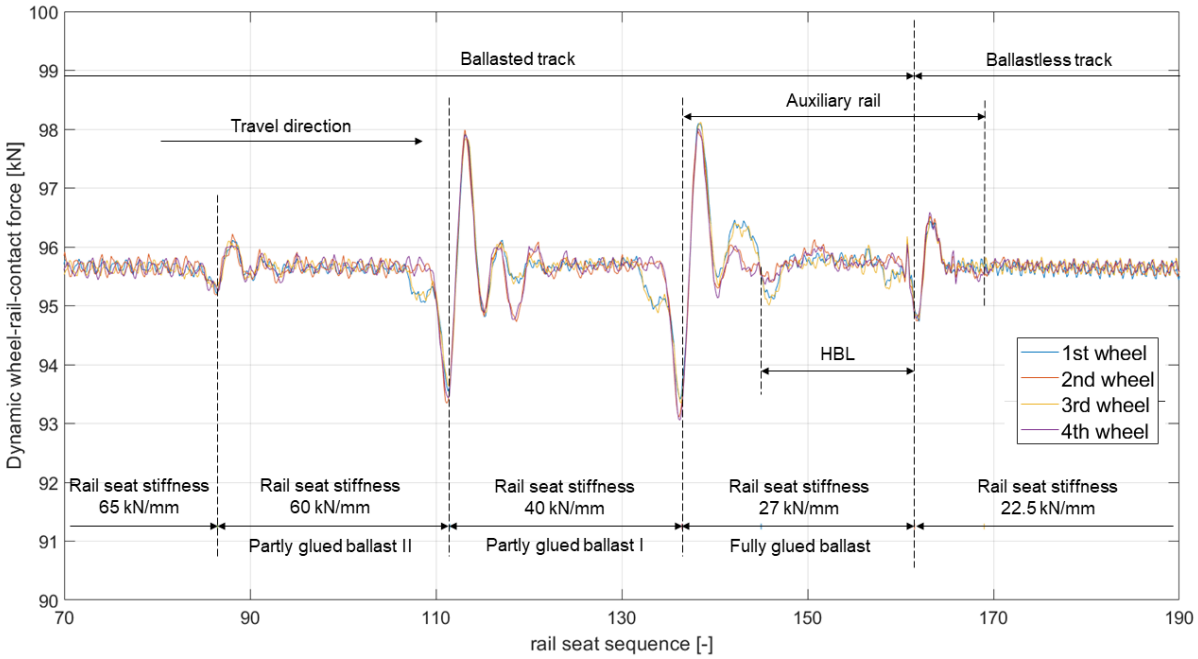

Figure 5-5: Determined dynamic wheel-rail contact force, case 'P-300-B-S'

It can also be observed that the contact force of the 1st wheelset and 3rd wheelset is slightly different from the 2nd and 4th wheelset, for example in the range between 106th rail seat and 109th rail seat, between 117th and 120th rail seat, between 131st and 135th rail seat, between

141st and 147th rail seat. This is caused by the interaction of the two adjacent wheelsets of the same bogie.

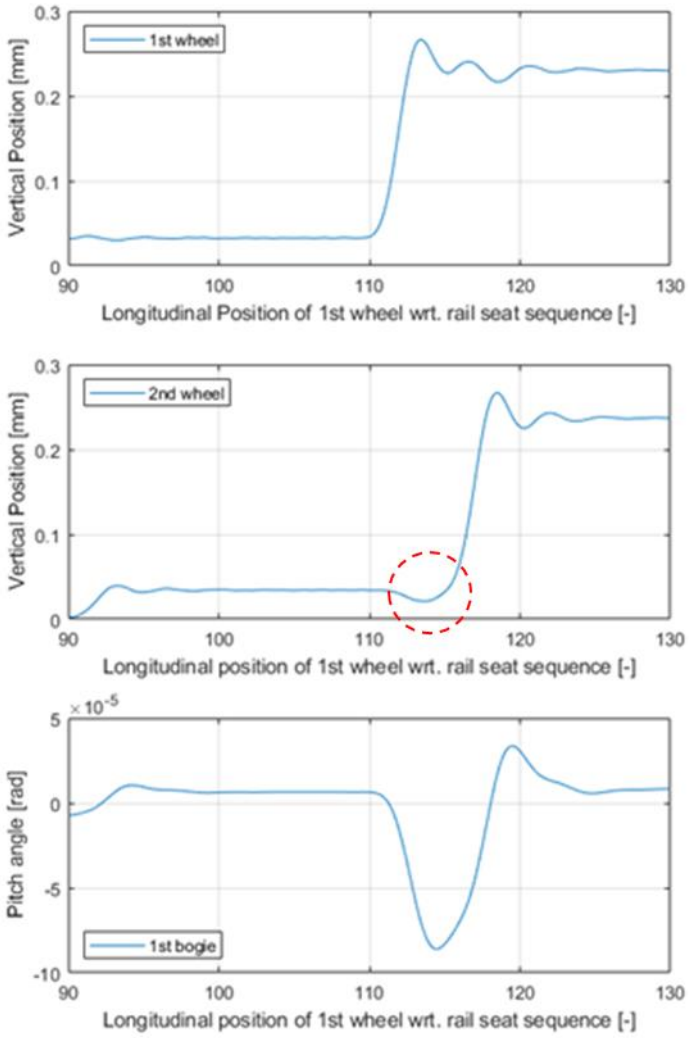

Figure 5-6: Movement of the first bogie and its two wheelsets during passing 112th rail seat

A detailed investigation is performed at the section between 106th rail seat and 109th rail seat as an example. In Figure 5-6, the vertical position of the 1st and 2nd wheelset and the pitch angle of the 1st bogie is demonstrated when the first bogie passes the stiffness discontinuity at the 112th rail seat. All three curves are plotted against the longitudinal position of the 1st wheelset, so that the three curves are timely synchronized. Positive translation in vertical direction indicates movement downwards. Negative rotation indicates anticlockwise pitch rotation of the bogie. It can be observed that when the 1st wheelset passes the stiffness discontinuity zone, it moves downwards due to the reduction of track stiffness. The downward

movement of the 1st wheelset leads to the pitch rotation of the bogie and furtherly to the upward movement of the 2nd wheelset (as indicated by the red circle in Figure 5-6). This phenomenon explains why the distribution of the WRC force of the 1st wheelset and 2nd wheelset is different from each other at around 112th rail seat, i.e., why the dynamic contact force between the 2nd wheelset and rail decreases before the 2nd wheelset passes the 112th rail seat. Due to the same reason, other variance of dynamic WRC force among wheelsets can also be explained.

To investigate the influence of travel direction on the dynamic behaviour of the standard track transition design, case 'P-300-S-S' is calculated, i.e., the same passenger power car travels along the same track transition at the same speed of 300 km/h but in the opposite direction. The calculated dynamic WRC force is demonstrated in Figure 5-7.

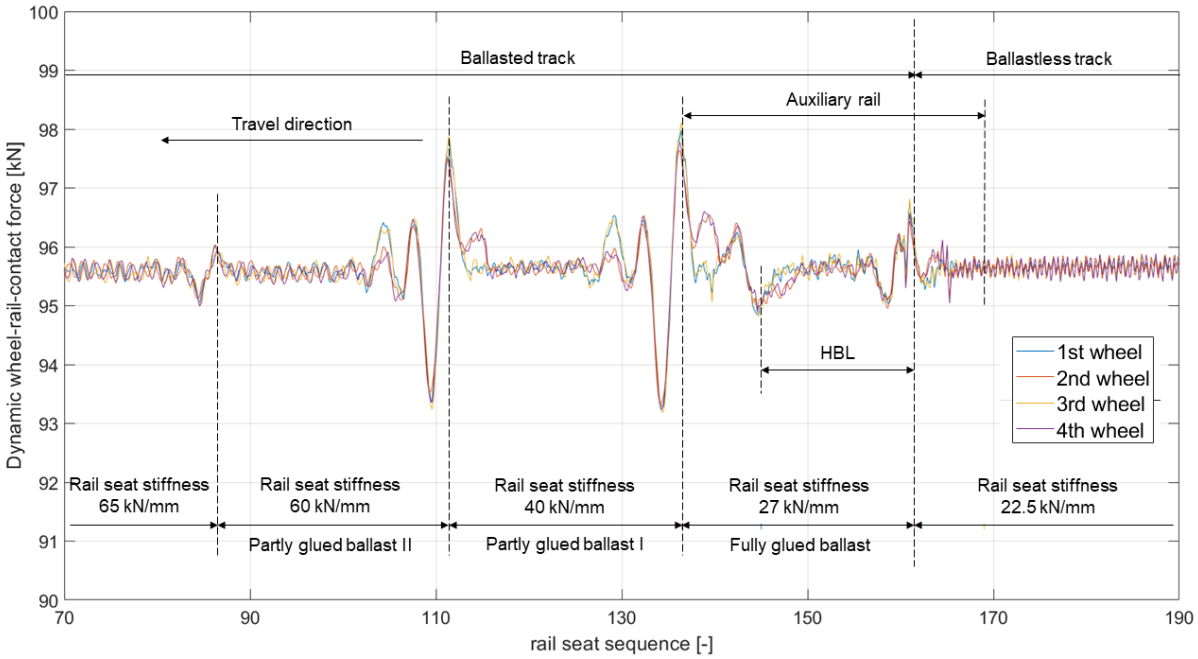

Figure 5-7: Determined dynamic wheel-rail contact force, case 'P-300-S-S'

It can be concluded that the travel direction has not influenced the extreme values of the dynamic force in this case, but it has led to change of the location of its extremum values. When a wheelset travels from a stiffer track to a softer track, the maximal WRC force is observed at rail seat behind the boundary. In contrast, when a wheelset travels from a softer track to a stiffer track, the maximal wheel-rail contact force is observed directly at the boundary.

In Figure 5-8 and Figure 5-9, the dynamic WRC force in case ‘P-230-B-S’ and case ‘P-160-B-S’ are demonstrated. With the decrease of travel speed, the maximal dynamic wheel-rail contact force decreases, too. At the speed of 230 km/h, the dynamic factor is 1.8%. And it decreases to 0.8% when the speed is 160 km/h.

Finally, the case ‘G-160-B-S’ is calculated. Parameters of the employed freight wagon is shown in Appendix 3-2, whose nominal wheel load is 125 kN. The calculated dynamic WRC force is demonstrated in Figure 5-10. The dynamic effect is negligible as in case ‘P-160-B-S’.

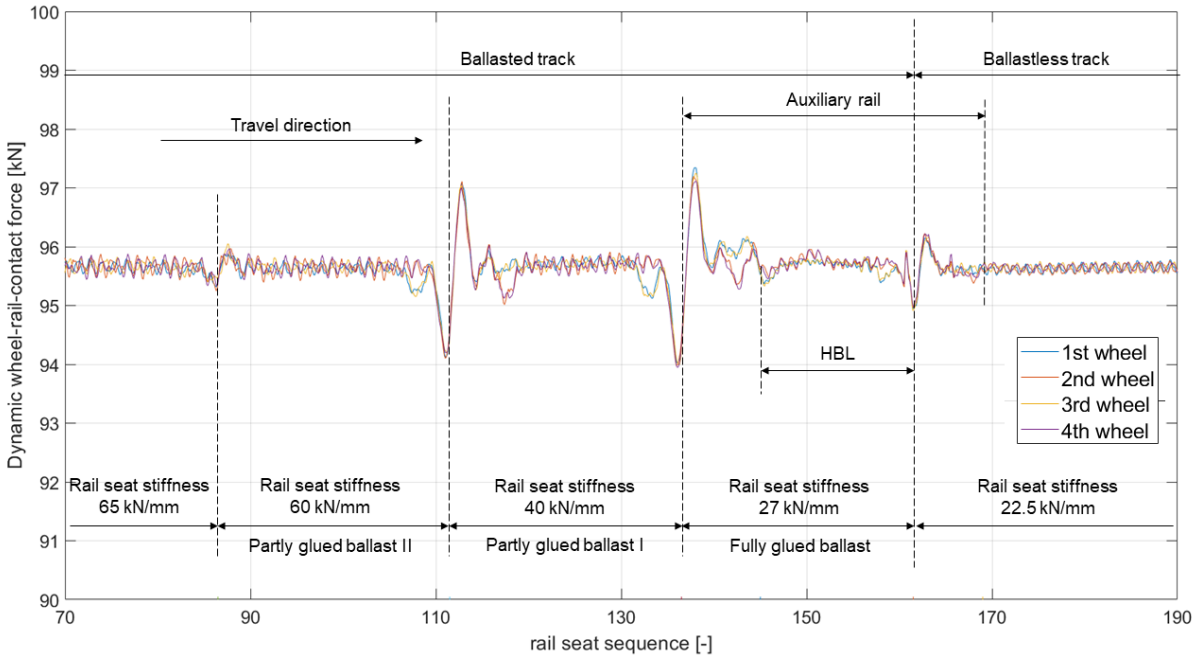

Figure 5-8: Determined dynamic wheel-rail contact force, case ‘P-230-B-S’

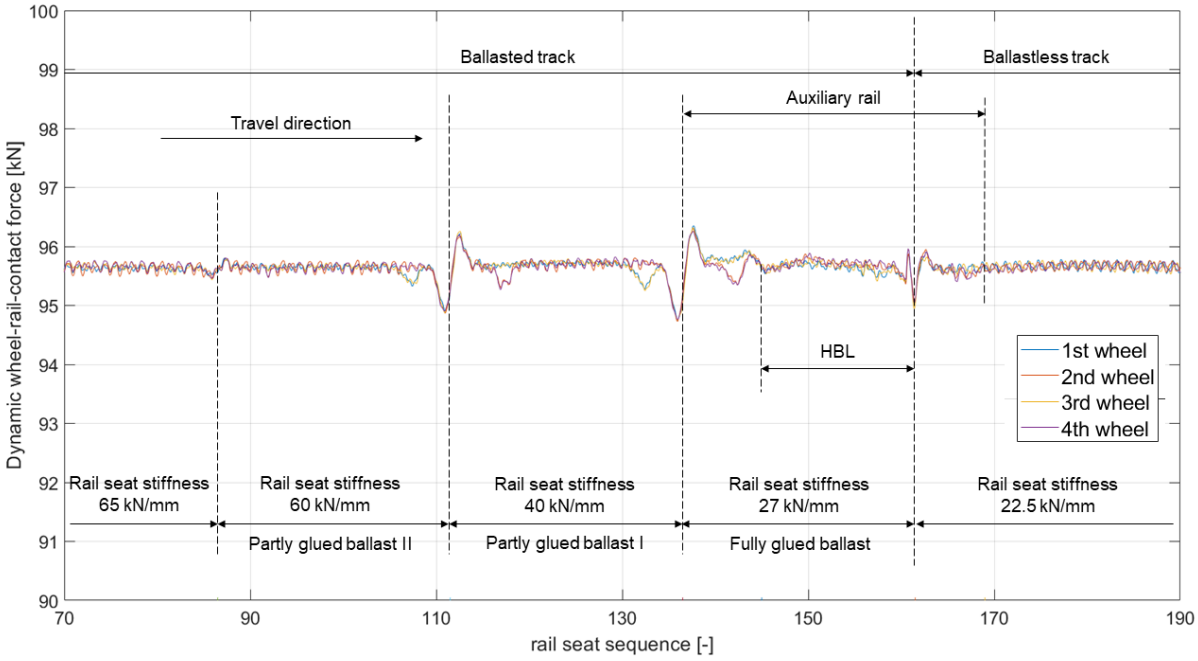

Figure 5-9: Determined dynamic wheel-rail contact force, case ‘P-160-B-S’

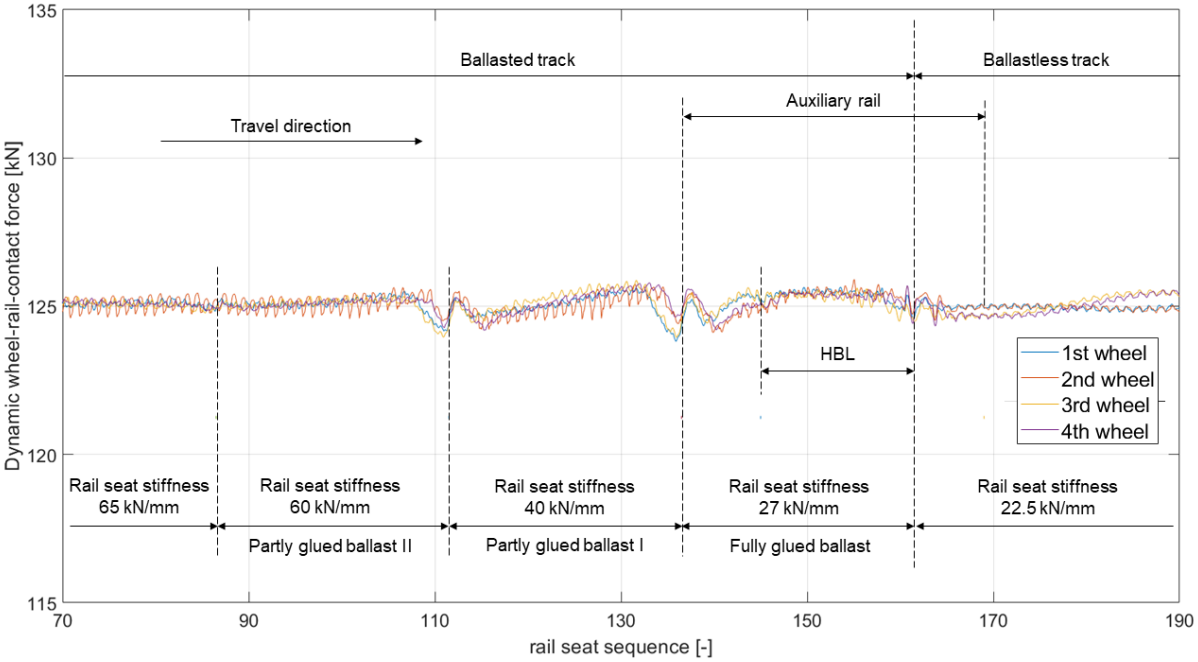

Figure 5-10: Determined dynamic wheel-rail contact force, case ‘G-160-B-S’

5.5 Investigation of the influence of auxiliary rail

In this chapter, the influence of auxiliary rails on track behaviour is investigated. For this purpose, vehicle-track-interaction along a new track with/without auxiliary rail are calculated and compared.

In Figure 5-11, comparison of the dynamic WRC force of the last wheel in case with and without auxiliary rail is demonstrated. It can be observed that the implementation of auxiliary rail has nearly no influence on the dynamic wheel-rail contact force along a new track.

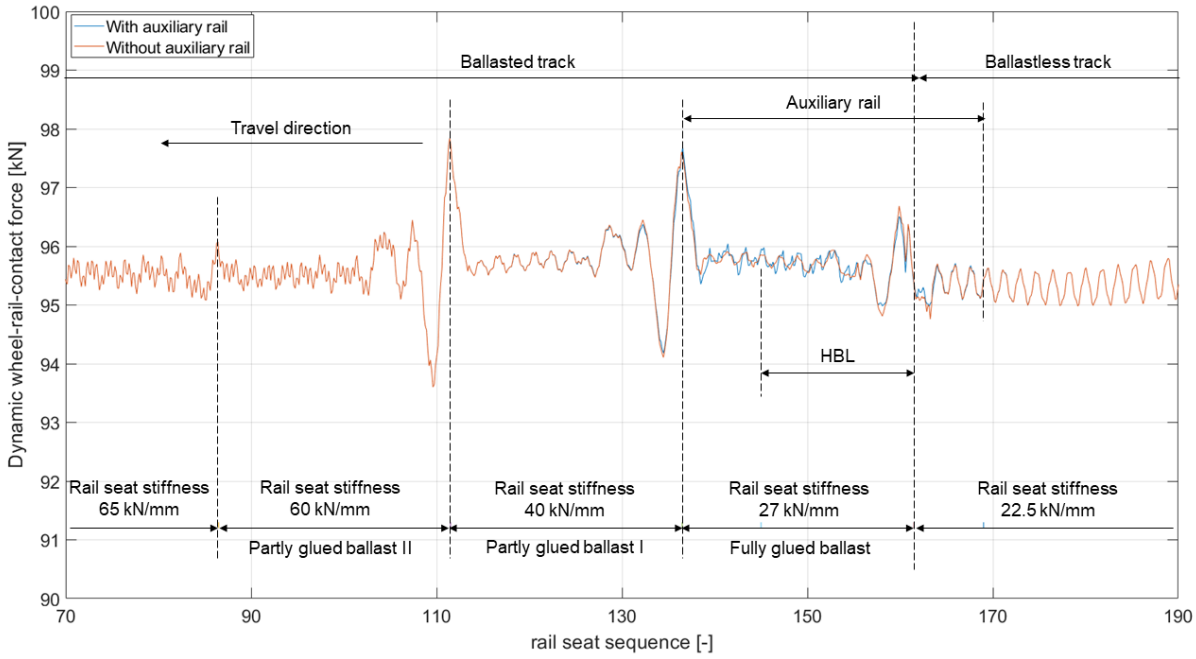

Figure 5-11: Influence of auxiliary rail on wheel-rail contact force, based on case 'P-300-B-S'

In Figure 5-12, the deflection of rail, sleeper, ballast layer and auxiliary rail at the 155th rail seat in both cases are compared as example. It can be observed that the deflection of track components in the case with auxiliary rail are the same as in the case without auxiliary rail. The reason is the relative deflection between sleeper and auxiliary rail does not exceed the gap between the middle ring of the rail tension clamp and rail foot. In this case, the stiffness of rail tension clamp for the auxiliary rail is low (see Figure 5-2).

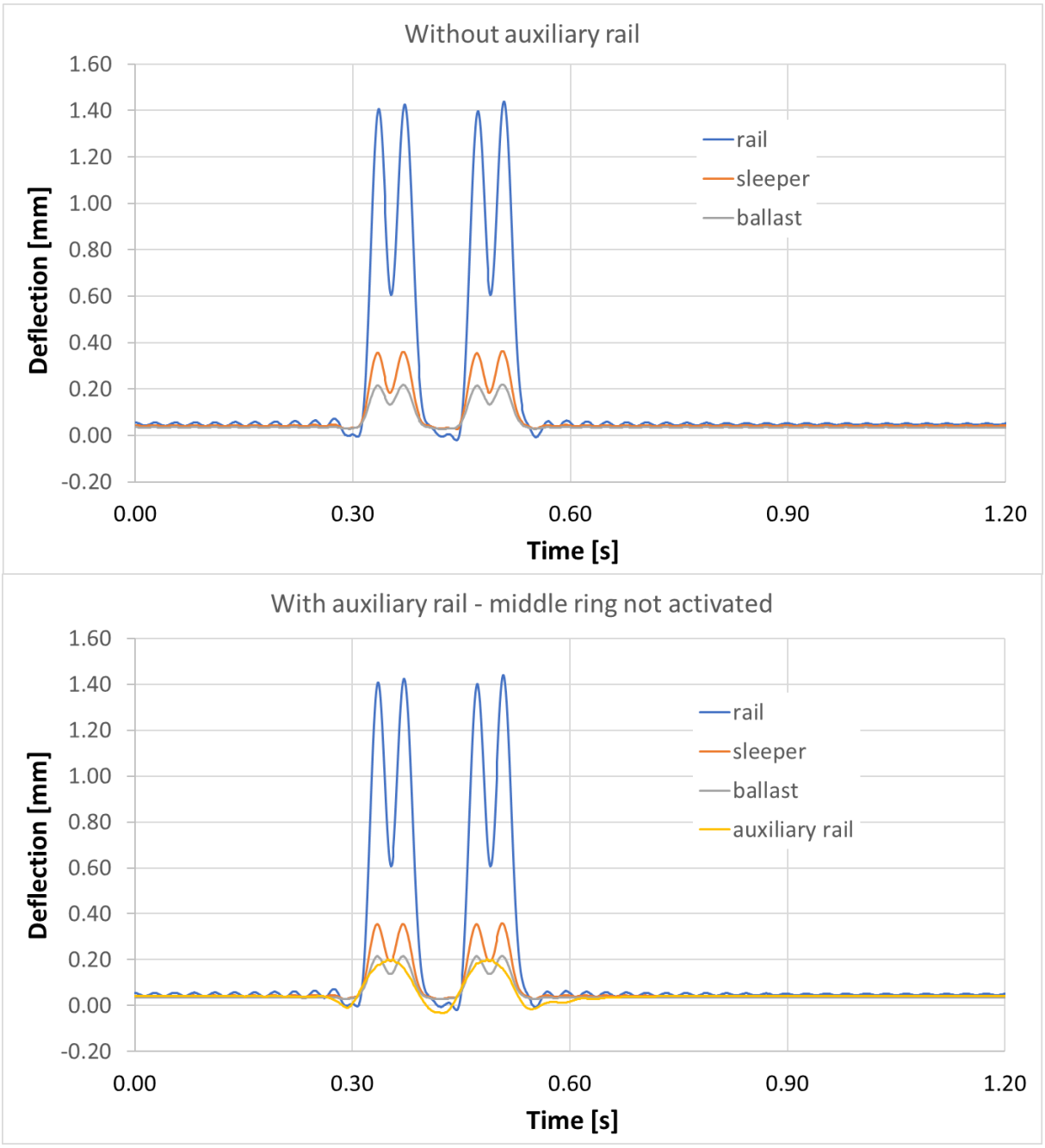

Figure 5-12: Comparison of dynamic deflection of rail, sleeper, ballast layer and auxiliary rail at 155th rail seat

In Figure 5-13, the rail deflection and ballast deformation are shown, when the tension stiffness of the fastening system in the first phase is increased to be the same as the value in the second phase.

Compared with previous situation, with the increase of rail tension clamp stiffness, the maximal ballast deformation is reduced 9%. But the rail deflection is nearly not changed. That is

because the rail pad deflection between the main rail and the sleeper is the dominant part of rail deflection under compression, which is nearly not influenced by auxiliary rail. That fits the conclusion drawn above that the auxiliary rail has insignificant influence on designed track stiffness.

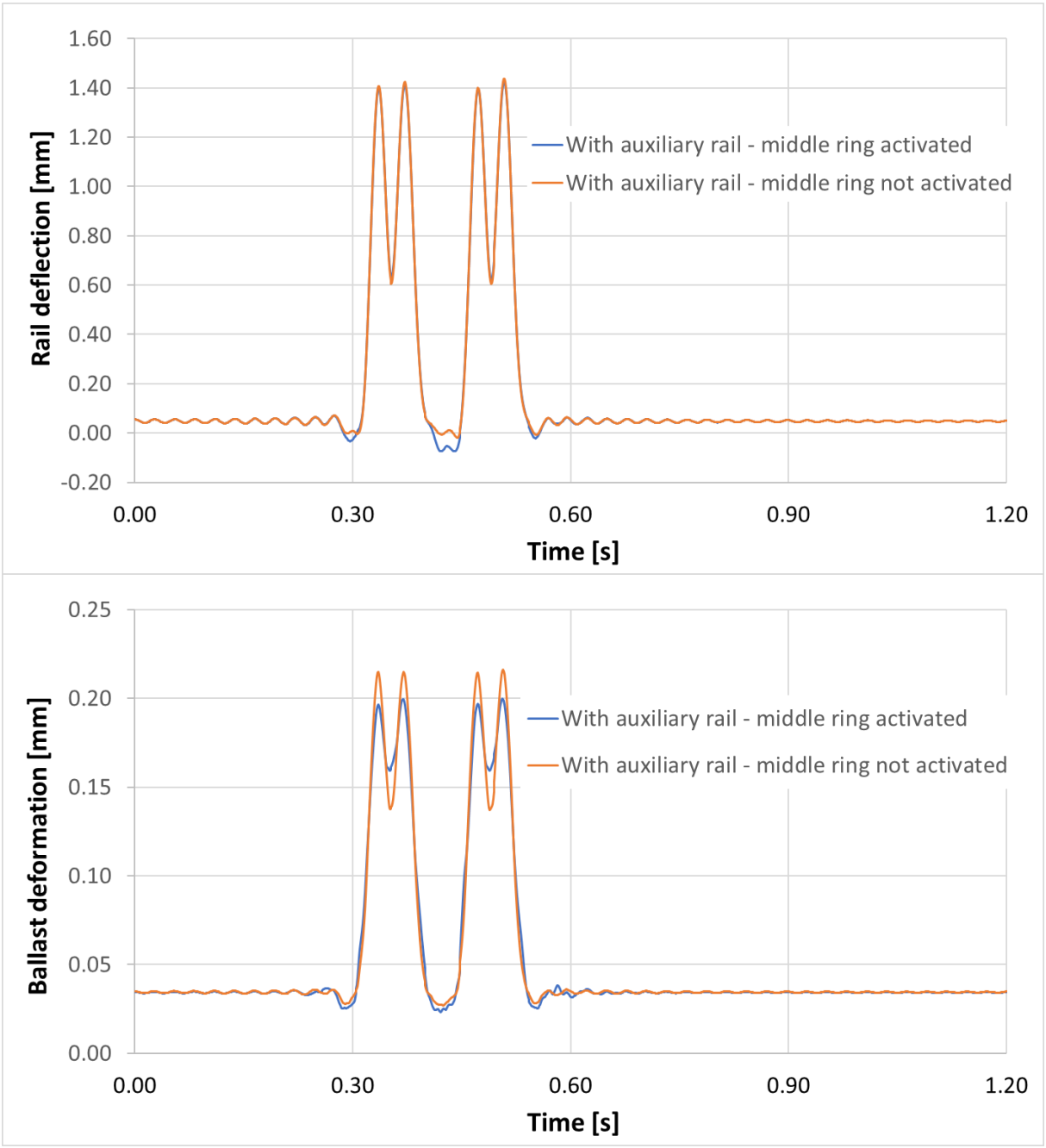

Figure 5-13: Comparison of dynamic rail deflection and ballast deformation at 155th rail seat when the middle ring is activated and not activated

As discussed in chapter 4, pressure on ballast is the dominate parameter for ballast settlement. It can therefore be inferred that reduction of ballast pressure can decelerate the development of ballast settlement. Implementation of auxiliary rail can therefore contribute to improve the long-term performance of track transitions.

It can be concluded that the effect of auxiliary rail is strongly influenced by the rail fastening system stiffness. Initially along new track, auxiliary rail is nearly not activated due to the existence of air gap between the rail tension clamp and rail foot. It is therefore inferred, increase of the initial stiffness of the rail tension clamp can advance the time point when the auxiliary rail begins to work, and thus improve the long-term track performance. This hypothesis is proved in chapter 6.4.

5.6 Discussion and conclusions

Based on the simulation results and discussion above, it can be concluded that the design plan proposed in current standards has successfully smoothed the stiffness discontinuity between the ballasted track and the ballastless track, which is mainly achieved by the implementation of rail pads with continuously changed stiffness. In contrast, auxiliary rail and glued ballast hardly contribute to static track stiffness. Extension of HBL according to current design plan leads to extra stiffness discontinuity. These countermeasures are mainly implemented for eliminating settlement difference in long-term view.

The dynamic calculation results suggest that the dynamic effect along the standard transition is generally low. The maximal dynamic force is determined as 98.1 kN in case ‘P-300-B-S’ and ‘P-300-S-S’, corresponding to a dynamic factor of 2.6%. The calculation has also demonstrated that the travel direction has nearly no influence on the amplitude of the wheel-rail contact force, but it alters the distribution of the force. The wheel-rail contact force increases with vehicle speed. The dynamic effect of freight traffic is insignificant in this case due to its low speed.

The role of auxiliary rail is investigated. It is found that auxiliary rail has nearly no influence on the design track stiffness, but it can reduce ballast pressure when the rail fastening stiffness is increased. It is inferred that increase the initial rail tension clamp stiffness in the first phase can optimise its effect on the long-term performance of track transition, which is proved in chapter 6.4.

In (D. Liu, 2015), Liu has measured the track stiffness quality and track geometry quality along several open track sections. Using the measurement results as input, he has furthermore determined the dynamic factor of WRC force. According to Liu's research, the dynamic factor of high-speed ballastless track with excellent quality compared to the AKFF requirement (Deutsche Bahn AG, 2002) at 300 km/h was 11.1%, and the dynamic factor of high-speed ballasted track after one year of service at 250 km/h was 25.2%. As comparison, the dynamic factor at the investigated transition determined in this research, which is activated by the designed stiffness change along the section (perfect track geometry and stiffness quality), is much lower. In fact, it can be calculated that even without any countermeasures, the dynamic factor along the investigated ballasted-ballastless track transition is 3.9%.

The result should however not be interpreted as that the track quality of the transition built according to standard design is higher than an open track section of a ballastless track with excellent quality, while different excitations have been included in these two calculations. The calculation in (D. Liu, 2015) has employed measured track geometry quality and track stiffness quality along the track, which takes the variation of track vertical level and track stiffness among rail seats into consideration. In contrast, in the investigation here it is assumed that stiffness of each rail seat within both subsections remain homogenous, and the discontinuity of track quality comes merely from the change of track design at the boundary. It can be inferred that for a transition in real life, the dynamic effect should be caused by track geometry and both types of track stiffness variance. From this point of view, a proper interpretation is that the short-term dynamic effect caused by transition makes up a small proportion of the total effect, when investigating new tracks.

This conclusion leads to the reconsideration of track transition treatment. If the influence of the stiffness discontinuity due to track design change on the short-term behaviour of transition is insignificant, why should the track stiffness be homogenized then? The answer lies in the long-term view, which is illustrated in coming chapter.

6. Investigation of the ballastless-ballasted-track-transition in long-term view

6.1 Introduction

Besides the stiffness discontinuity between the ballasted track and the ballastless track, the long-term settlement difference between these two sections is another issue to be addressed during the design of the ballastless-ballasted track transition. In this chapter, the standard design plan (see Figure 5-1) is optimised in the long-term view.

As mentioned at the beginning of this research, it is assumed that the bearing capacity of subgrade is sufficient, and the settlement of subgrade is negligible. Consequently, the ballastless track is treated as settlement-free in this research. In this regard, the difference of settlement at the ballasted-ballastless-track-transition equals to the ballast settlement of the ballasted track.

6.1.1 Selection of countermeasures in the new design plan

As summarised in Table 6-1, the countermeasures listed in the standard design plan can be divided into two categories based on their effect on ballast settlement.

Table 6-1: Categorisation of the countermeasures in the standard design plan

Category	Countermeasure	Effect
1	Glued ballast	Elimination of ballast settlement (Kennedy et al., 2013; J. Liu, Geisler, Lechner, & Freudenstein, 2012).
2	Extended HBL	Increase of the supporting stiffness of ballast layer, and reduction of ballast settlement (Holtzendorff, 2003; Kumar et al., 2019; Raymond & Richard, 1987; Sol-Sánchez et al., 2016; Sol-Sánchez et al., 2015).
	Auxiliary rail	Better distribution of track load, reduction of the ballast pressure and settlement (see Chapter 5.5)
	Rail seat stiffness adjustment	Reduction of stiffness discontinuity, reduction of ballast settlement (see Chapter 6.5)

According to (Kennedy et al., 2013; J. Liu et al., 2012), glued ballast can eliminate ballast settlement. If so, the track longitudinal level and the track stiffness discontinuity would remain unchanged in long-term view. Consequently, the performance of the transition design in long-term is the same as in short-term. As discussed in chapter 5, the standard design has already reduced the dynamic factor to insignificant level. No extra long-term investigation is needed.

In (Mattner & Eisenmann, 1990), effect of glued ballast was also investigated through field measurement. Nevertheless, the results revealed that settlement of glued ballast along the measurement section has been reduced but not eliminated. Besides, glued ballast has also led to new discontinuity between the ballasted track section with glued ballast and the ballasted track section with free ballast. Based on measurement result, Mattner and Eisenmann have concluded that glued ballast might has only transferred the settlement problem spatially along the track, rather than solved the problem. In this case, optimisation of this transition should additionally focus on the new discontinuity formed between the ballasted track with glued ballast and normal ballasted track with free ballast.

The discussion above reveals that the behaviour of track sections with glued ballast can be various. More measurement data is needed to interpret the effect of glued ballast more realistic and exactly. Therefore, the research here focuses on the countermeasures of Category 2 in Table 6-1. Alternative transition designs with free ballast are studied.

A general consideration on such a solution is that compared to the solution with glued ballast, unglued ballast may experience more abrasion and deteriorates more quickly, especially along the sections where it is supported by rigid layers like HBL. In the praxis, following two methods are usually used to solve this problem:

- Implementation of flexible pavement instead of the rigid HBL, for example using bituminous layers as in Japan and Italy (Castillo-Mingorance, Sol-Sánchez, Moreno-Navarro, Pérez, & del Carmen Rubio-Gámez, 2021; Teixeira, López-Pita, Casas, Bachiller, & Robuste, 2006).
- Implementation of elastic components such as USP, UBM can also protect ballast particles (Baeßler, 2008; Loy & Augustin, 2013; Sol-Sanchez & D'Angelo, 2017).

In this research, implementation of USP is proposed as a part of the final design plan (see chapter 6.6).

6.1.2 Definition of research aim and process

Based on the rail seat stiffness, the transition can be divided into three subsections. For convenience of reference, the subsections next to the ballastless track is designated as the 1st subsection, and the subsection next to the ballasted track is designated as the 3rd subsection. As already discussed, in this research, it is assumed that the ballastless track is free of settlement. Meanwhile, the settlement of a rail seat in the ballasted open track is not influenced by the design of the track transition, given it is far enough away from the transition. Therefore, the settlement difference at both ends of the transition is fixed.

In this context, it is proposed to optimize track transition performance by finding out a track transition design, which enables continuous change of track settlement along the transition in three steps. The result of this research demonstrates that following this design principle, the vehicle-track-interaction and track geometry deterioration can both be reduced significantly. It is not excluded that there might exist other design principles that could also optimize the standard transition design, but ergodic research of all possibilities is out of the scope of this research.

Starting from the standard transition design demonstrated in Figure 5-1, the investigation is performed stepwise as shown in Figure 6-1. Based on the discussion in chapter 5, the dynamic effect in following condition is the most severe:

- Vehicle type: passenger power car with nominal wheel load of 95.6 kN (see Appendix 3-1)
- Speed level: 300 km/h
- Travel direction: from the ballastless track to the ballasted track.

Therefore, the long-term calculation is performed under this condition. Finally in chapter 6.7, it is proved that the proposed design plan is also effective when traffic is in the other direction.

To investigate the long-term effect, 4.1 million axle loadings are introduced. With the axle load as 19.5 tonnes, it corresponds to 80 million gross tons (MGT). According to (Eisenmann & Leykauf, 2003), the maintenance interval of railway track is usually 20 MGT ~ 40 MGT. Therefore, 80 MGT is considered as sufficient to study a complete life cycle of a railway track transition.

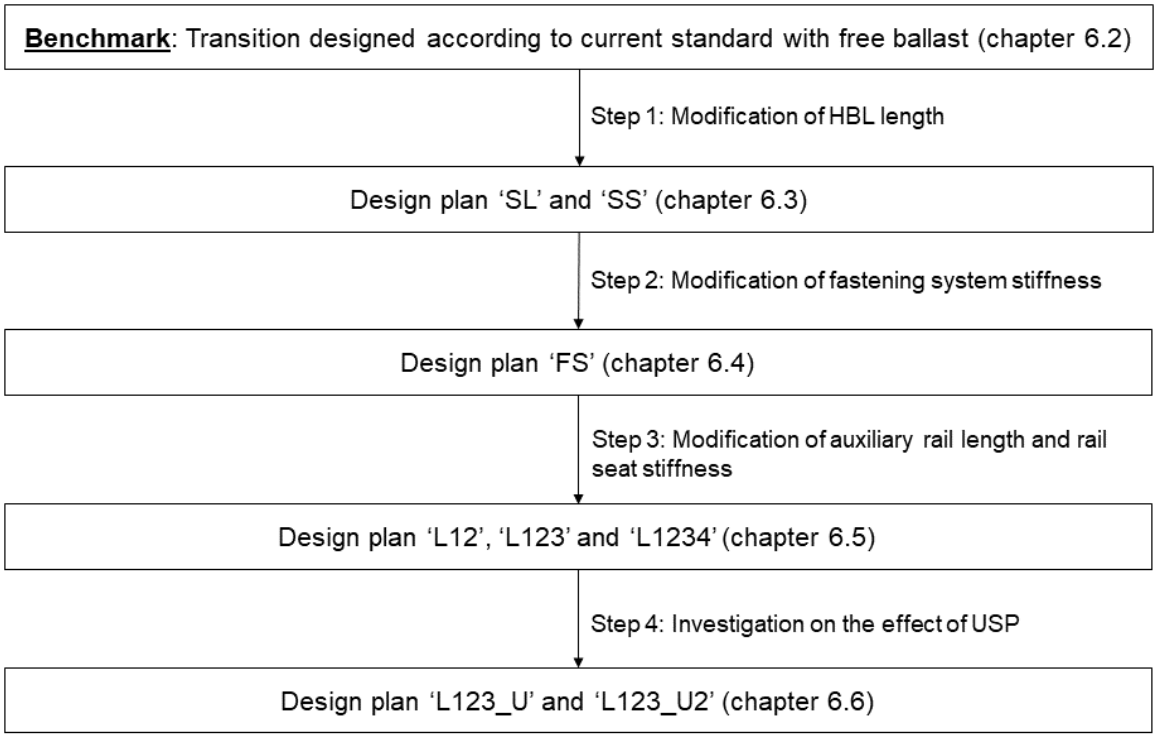

Figure 6-1: Overview of the investigation process

The steps are illustrated shortly as follows:

- **Benchmark**

  The dynamic performance of the track transition following standard design but with free ballast is first investigated, serving as benchmark for following modifications.

- **Modification of HBL length**

  In the benchmark design, the length of HBL is 10 m. In this chapter, two variations, i.e., case 'SS', in which the HBL is reduced to 7.2 m, and case 'SL', in which the HBL is extended to 15 m are investigated.

- **Modification of the rail fastening stiffness of auxiliary rail**

  In this chapter, the effect of increasing the initial rail fastening stiffness of auxiliary rail is investigated. Without losing generality and to reduce calculation time, it is increased to be the same as the stiffness in the second phase.

- **Modification of the length of auxiliary rail**

  In the benchmark design plan, auxiliary rails are mounted from the ballastless track to the 1st subsection of the transition. In this chapter, following variations of extending the auxiliary rails are studied:

  - plan 'L12': extended to the 2nd subsection,
  - plan 'L123': extended to the 2nd and the 3rd subsection,
  - plan 'L1234': extended to the 2nd, the 3rd subsection and extra 5 m into the ballasted open track. This design is inspired by how the auxiliary rail is implemented in the ballastless track in the standard design plan.

- **Modification of the distribution of rail seat stiffness**

  As demonstrated in Chapter 6.5, larger stiffness difference leads to larger settlement difference in the long-term view. In the benchmark design plan, the change of track stiffness along the transition is nevertheless not continuous (see Figure 5-4). It is therefore proposed to investigate the effect when the track stiffness distribution is homogenized by tuning rail seat stiffness.

- **Implementation of under sleeper pad (USP)**

  Implementation of USP at the bottom of concrete sleepers can increase the contact area between sleepers and ballast, which consequently reduces the pressure on the ballast layer and reduces the ballast settlement (Loy, 2008). In the same publication, Loy has pointed out that the implementation of USP with static bedding modulus of 0.2 N/mm^3 can reduce the ballast pressure up to 25%. In chapter 6.6, the feasibility to reduce the settlement difference by implementation of USP is studied.

  As discussed at the very beginning of this chapter, USP should be implemented at least in subsection 1 to reduce ballast abrasion. Based on Figure 6-25, it can be inferred that further reduction of settlement in subsection 2 can further reduce the maximal global settlement difference. It is therefore proposed to implement USP in subsection 1 and 2. USP is not installed in subsection 3, because it would increase the settlement difference between the 3rd subsection and open track. The effect of using USP with different bedding modulus in subsection1 and 2 is also investigated.

To illustrate the influence of each single countermeasure clearly, in each investigation only one countermeasure should be modified/introduced. However, considering it is already proved that auxiliary rail has nearly no influence on the track stiffness, the length of auxiliary rail and the distribution of rail seat stiffness are investigated together. As a results, the investigated cases can be summarised as in Table 6-2.

Table 6-2: Summary of performed long-term investigations

Group 1: influence of the length of HBL		
Designation	**Length of HBL**	
'SL'	15 m	
'SS'	7.2 m	
Group 2: influence of the rail fastening stiffness for auxiliary rail		
Designation	**Rail fastening stiffness of auxiliary rail**	
'FS'	Increased (see the illustration in the text above)	
Group 3: influence of the length of auxiliary rail and rail seat stiffness distribution		
Designation	**Range of auxiliary rail**	**Distribution of rail seat stiffness**
'L12'	Mounted in subsection 1 and 2	3 Steps with uniform deflection difference
'L123'	Mounted in subsection 1, 2 and 3	
'L1234'	Mounted in subsection 1, 2, 3 and 5 m in the ballasted open track	
Group 4: influence of implementation of USP		
Designation	**Range of USP implementation and its bedding modulus**	
'L123_U1'	Mounted in subsection 1 and 2, the same bedding modulus in two subsections	
'L123_U2'	Mounted in subsection 1 and 2, different bedding modulus in two subsections	

It should be pointed out that the benchmark case is selected to set up a starting pointing for the following optimization steps. The comparison of further design variations with benchmark does not mean that the design plan proposed here is better than the plan in current standard, while the benchmark design is used together with glued ballast in the praxis, which is not considered here. Instead, the aim of this research is to find a design plan with suitable countermeasures and proper parameters alternative to the standard plan.

It is also worth mentioning that the objective of the new design plan is to realise the globally optimized performance of the track transition. Therefore, the new design does not always lead to local improvement. It however does not harm the significance of the research.

6.2 Long-term behaviour of the benchmark design

The long-term behaviour of track transition is predicted using Modul I, II and III of the MATLAB programmes. The calculation process is illustrated taking case ‘P-300-S-Benchmark’, i.e., a passenger power car moves from the ballastless track to the ballasted track at the speed of 300 km/h.

6.2.1 Calculation under repeated axle loading

First, the vehicle-track interaction model is brought to equilibrium using Modul I. Then the dynamic calculation is performed using Modul II of the program. This procedure is the same as discussed in chapter 5. Based on the determined ballast pressure, the increment of settlement after this axle loading cycle can be calculated. Based on the calculated ballast settlement, the unloaded track geometry and under sleeper gap are determined using Modul I again. Repeating this calculation process, a looped calculation for prediction of the long-term behaviour of track transition is realized.

It is self-evident, before the increment of ballast settlement exceeds a limit Δs, the wheel-rail contact force would only change insignificantly. Therefore, it is unnecessary to perform a new dynamic calculation at each iteration step. Since module II, i.e., the short-term vehicle-track interaction module is the most time-consuming part in the whole calculation process, reducing the needed short-term calculation can significantly reduce the needed calculation time. Based on this consideration, the workflow showed Figure 6-2 is proposed. After parameter study, step size Δs = 0.2 mm is chosen for further calculation, which provides a good compromise between the calculation time and accuracy.

The development of ballast settlement with respect to the number of load cycles is shown in Figure 6-14. Under traffic in the direction from ballastless track to ballasted track, the ballast settlement increases in quasi two steps from 2.4 mm to 8.1 mm after 80 MGT traffic load. Inhomogeneous ballast settlement is observed at the boundaries between subsections, especially between the ballastless track and subsection 1, and at the end of HBL, due to stiffness variance and different ballast supporting condition.

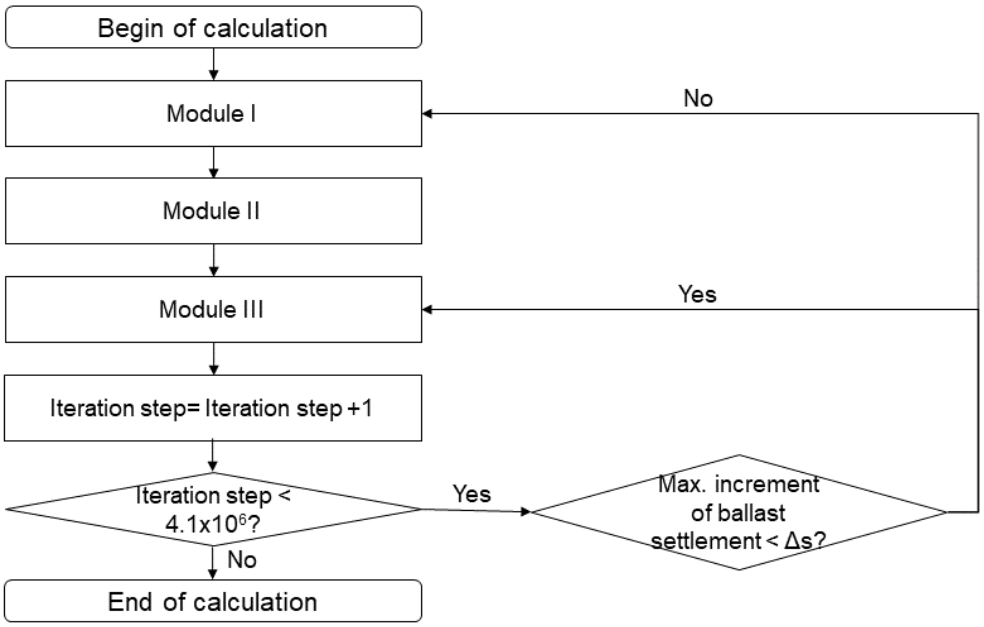

Figure 6-2: Workflow of the repeated calculation

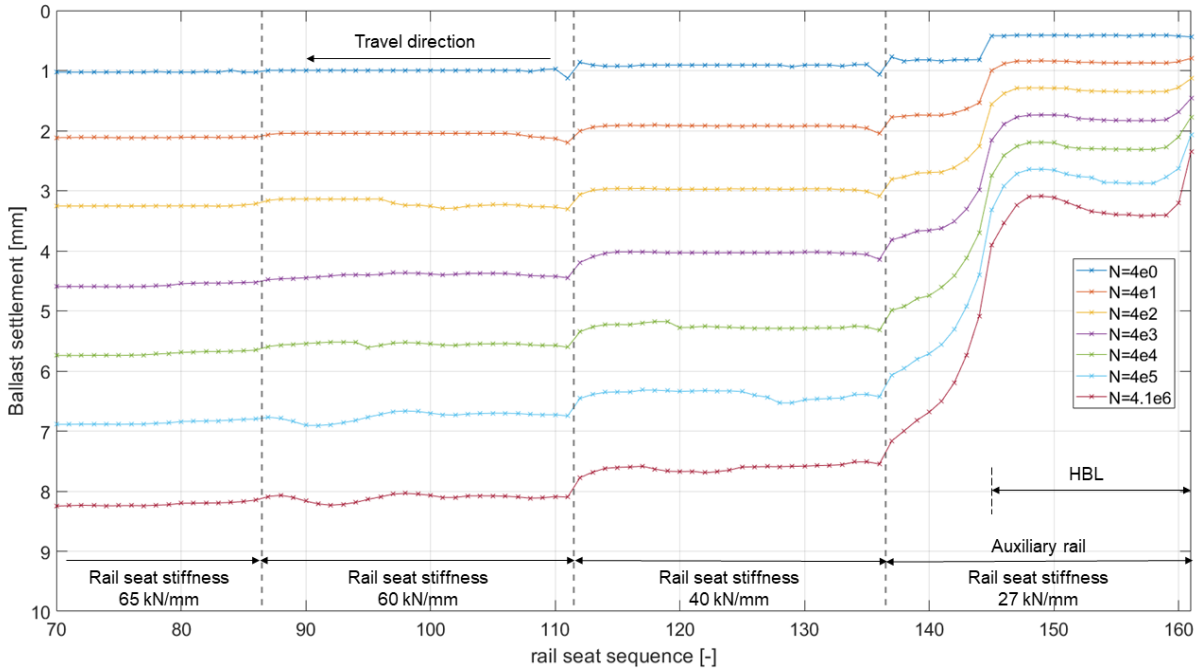

Figure 6-3: Development of ballast settlement with respect to the number of axle loadings

In this research, only the longitudinal level caused by design track stiffness discontinuity and uneven ballast settlement is considered. Therefore, the ballast settlement at those rail seats that are not influenced by the transition zone effect turns out to be homogenous. Due to the

same reason, the maximal settlement is also lower than empirical value, for example around 11 mm after 80 MGT as suggested in (Klotzinger, 2008b).

6.2.2 Evaluation

As a result of the varying ballast settlement, under sleeper gaps are formed, which can be calculated as the distance between the vertical position of sleeper bottom and ballast layer surface in unloaded equilibrium state. The determined amplitude of under sleeper gap along the transition after 80 MGT traffic load is demonstrated in Figure 6-4. It can be observed that under sleeper gaps are mainly observed at the boundary of discontinuities. Between the ballastless track and the 1st subsection, 6 rail seats are not fully supported. The maximum amplitude of under sleeper gap there is 1.8 mm. In (Rump, 1997), field measurement on the high speed line Hannover – Würzburg in Germany revealed that it was possible that maximal 9 sleepers in a row became unsupported. At the end of HBL within the 1st subsection, another 5 sleepers are not fully supported. The maximal amplitude of under sleeper gap is 0.4 mm. At the boundary between the 1st subsection and the 2nd subsection, and between the 2nd subsection and the 3rd subsection, under sleeper gaps with amplitude of 0.1 mm are also detected.

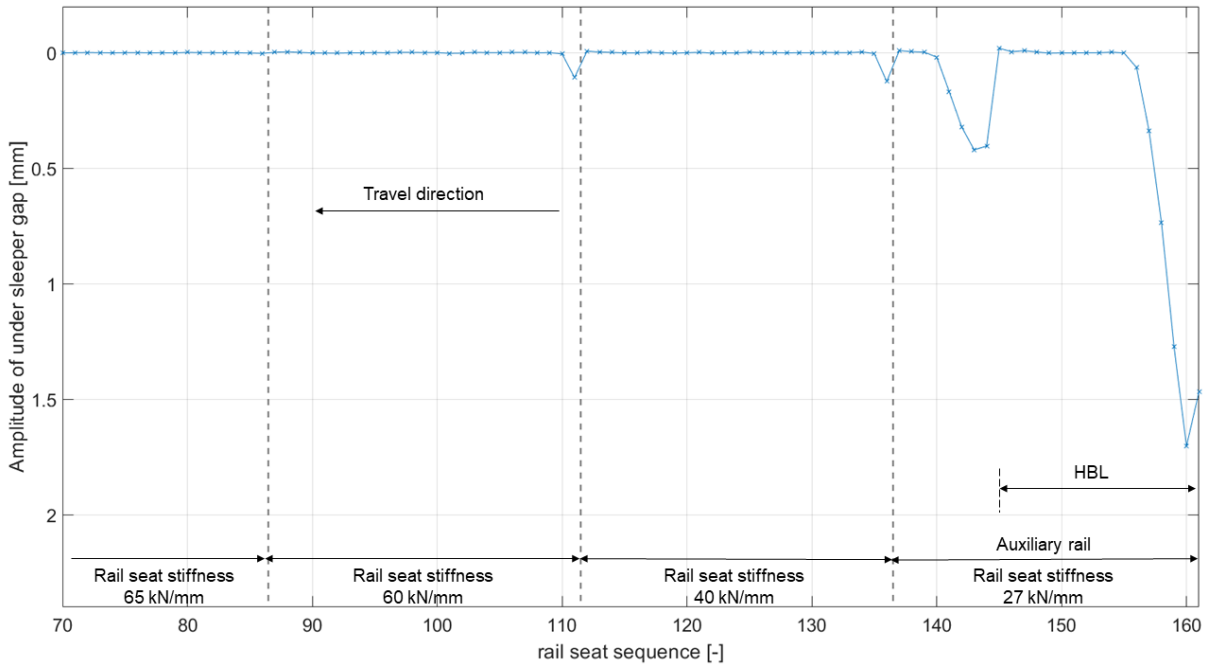

Figure 6-4: Under sleeper gap level after 80 MGT traffic load

For evaluation of track service life, the vertical SR-value, which is used as the indicator for planning track maintenance activities in Ril 821.2001 (DB Netz AG, 2010), is used to assess the deterioration of track quality. SR-value can be determined by conversion of the actual longitudinal level using chord-based measurement method, which is graphically illustrated in Figure 6-5 according to (Wolter, 2013).

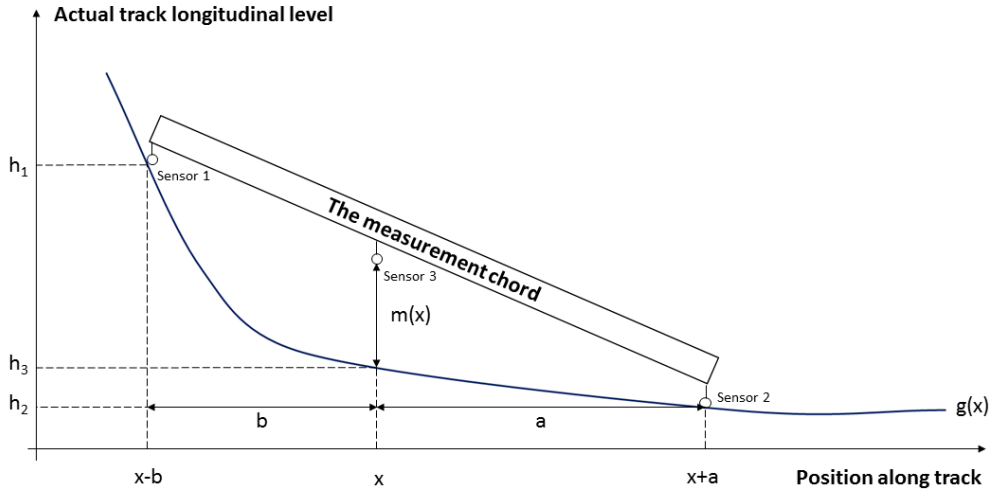

Figure 6-5: Principle of chord-based method measurement

In Figure 6-5, $\mathrm{g(x)}$ represents the actual rail longitudinal level. The measurement chord carries three position sensors. The versine $m(x)$ is considered as the measured longitudinal level of track position x. It can be observed that the measured longitudinal level in this way is different from the actual rail longitudinal level. The relationship between them is illustrated as follows (Wolter, 2013):

$$\mathrm{m(x)} = h_3 - \frac{a}{a+b} \cdot h_1 - \frac{b}{a+b} \cdot h_2 \qquad (16)$$

with

$m(x)$: longitudinal level determined using chord-based method [mm]

a, b : length of the two chords [m],

h_1, h_2 : accurate longitudinal level at both ends of the chords [mm]

h_3 : accurate longitudinal level at the calculation point [mm]

In case of longitudinal level measurement, $a = 2.6\,m, b = 6.0\,m$.

In Ril 821.2001 (DB Netz AG, 2010), SR values are determined as the “peak-peak” values of the chord-based measurement results. The threshold of single fault of track longitudinal level is summarised in Table 6-3.

Table 6-3: Assessment criteria of the single fault of track longitudinal level in Ril 821.2001 (DB Netz AG, 2010)

Assessment criterion	v ≤ 80	80<v ≤ 120	120<v ≤ 160	160<v ≤ 230	v>230
SR_A [mm]	12	10	8	6	5
SR_{100} [mm]	15	13	11	9	7
SR_{lim} [mm]	21	17	14	11	9

The assessment criteria are illustrated as follows:

- SR_A: if this value is exceeded, the preparatory planning for a maintenance measure is needed.
- SR_{100}: if this value is exceeded, maintenance should be performed before next inspection.
- SR_{lim}: if this value is exceeded, it is expected that the track functionality has been damaged. Maintenance should be performed as soon as possible.

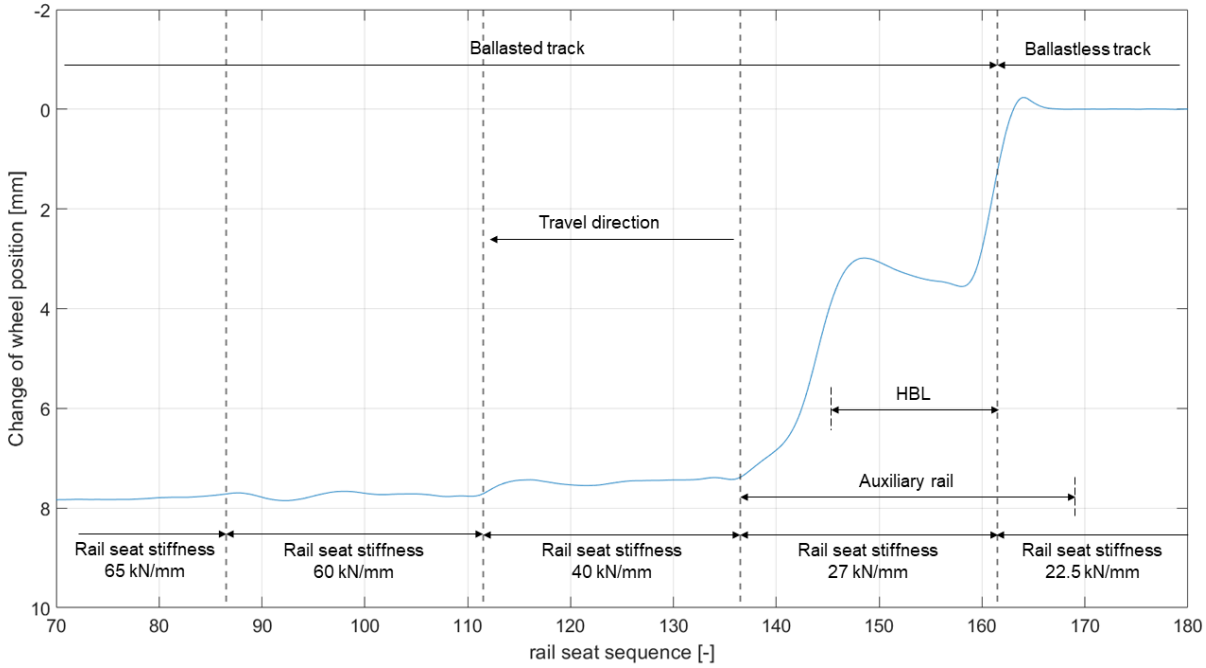

Figure 6-6: Loaded longitudinal level after 4.1 million axle loadings in the benchmark case

In Figure 6-6, the determined loaded longitudinal level after 4.1 million axle loadings in the benchmark case is demonstrated. A quasi-two-step transition between the ballastless track and the ballasted track has formed, along which the longitudinal level increases from 0 mm in the ballastless track, over approximately 3.0 mm in the 1st subsection with HBL, over appr. 7.5 mm in the 2nd subsection. The longitudinal level does not change significantly afterwards. In the 3rd subsection and in the open track, the longitudinal level are approximately 7.9 mm. Discontinuities of longitudinal levels can be observed at the boundaries of subsections and discontinuities due to the different stiffness and settlement behaviour there.

The SR-value curve along this section in this case can therefore be determined according to formula (16). The result is shown in Figure 6-7.

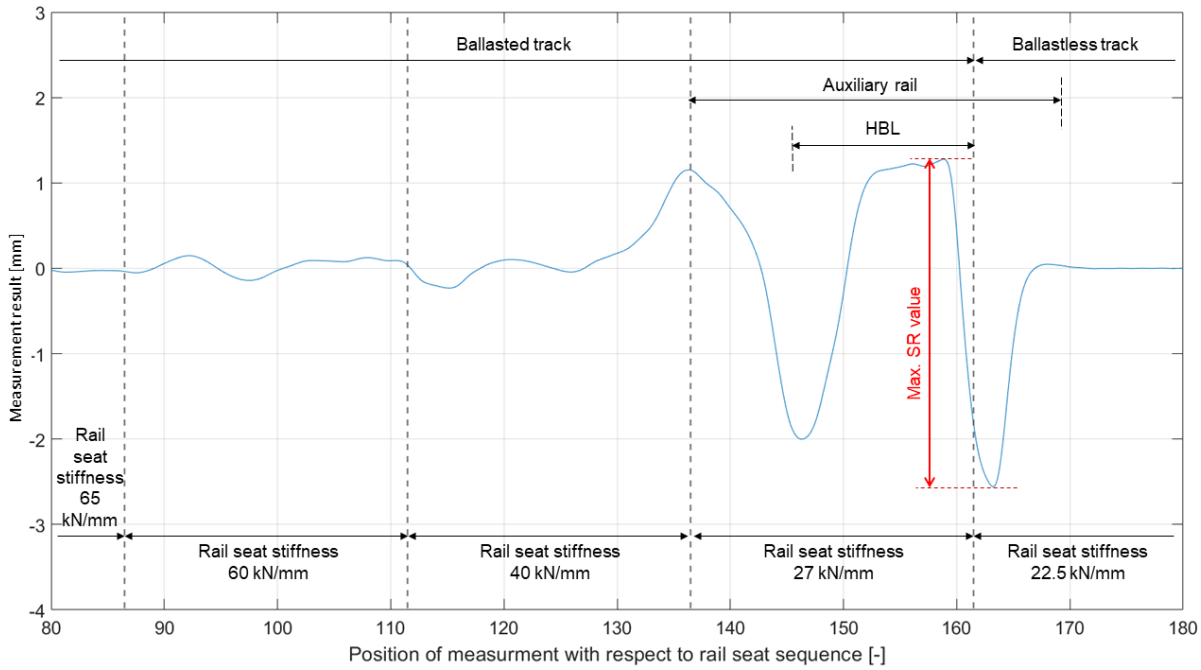

Figure 6-7: SR-value curve after 4.1 million axle loadings in benchmark case

First, it can be observed how the SR values differ from the track longitudinal level regarding both the amplitude and phase. Second, the SR value correlates with the change of loaded longitudinal level curve: if the longitudinal level remains unchanged, the SR value in this range lie also around zero. Otherwise, abruptly changed longitudinal level leads to higher SR value. Along the whole section, the maximal SR value along the section is also observed at the boundary between the ballastless track and the 1st subsection., whose peak-to-peak value as required in Ril 821.2001 (DB Netz AG, 2010) is determined as 3.8 mm (see the arrow in

Figure 6-7). The second highest SR value is observed at the boundary between the 1st subsection and the 2nd subsection with an amplitude of 3.2 mm. Compared with Table 6-3, the maximal SR value lies below SR_A value.

In Figure 6-8, the development of the maximal SR value of the whole section with respect to load cycles is demonstrated. For the plot a base-10 logarithmic scale on the x-axis and a linear scale on the y-axis are used. In the figure, a quasi-linear relationship between the logarithm of the number of load cycles and the maximal SR value of the whole transition section can be observed.

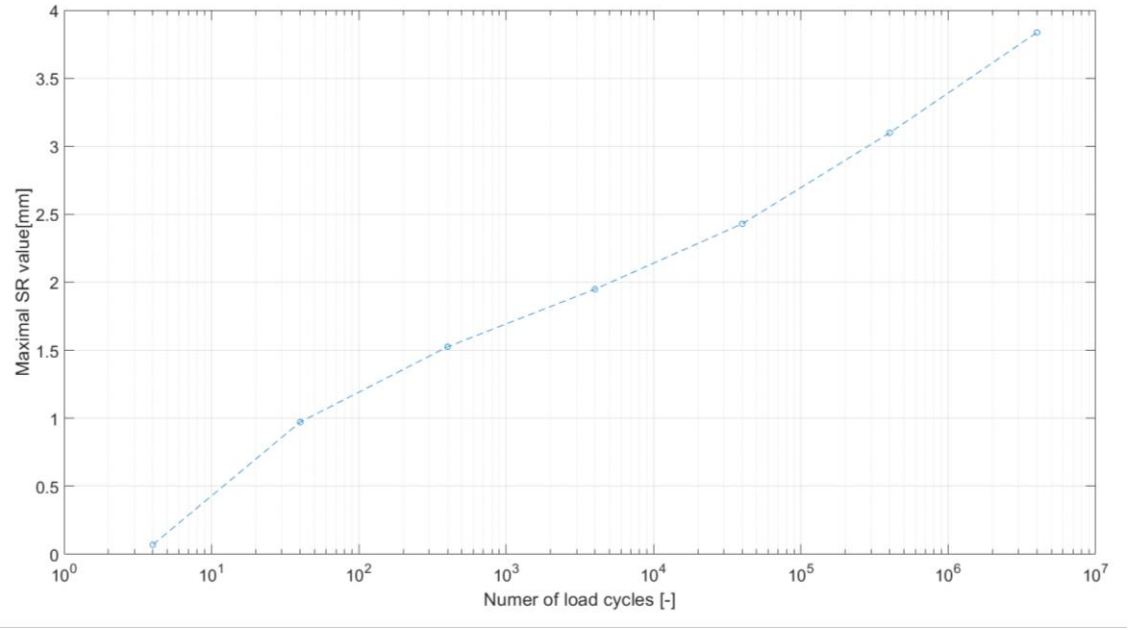

Figure 6-8: Development of maximal SR value with respect to load cycles

The dynamic WRC force after 4.1 million load cycles is plotted in Figure 6-9. The maximal WRC force of 132.8 kN is observed at the boundary between the ballasted track and the ballastless track, corresponding to a dynamic factor of 38.9%. At the end of HBL in the 1st subsection, the dynamic WRC force is increased 7.5% to 102.8 kN compared to the static wheel load.

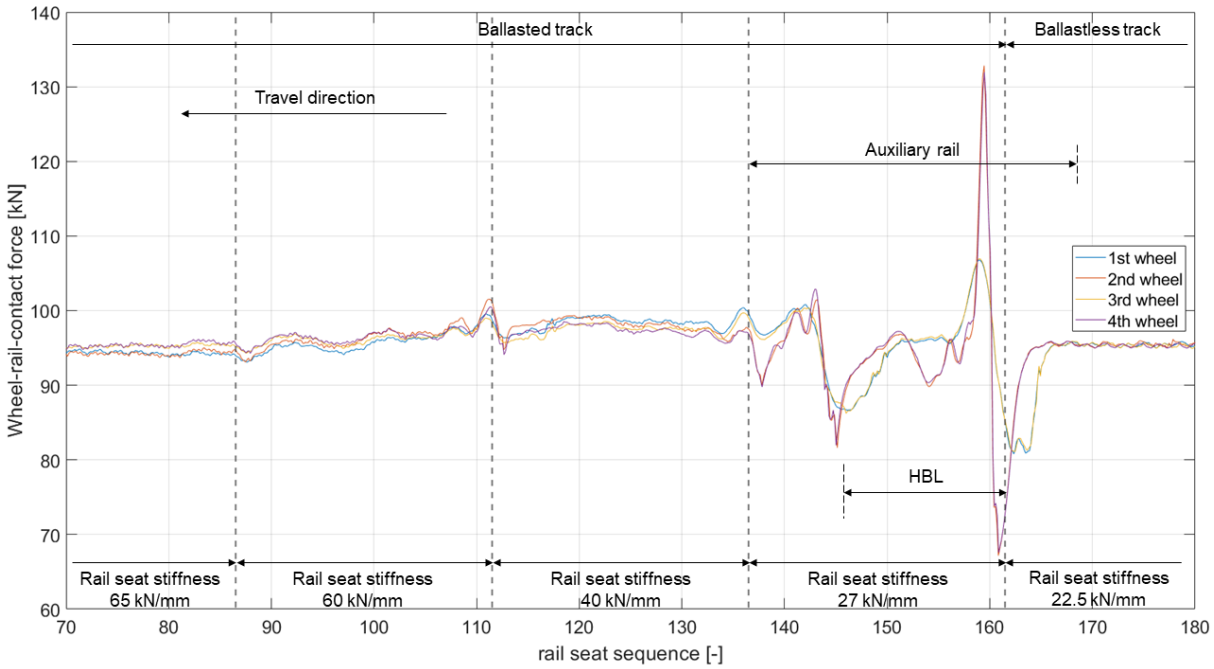

Figure 6-9: Dynamic wheel-rail contact force after 4.1 million load cycles

6.3 Modification of HBL length

6.3.1 Influence of reducing HBL length

In this chapter, the influence of HBL length on transition performance is investigated.

First the case ‘SS’ (Standard design with Shorter HBL) with 7.2 m HBL is investigated as an example to investigate the influence of reducing HBL length. Its static stiffness is shown in Figure 6-10.

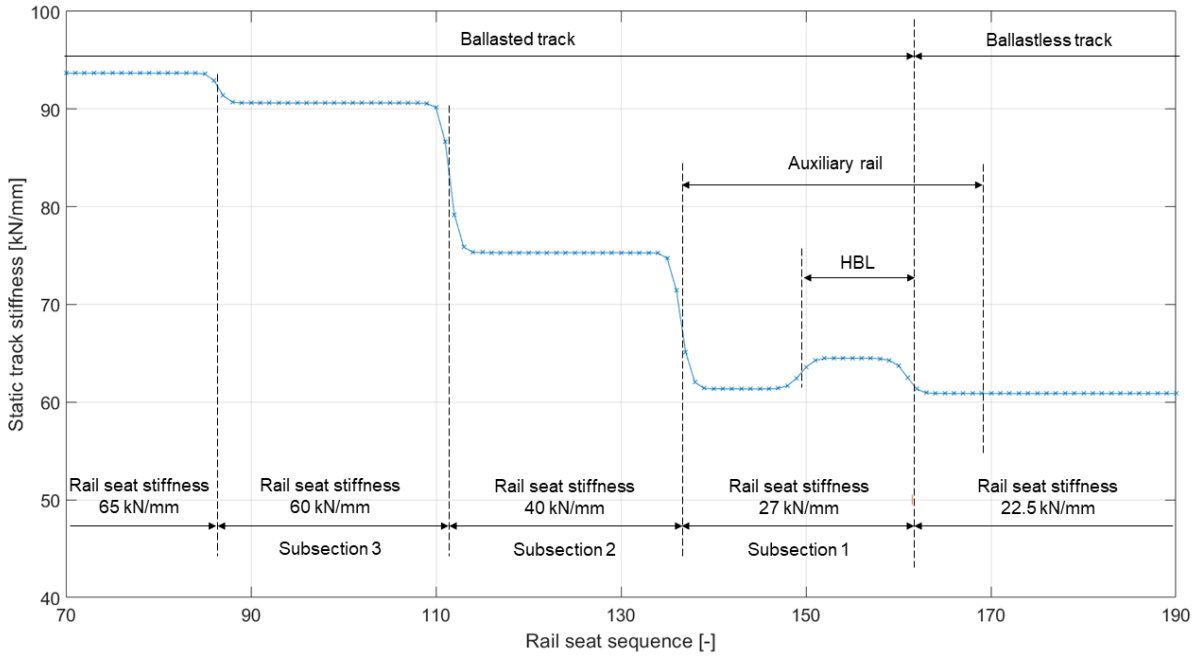

Figure 6-10: Sketch of the design plan 'SS' with 7.2 m HBL

The influence of reducing HBL length to 7.2 m on the long-term behaviour of track transition is demonstrated by Figure 6-11 and Figure 6-12, from which it can be concluded that reducing HBL length has nearly no influence on either the amplitude of dynamic WRC force or ballast settlement. It has only led to shift of the calculation results towards the new end of the HBL.

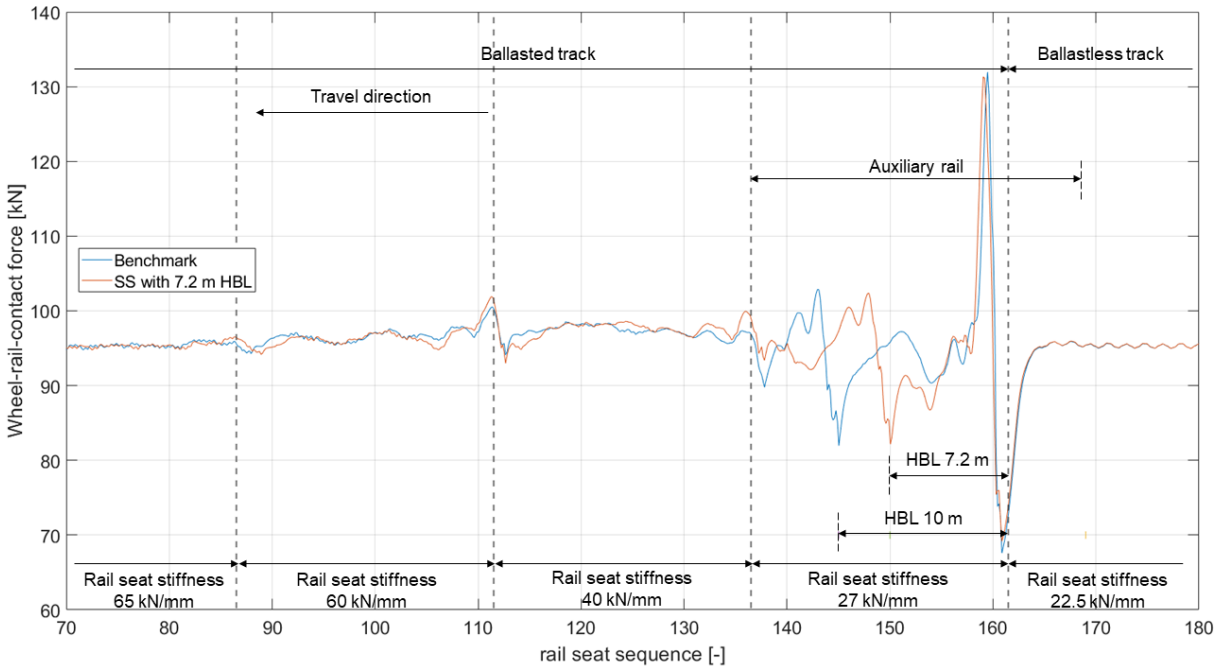

Figure 6-11: Comparison of dynamic WRC force after 80 MGT in case benchmark and 'SS'

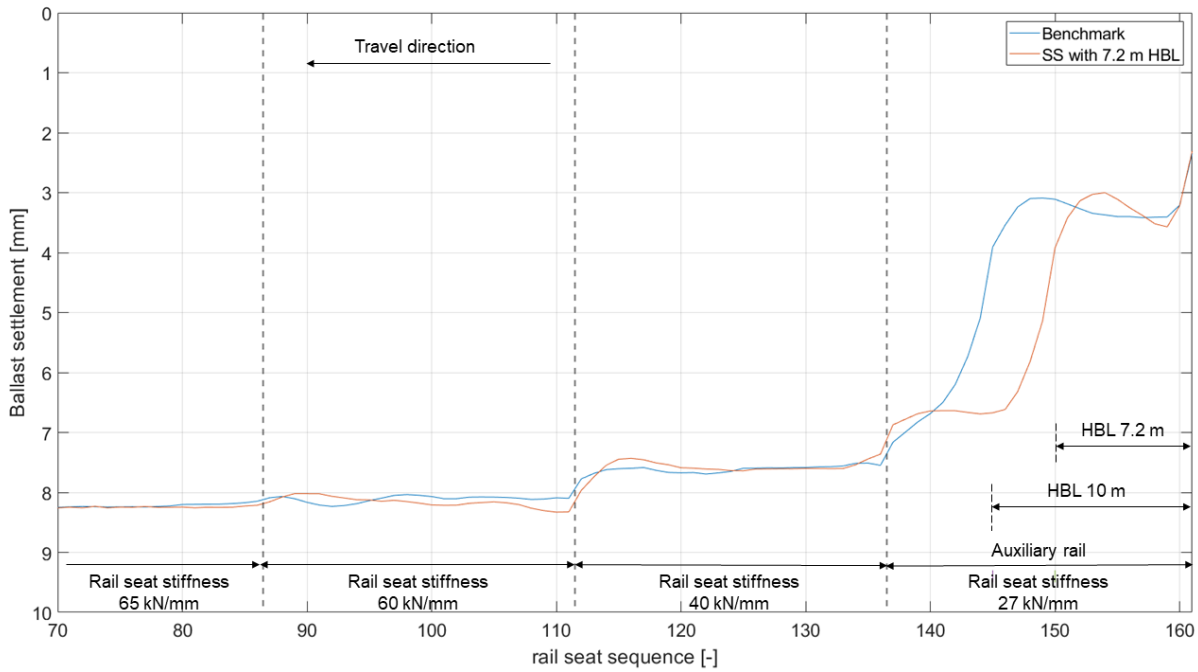

Figure 6-12: Comparison of ballast settlement after 80 MGT in case benchmark and 'SS'

6.3.2 Influence of increasing HBL length

It can be observed from the calculation results of the previous two cases (benchmark and 'SS') that the transition of the track settlement from the ballastless track to the ballasted track is almost achieved in the 1st subsection already. For example, in case benchmark, the settlement at the end of 1st subsection, the settlement has already increased from 0 to 7.55 mm, whereas the settlement has only increased to 8.23 mm afterwards along the 2nd and 3rd subsection until the open track. Consequently, the increase of dynamic WRC force is also mainly observed within the 1st subsection. It can therefore be concluded that the benchmark design has not effectively used the full length of the transition, which is to be optimized in the following context.

The aim of the new design is to enable a continuous three-step transition of ballast settlement along the whole section to achieve optimized global performance of the transition section. To accomplish this goal, the discontinuity within the 1st subsection caused by the inconsistent HBL length is eliminated first. Therefore, it is proposed to extend the HBL length to 15 m, same as the length of the 1st subsection. This design plan is designated as 'SL' (standard design with longer HBL), which is shown in Figure 6-13.

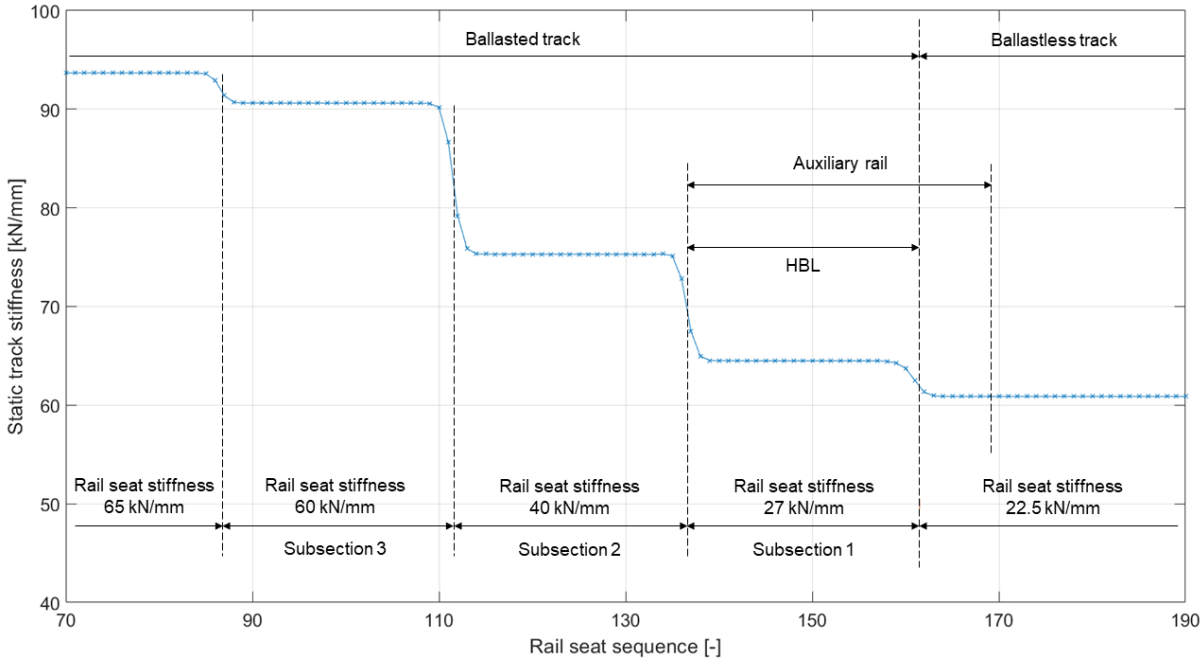

Figure 6-13: Sketch of the design plan 'SL' with 15 m HBL

Below the performance of the design plan 'SL' in long-term view is demonstrated. It can be observed that by extending the HBL to 15 m, the origin discontinuity within the 1st subsection caused by HBL is shifted to the boundary between the 1st and 2nd subsection. Compared with benchmark case, this modification has generally led to decrease of track performance locally.

As already explained, the change is intended. Extension of HBL to 15 meters makes the design stiffness within each subsection homogonous, which facilitates further optimization. It is also demonstrated in following chapters that this worsening is only temporary. By introducing other countermeasures and tuning their parameters, its negative effect vanishes.

For example, the development of ballast settlement with respect to the number of axle loadings is shown in Figure 6-14. As expected, the discontinuity within the 1st subsection is eliminated at the cost of increasing the settlement difference at the boundary between the 1st and 2nd subsection.

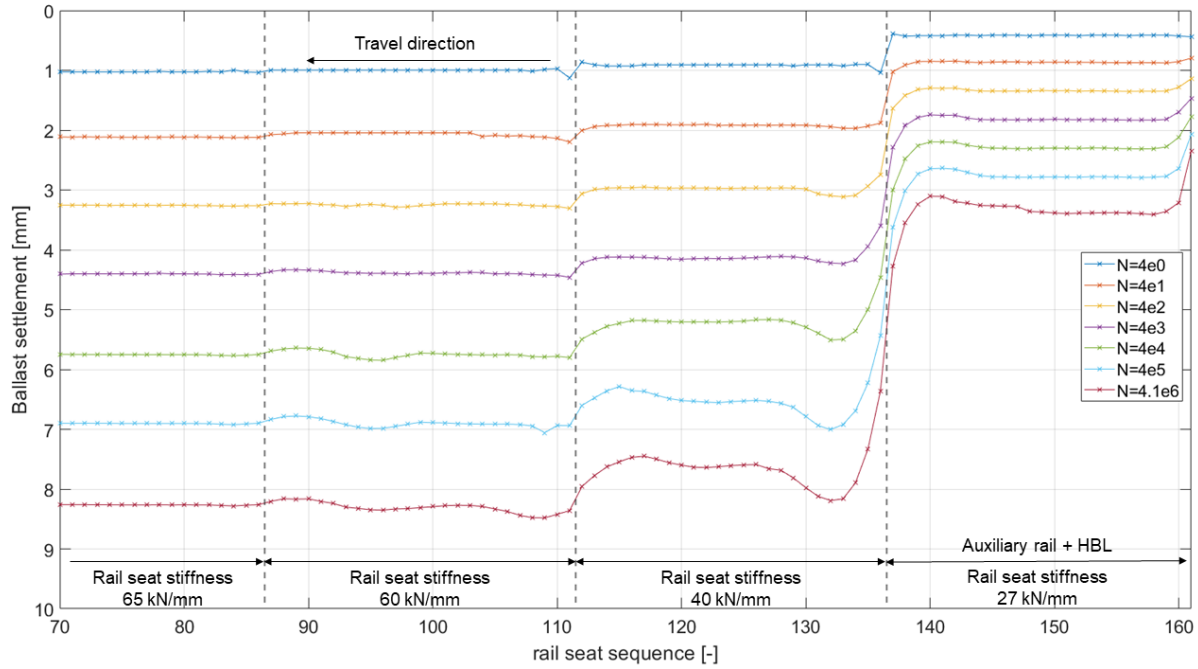

Figure 6-14: Development of ballast settlement with respect to the axle loadings in case 'SL'

As a result of the varying ballast settlement, under sleeper gaps are formed (see Figure 6-15). Compared to benchmark case, the amplitude of under sleeper gap between the ballastless track and the 1st subsection remains unchanged, whereas the amplitude of under sleeper gap between the 1st and 2nd subsection increases to 1.2 mm.

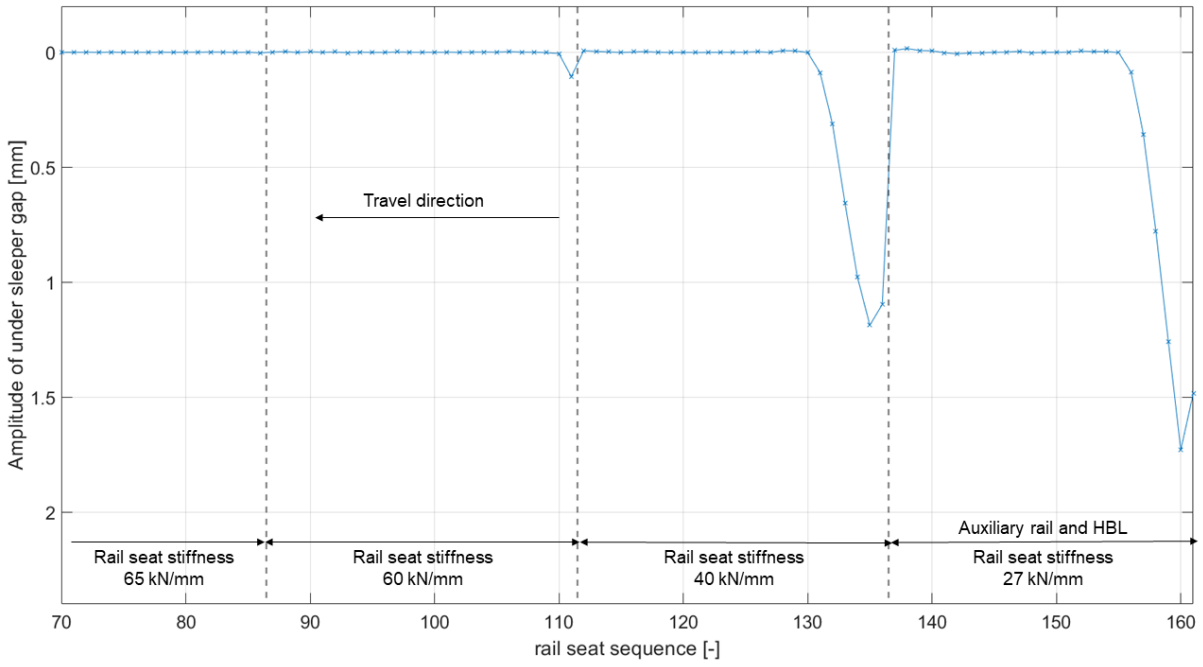

Figure 6-15: Amplitude of under sleeper gap after 4.1 million axle loadings in case 'SL'

The dynamic WRC force after 4.1 million load cycles is plotted in Figure 6-16. The maximal WRC force of 132.8 kN at the boundary between the ballasted track and the 1st subsection remains unchanged. The dynamic WRC force between the 1st subsection and the 2nd subsection increases from 100 kN to 117.2 kN.

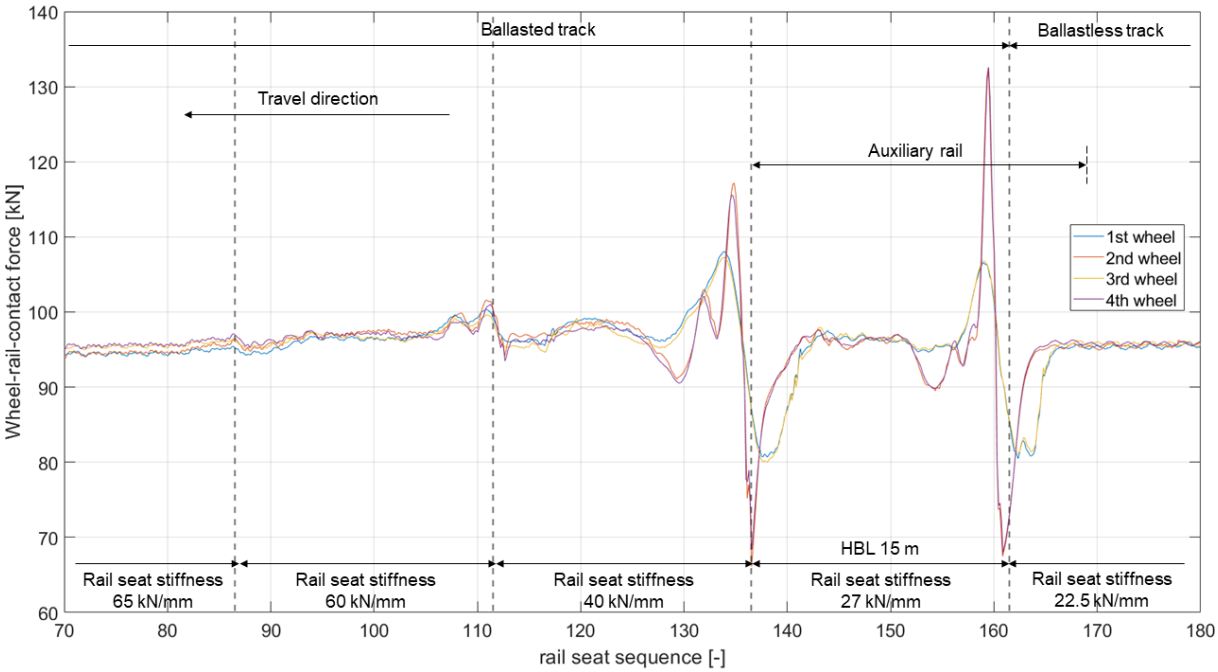

Figure 6-16: Dynamic wheel-rail contact force after 4.1 million axle loadings in case 'SL'

6.4 Optimization of the rail fastening system stiffness of auxiliary rail

As discussed in chapter 5.5, the effect of increasing the rail fastening system stiffness of auxiliary rail on the long-term behaviour of track transition is investigated to optimize design plan 'SL' in this chapter. The modification is illustrated below based on Figure 6-17.

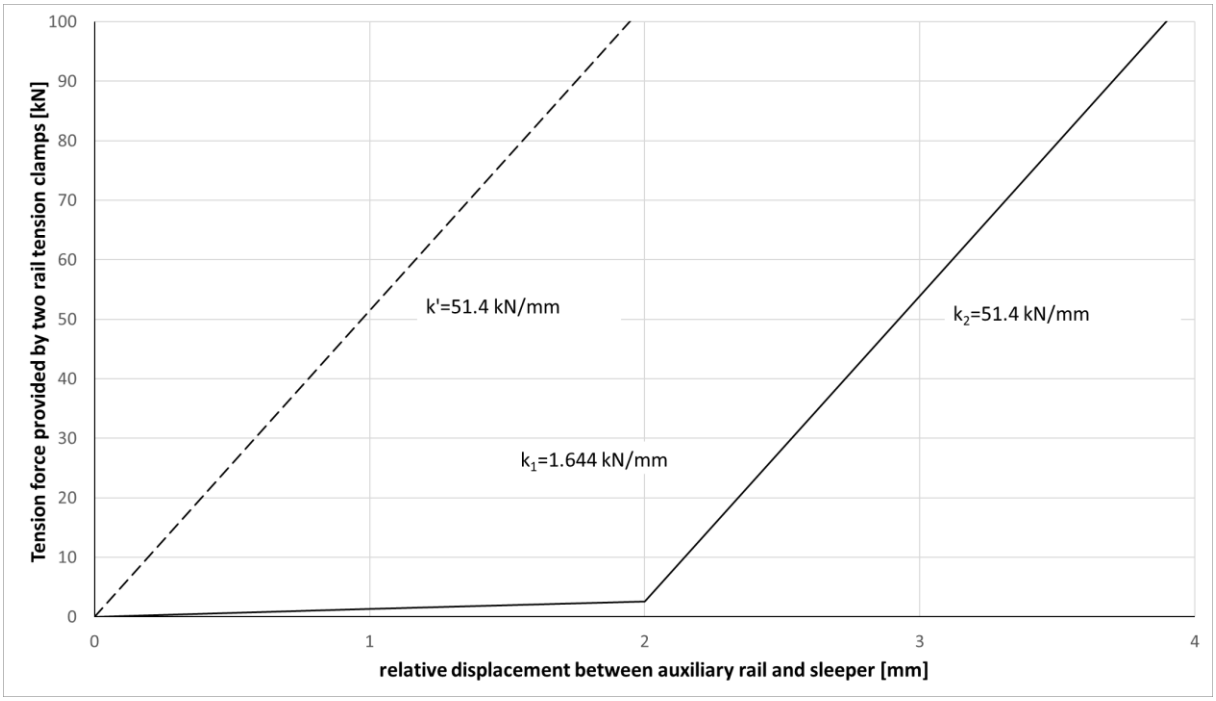

Figure 6-17: Modification of the rail fastening stiffness used in calculation

The solid curve in Figure 6-17 represents the tension stiffness of a rail fastening system with rail tension clamp SKL 24, which is a normal choice for auxiliary rails. In the first phase, when the relative deflection between auxiliary rail and sleeper is less than 2 mm, the stiffness is 1.644 kN/mm (two rail tension clamps). In the second phase, when the relative deflection exceeds 2 mm, the middle ring of the rail tension clamp contacts the rail foot and the stiffness increases to 51.4 kN/mm consequently (two rail tension clamps). In following calculation, the effect of increasing rail fastening stiffness is demonstrated by increasing the stiffness in the first phase to be the same as in the second phase (see the dashed line in Figure 6-17). This calculation case is designated as case 'FS'.

Figure 6-18 and Figure 6-19 demonstrate its positive effect on track settlement development. Compared to case 'SL', the amplitude of under sleeper gap is reduced from 1.7 mm to 1.1 mm at the 161st rail seat. It is also observed that the reduction of ballast settlement is also mainly observed at the boundary between the ballastless track and the 1st subsection, where sleepers are not fully supported. That is because increase of rail fastening stiffness helps to avoid the contact between sleepers and ballast.

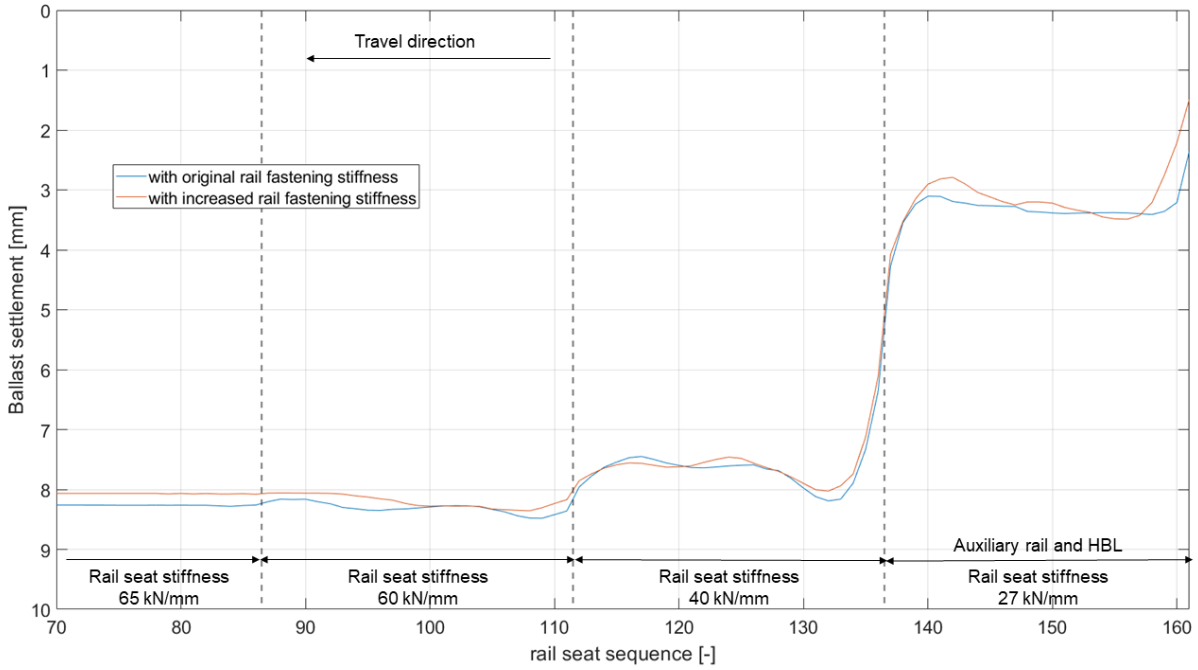

Figure 6-18: Comparison of ballast settlement after 80 MGT in case 'SL' and 'FS'

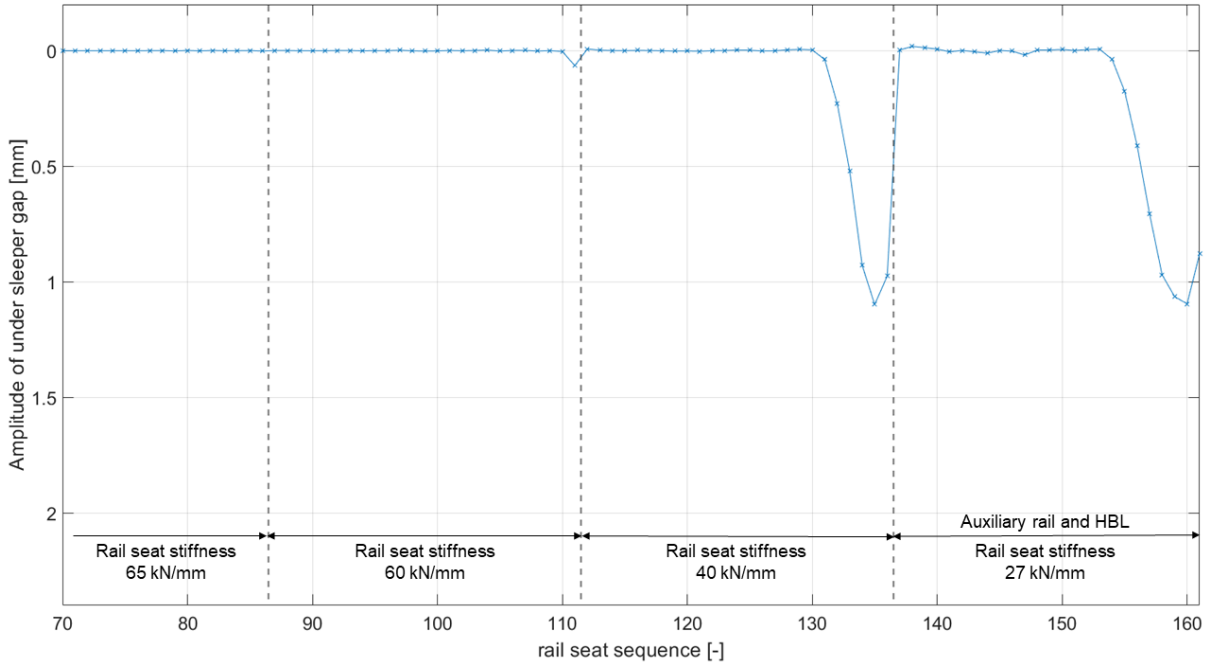

Figure 6-19: Amplitude of under sleeper gap after 4.1 million axle loadings in case 'FS'

Consequently, the dynamic WRC force there is also reduced from 132.8 kN to 113.2 kN (see Figure 6-20).

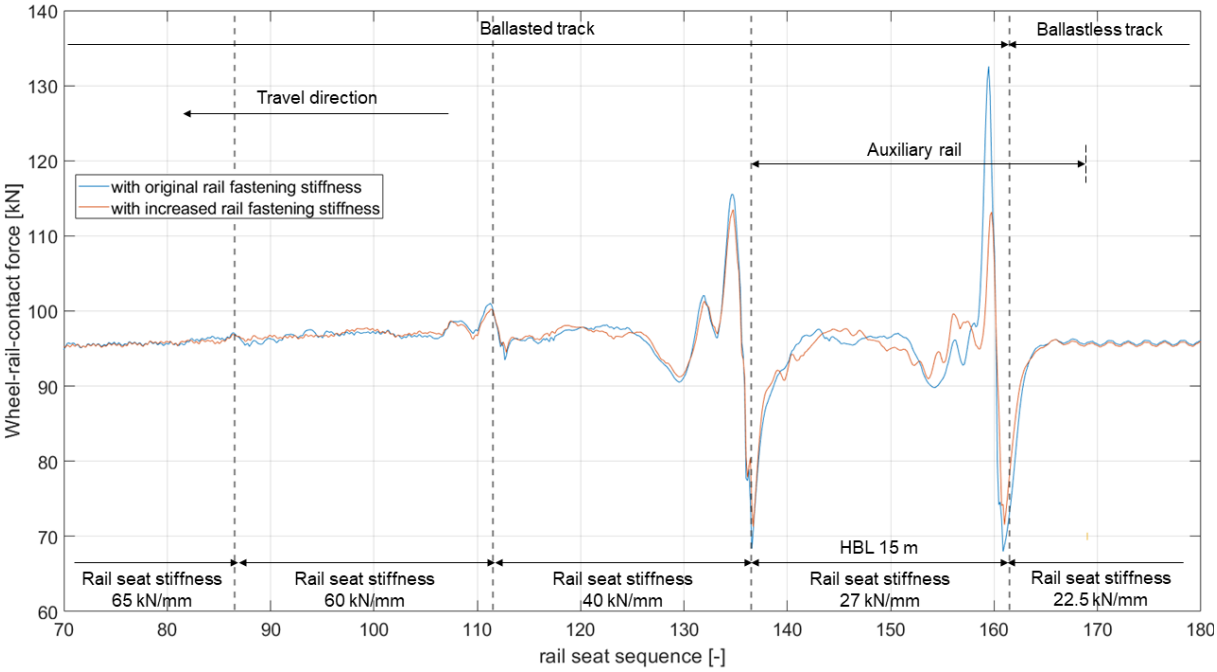

Figure 6-20: Comparison of dynamic WRC force after 80 MGT in case 'SL' and 'FS'

As conclusion of this chapter, increase the tension stiffness of rail fastening of auxiliary rail is an effective way to optimize long-term performance of transition. It is used for all following calculation. It is nevertheless worth mentioning that this modification might lead to higher requirement on the dynamic fatigue resistance of rail tension clamps. Related investigation should be performed before industrial implementation.

6.5 Optimization of auxiliary rail length and rail seat stiffness

6.5.1 Influence of stiffness difference on the long-term behaviour of track transition

To optimise track transition design, one central task is to handle the track stiffness discontinuity. Based on the analysis in chapter 5, it can be concluded that the influence of track stiffness on short-term vehicle-track interaction in track transition zone is not significant in case the track design follows the requirement of AKFF (Deutsche Bahn AG, 2002), respectively the recommendation of current standards including BetonKalender 2015 (Freudenstein et al., 2015), DB regulation Ril. 820.2020 (DB Netz AG, 2018) and the European standard DIN EN 16432-2:2017-10 (Deutsches Institut für Normung e. V., 2017). In this chapter, the influence

of track stiffness difference at track transition on the development of track settlement is demonstrated.

First, the influence is demonstrated with a simplified model shown in Figure 6-21. To underline the influence of track stiffness, auxiliary rail, extended HBL and glued ballast are not implemented. By altering the rail seat stiffness, three scenarios with different design track stiffness are created (see Table 6-4). The three calculation scenarios are designated as ‘P-300-S-S1’, ‘P-300-S-S2’ and ‘P-300-S-S3’ respectively.

Table 6-4: Summary of the parameters in the investigation

Scenario NO.	Rail seat stiffness in ballasted track [kN/mm]	Rail seat stiffness in ballastless track [kN/mm]
1	56.0	25.0
2	65.0	22.5
3	90.0	20.0

The numerical model is built similarly as described in chapter 5.4. The calculation process is the same as illustrated in chapter 6.2.1. As the first step, the initial variance of static track stiffness and static track deflection (under wheel load 95.6 kN) are calculated using Modul I of the MATLAB program as illustrated in the previous chapter. The results are summarised in Table 6-5.

Table 6-5: Calculated track stiffness and the static track deflection

Case NO.	Ballasted track stiffness [kN/mm]	Ballastless track stiffness [kN/mm]	Deflection in ballasted track [mm]	Deflection in ballastless track [mm]	Deflection variation [mm]
1	87.7	65.5	1.09	1.46	0.37
2	93.7	60.9	1.02	1.57	0.55
3	106.2	56.2	0.90	1.70	0.80

Track settlement is predicted using Modul I, II and III of the MATLAB programs.

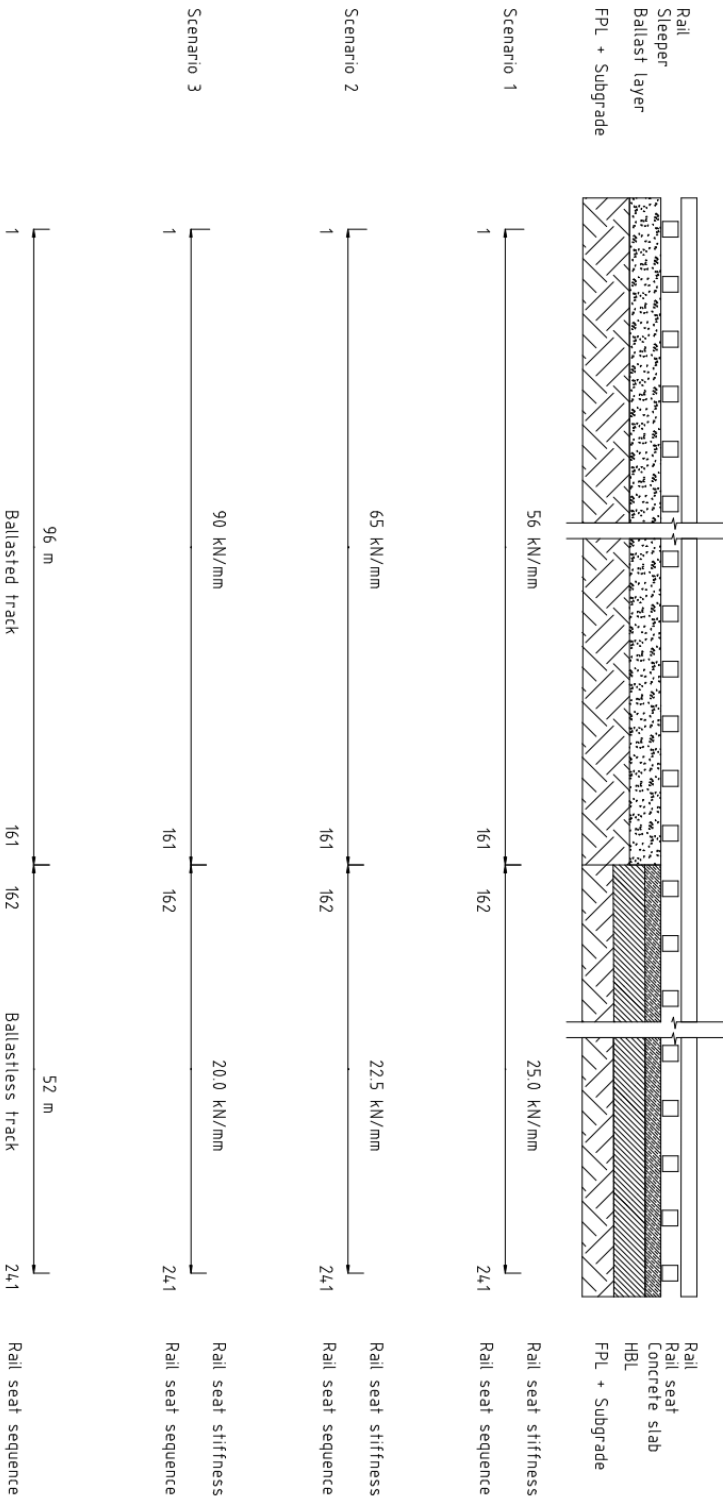

Figure 6-21: Sketch of track transition model and three calculation scenarios, not to scale

As evaluation of the Influence of designed stiffness/deflection difference on the deterioration speed of track quality at track transition, development of SR-value with respect to axle loading in three cases are demonstrated in Figure 6-22. With the increase of the designed deflection difference, the deterioration of track geometry accelerates. The number of experienced axle loadings before exceeding the SR_{lim} value in case 1, 2 and 3 is $3x10^5$, $1.2x10^5$ and $5x10^4$, respectively.

The calculation results illustrate the significant influence of designed deflection difference on the deterioration speed of track geometry. It is proved theoretically that reduction of designed deflection difference can reduce the speed of track longitudinal level deterioration.

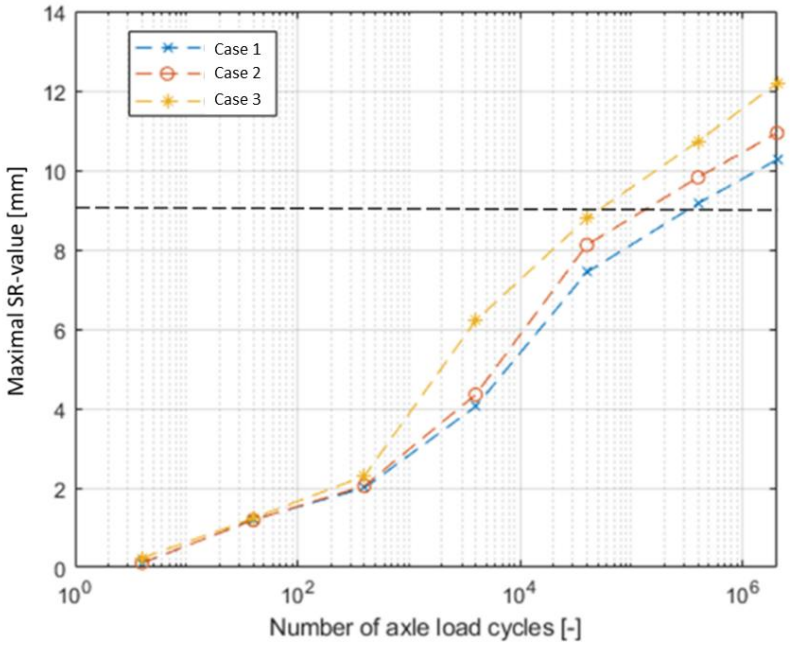

Figure 6-22: Influence of designed deflection difference on the development of SR-value, the horizontal dash line indicates the SR_{lim} value in this case 9 mm

6.5.2 Determination of rail seat stiffness based on aimed static deflection

The purpose of this chapter is to determine the aimed rail seat stiffness distribution. The distribution of track transition stiffness can be described by following parameters:

- Number of subsections: n
- Rail seat stiffness in each subsection: $k_1, k_2, \ldots k_n$.

Based on the assumption that the total deflection difference between the ballasted track and the ballasted track is equally distributed among the subsections, rail seat stiffness can be determined following the steps below:

1. First, determine the number of subsections n.
2. Then, the static deflection of each subsection is determined by uniform interpolation between the static deflection of the ballasted track (1.02 mm) and the ballastless track (1.57 mm) as in formula (17).
3. Based on the bedding modulus and the desired static deflection s_i, the rail seat stiffness $k_1, k_2, \ldots k_n$ are determined.

$$s_i = 1.02 + \frac{1.57 - 1.02}{n + 1} * \mathrm{i} \qquad (17)$$

with

n: Number of subsections [-]

i: Sequence of the subsection, $i = 1,2, \ldots n,$

s_i: Static deflection of i_{th} subsection [m]

To facilitate step 3, the relationship between rail seat stiffness and static track deflection with given bedding modulus is firstly determined and plotted as curves. Later, the design rail seat stiffness can be directly read from the figure when the bedding modulus and desired track deflection are determined.

For this purpose, the same point-load-on-track model as proposed in chapter 5.3 is employed. The deflection has been determined with bedding modulus 0.10 N/mm^3 (normal subgrade) and 0.16 N/mm^3 (HBL) respectively. The stiffness of rail seat ranges from 22.5 kN/mm to 65 kN/mm.

The calculation process is as follows:

1. Apply selected rail seat stiffness and bedding modulus
2. Bring track to equilibrium under self-weight
3. Apply a point load of 95.6 kN on the rail seat in the middle of the track.
4. Calculate track stiffness according to formula (15) proposed in chapter 5.3.

The calculated results are shown in Figure 6-23.

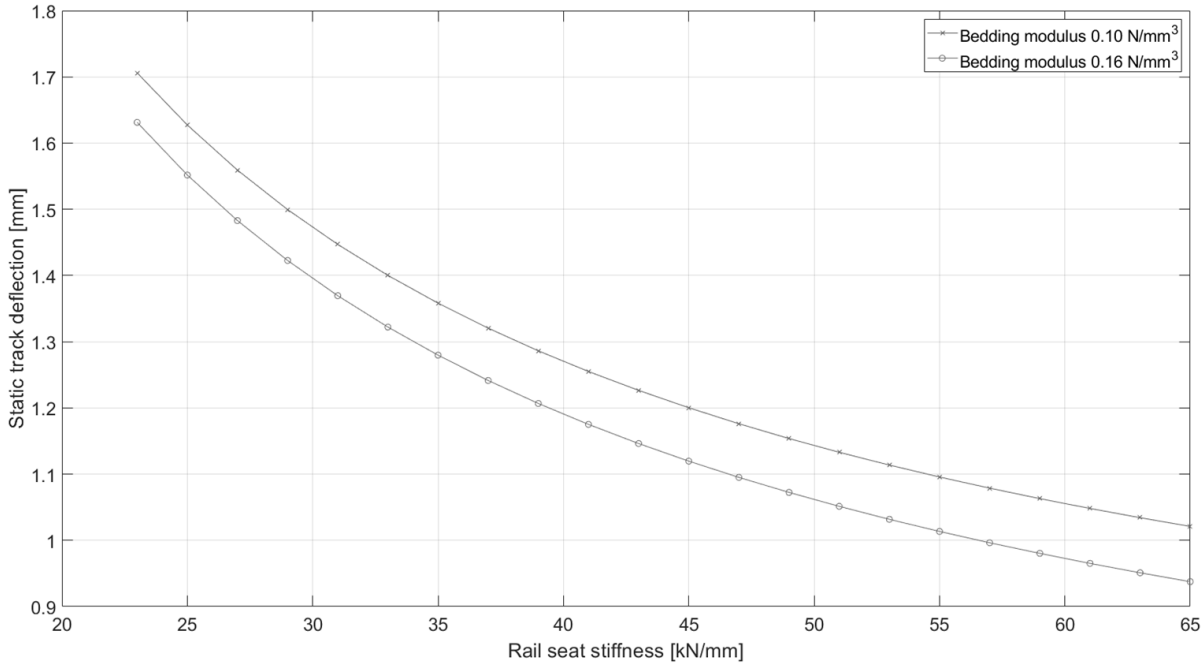

Figure 6-23: Relationship between rail seat stiffness and static track deflection with given bedding modulus

6.5.3 Investigation of the design variations

In this chapter, the short-term and long-term performance of the three new design plans ‘L12’, ‘L123’ and ‘L1234’ based on plan ‘FS’, are proposed and evaluated. The target rail seat stiffness is determined according to the method proposed in chapter 6.5.2. The result is summarised in Table 6-6. The three plans are demonstrated in Figure 6-24. It should be noticed that the static rail stiffness in the three design plans is the same, which is not influenced by how the auxiliary rail is montaged (see the discussion in chapter 5.5).

Table 6-6: Parameters of the design plan ‘L12’, ‘L123’ and ‘L1234’

Section	Static deflection (wheel load 95.6 kN) [mm]	Rail seat stiffness [kN/mm]	Bedding modulus [N/mm³]	Length [m]
Ballasted track	1.02	65	0.10	-
Subsection 3	1.16	48	0.10	15
Subsection 2	1.30	38	0.10	15
Subsection 1	1.44	28	0.16	15
Ballastless track	1.57	22.5	0.30	-

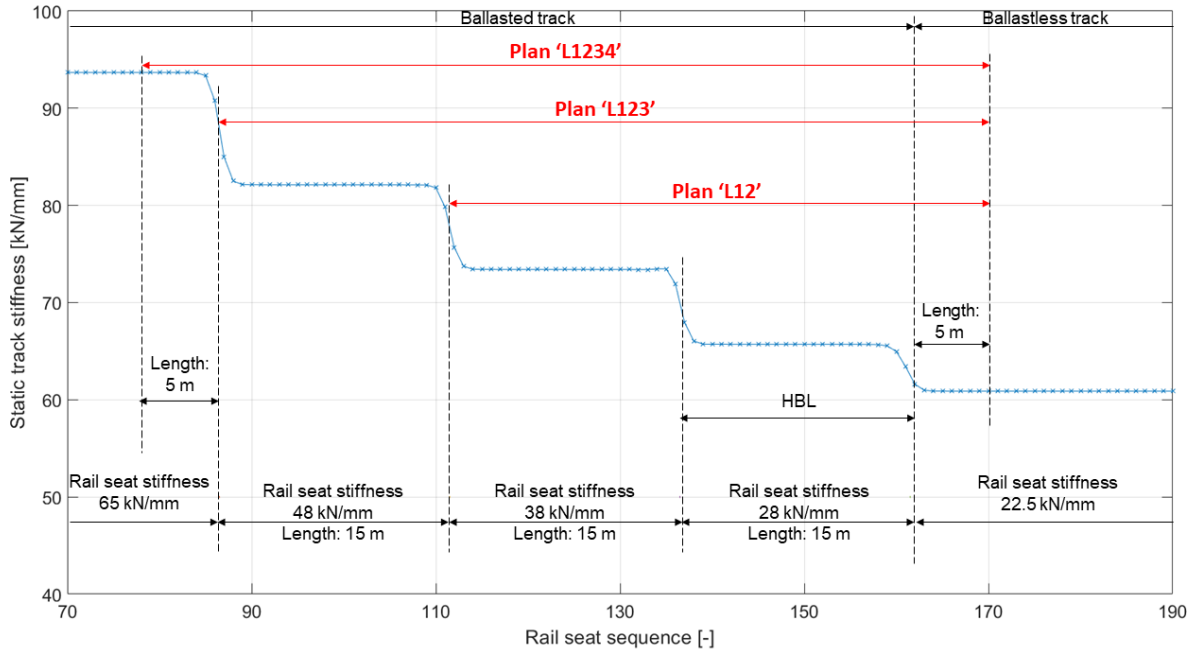

Figure 6-24: Design plan ‘L12’, ‘L123' and ‘L1234’ with position of auxiliary rail indicated

In Table 6-7, distribution of rail seat stiffness in plan ‘FS’ is compared with in new plan. It can be concluded, to achieve the continuous change of static track deflection, the difference of rail seat stiffness between subsection 3 and ballasted open track is increased from 5 kN/mm to 17 kN/mm. It is therefore inferred that such a new design can reduce the global maximum of dynamic factor, at the cost of increase of local maximum at the boundary between subsection 3 and open track. Its effect is validated through long-term calculation below.

Table 6-7: Comparison of rail seat stiffness in plan 'SL' and in the new plans

Section	Plan 'L12', 'L123' and 'L1234'		Plan 'FS'	
	Rail seat stiffness [kN/mm]	Difference to previous subsection [kN/mm]	Rail seat stiffness [kN/mm]	Difference to previous subsection [kN/mm]
Ballasted track	65	-	65	-
Subsection 3	48	17	60	5
Subsection 2	38	10	40	20
Subsection 1	28	10	27	13
Ballastless track	22.5	5.5	22.5	4.5

The long-term calculation is performed following the same process as described in chapter 6.2.1, so only the calculation results are demonstrated here.

In Figure 6-25, ballast settlement in these three cases after 4.1 million axle loadings are compared with each other. The difference between these three design plans lies merely in the length of auxiliary rail. In all three plans, the rail seat stiffness determined in Table 6-6 is used.

Comparing the results of plan 'L12' with plan 'L123', the settlement in plan 'L12' experiences an abrupt change at the boundary between subsection 2 and 3 (see Figure 6-25). Since the only difference between these two plans is the range of auxiliary rail, the role of auxiliary rail to distribute ballast pressure and to mitigate settlement difference is thereby proved. Comparing the results of plan 'L123' with plan 'L1234', the settlement in plan 'L1234' has generally reduced the settlement, but it has also led to an extra settlement near its end in the ballasted track. It is caused by the extension of auxiliary rail into the ballast track, which leads to the variance of ballast pressure distribution there.

Based on the ballast settlement, amplitude of under sleeper gap in each case can be determined. The maximal under sleeper gap in all cases are found at the boundary between the ballastless track and subsection 1. The amplitude amounts to 0.59 mm, 0.57 mm and 0.68 mm in case 'L12', 'L123' and 'L1234'. Besides, under sleeper gap of 0.15 mm can also be found in case 'L1234' at the end of the auxiliary rail in the ballasted track. From this point of view, plan 'L123' is the most optimal variance.

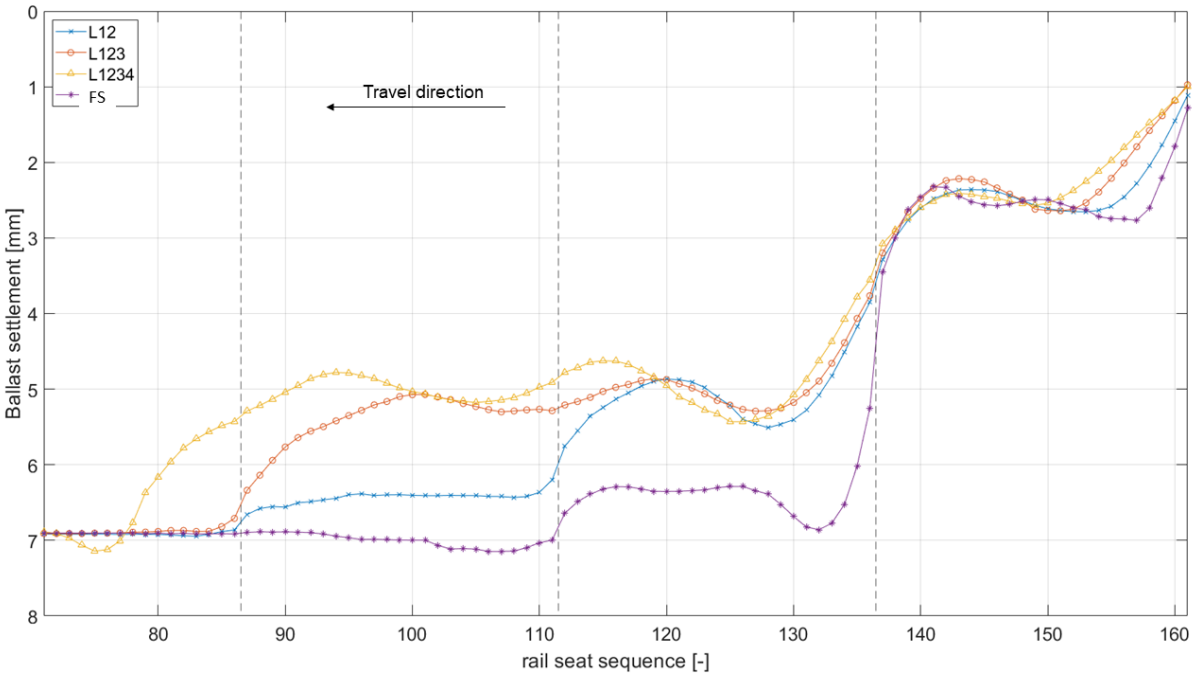

Figure 6-25: Comparison of ballast settlement after 4.1 million load cycles in the case 'FS', case 'L12', 'L123' and 'L1234'

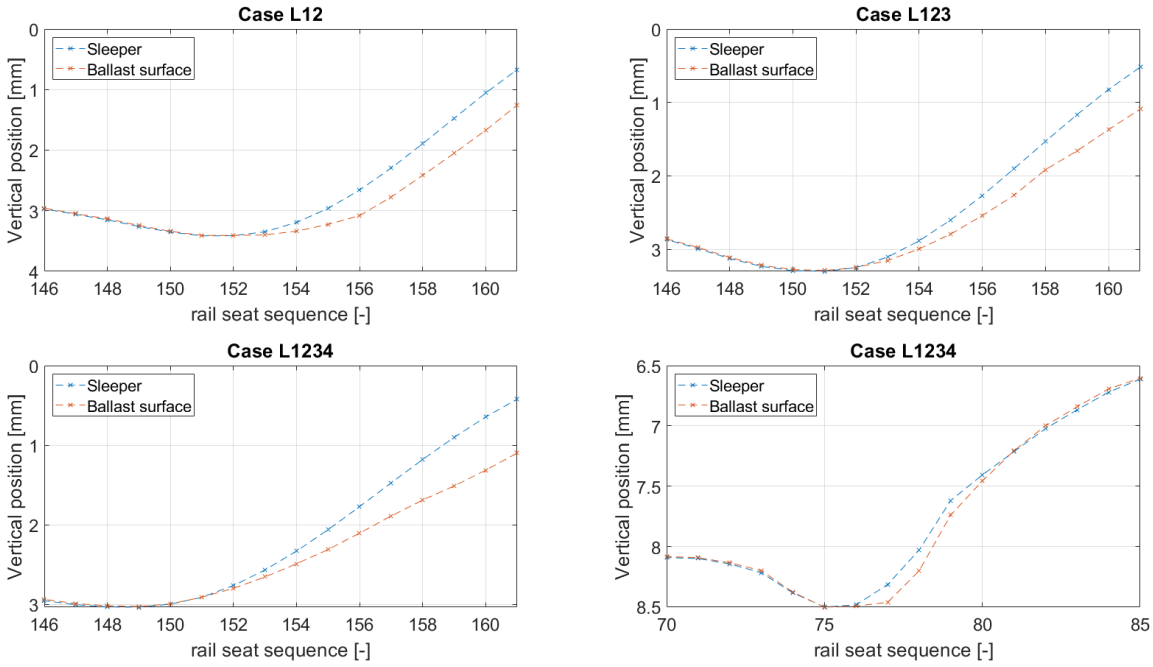

Figure 6-26: Under sleeper gap in case 'L12', 'L123' and 'L1234' after 4.1 million axle loadings

As evaluation of the influence of different transition design on track quality, the dynamic WRC force after 4.1 million load cycles in case 'L12', 'L123' and 'L1234' are compared with each

other in Figure 6-27. The maximal dynamic factor in case ‘L12’ is 12.3 %, whereas the maximal dynamic factor in case ‘L123’ is 3.9 %, both of which are lower than 20.5 % in case ‘FS’ (see Figure 6-20). The dynamic factor in case ‘L1234’ is 5.3%, which is higher than in case ‘L123’ but lower than ‘L12’. Besides in case ‘L1234’, additionally dynamic load can be observed at the end of auxiliary rail in the ballasted track. In all three cases, the dynamic load at the exit of the transition to the ballasted track increases compared to case ‘FS’, while the design stiffness difference there increases. The amplitude of the dynamic effect is nevertheless low. The comparison demonstrates that all the three new design improves the long-term behaviour of track transition, among which ‘L123’ is the most effective.

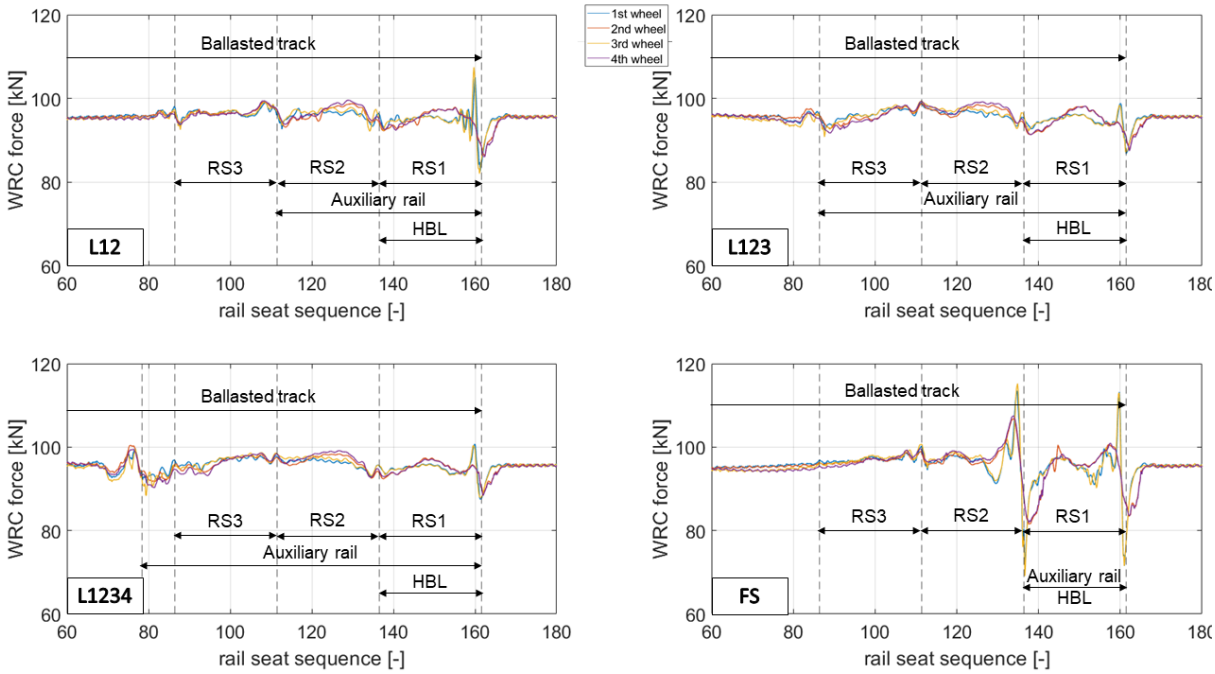

Figure 6-27: Dynamic WRC force (all 4 wheelsets) after 4.1 million axle loadings in case ‘L12’, ‘L123’, ‘L1234’ and ‘FS’

The effect of auxiliary rail on preventing the deterioration of track longitudinal level is also demonstrated in Figure 6-28 by the SR values in all three cases. Compared with the other cases, the maximal SR value after 4.1 million load cycles in case ‘L1234’ is the smallest.

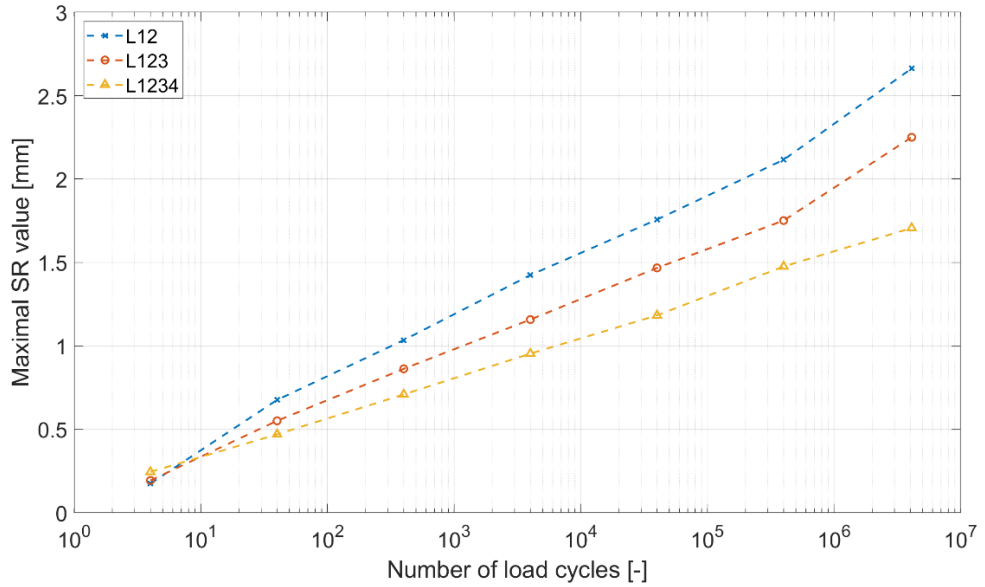

Figure 6-28: Development of maximal SR value of longitudinal level in three cases

The analysis shows that conclusion drawn based on dynamic factor and based on maximal SR value does not always consistent with each other. SR value is determined along a spatial interval (8.6 m in this case), while dynamic factor is directly related with the local wheel acceleration during train run. In Figure 6-29, the vertical acceleration of the first wheelset in three cases are compared, which can further prove this explanation. Since dynamic factor is a more direct parameter, it is used as the criterion in case of conflict.

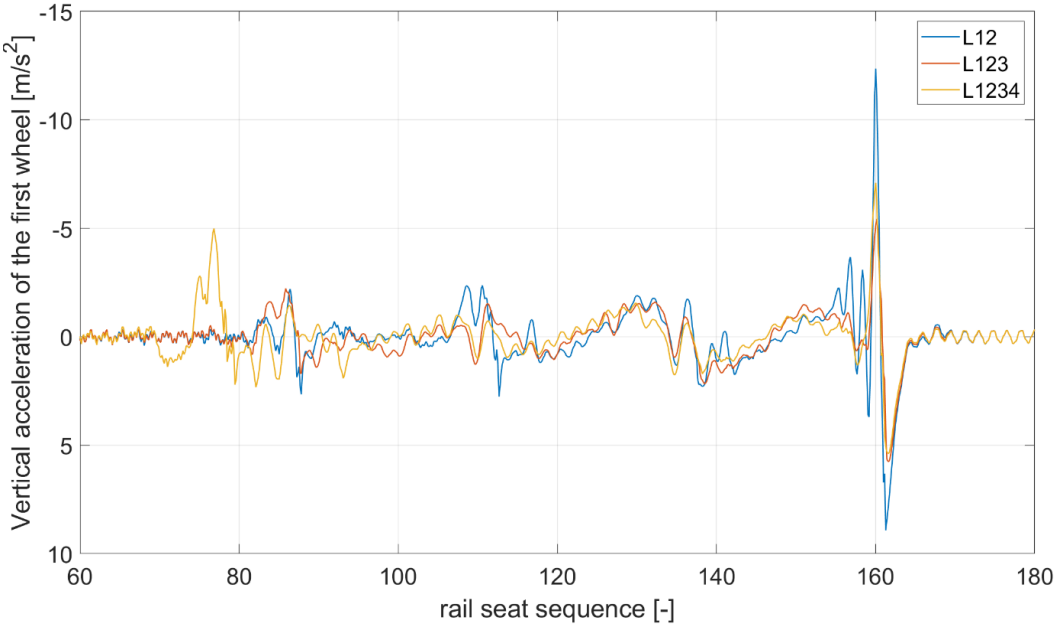

Figure 6-29: vertical acceleration of the first wheelset in case 'L12', 'L123' and 'L1234' (deteriorated track after 4.1 million axle loading)

6.6 Implementation of USP

In this chapter, it is investigated to further optimise the plan “L123” by implementation of USP. Two variations ‘L123_U’ and ‘L123_U2’ are investigated. In plan ‘L123_U’, USP with bedding modulus of 0.2 N/mm^3 is implemented along subsection 1 and 2 (see Figure 6-30), while in plan ‘L123_U2’, USP (0.2 N/mm^3) is implemented along subsection 2, and USP (0.1 N/mm^3) is implemented along subsection 1, see Figure 6-31. The reason of implementation of USP with different stiffness is that according to Zimmermann’s theory (Freudenstein, 2020b), USP with lower bedding modulus helps to distribute the rail seat force better along rail seats, which leads to decreased ballast pressure and settlement.

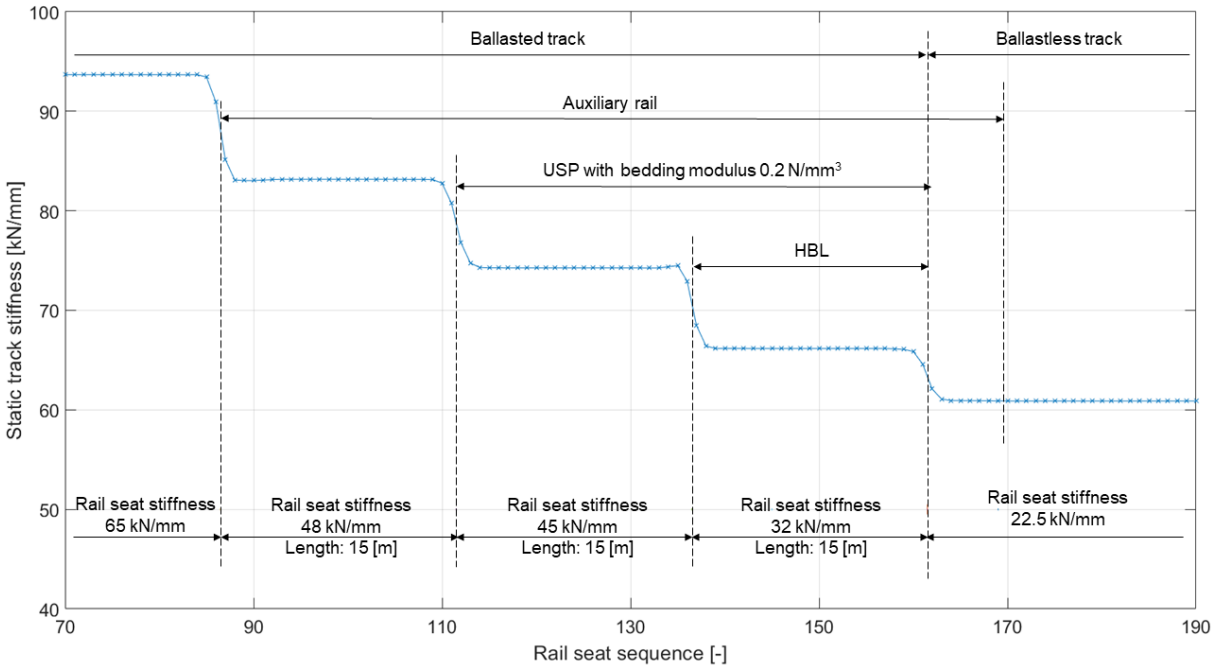

Figure 6-30: Overview of plan ‘L123_U’

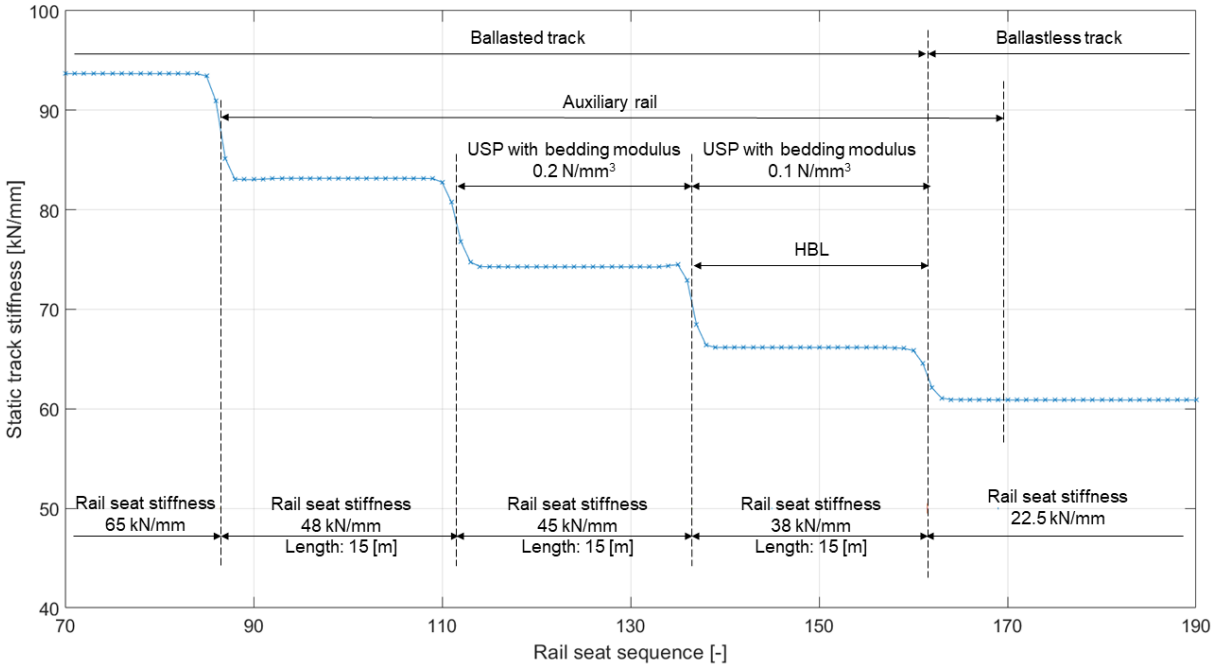

Figure 6-31: Overview of plan 'L123_U2'

Since implementation of USP changes track stiffness, the rail seat stiffness must be adjusted again to achieve the aimed track stiffness. The new design rail seat stiffness in both cases is demonstrated in Table 6-8, in Figure 6-30 and Figure 6-31.

Table 6-8: Rail seat stiffness in plan 'L123_U' and 'L123_U2'

Section	Plan 'L12', 'L123' and 'L1234'		Plan 'L123_U'		Plan 'L123_U2'	
	Rail seat stiffness [kN/mm]	Bedding modulus of USP [N/mm³]	Rail seat stiffness [kN/mm]	Bedding modulus of USP [N/mm³]	Rail seat stiffness [kN/mm]	Bedding modulus of USP [N/mm³]
Ballasted track	65	-	65	-	65	-
Subsection 3	48	-	48	-	48	-
Subsection 2	38	-	45	0.2	45	0.2
Subsection 1	28	-	32	0.2	38	0.1
Ballastless track	22.5	-	22.5	-	22.5	-

The USP is simulated in the numerical model by adding an addition spring between sleepers and the ballast layer at corresponding rail seats (see Figure 6-32). The spring constant is

determined as the product of its bedding modulus and the contact area. Because the damping of USP is not available, it is here assumed that the damping between ballast and sleeper did not change after installing USP. The results lie therefore on the safe side. Influence of USP on the long-term is introduced into simulation by reducing the pressure on ballast layer by 25% (Loy, 2008).

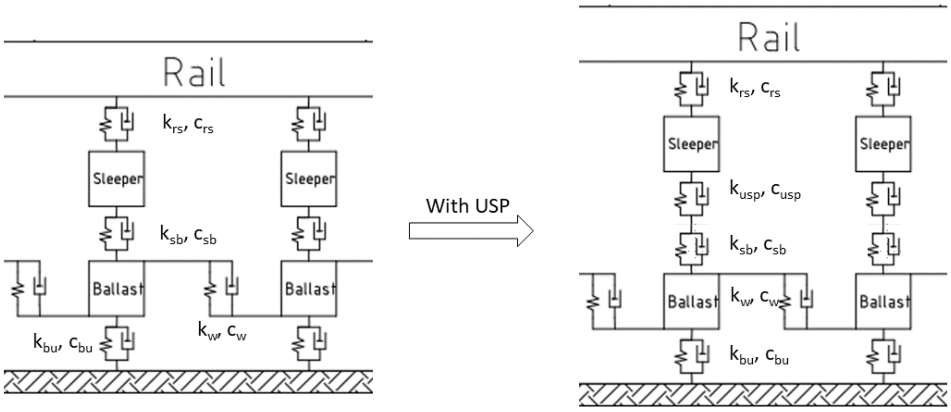

Figure 6-32: Simulation of USP in the numerical model (see chapter 3.1 for the meaning of symbols)

The long-term performance of plan ‘L123_U’, plan ‘L123_U2’ and plan ‘L123’ are compared in Figure 6-33, Figure 6-34 and Figure 6-35. In Figure 6-33, it can be observed that the implementation of USP has noticeably reduced the ballast settlement in the corresponding subsections. The difference of ballast settlement between adjacent subsections are nearly homogeneous in plan ‘L123_U’ and plan ‘L123_U2’. The under sleeper gap is further reduced to 0.5 mm in both cases. Nevertheless, the effect of adjusting USP bedding modulus is not significant. The same conclusion can be drawn when analysing dynamic WRC force and deterioration of track longitudinal level.

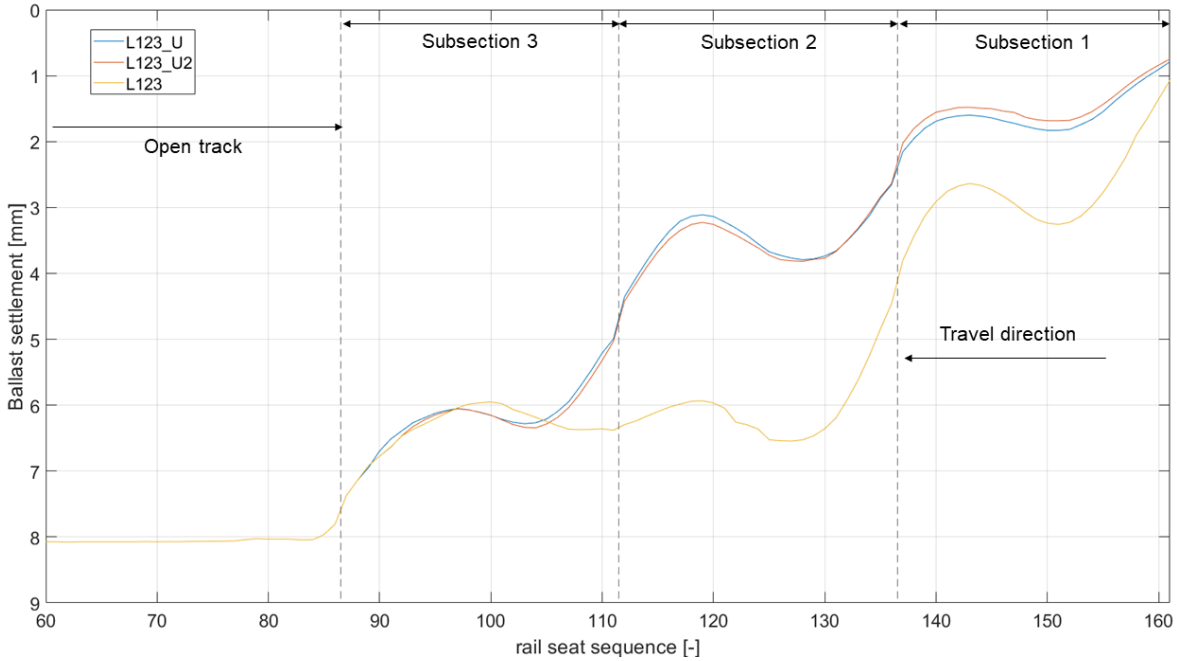

Figure 6-33: Ballast settlement after 4.1 million load cycles in case 'L123', 'L123_U' and 'L123_U2'

As a result of the implementation of USP, the maximal SR-value of longitudinal level after 4.1 million axle loadings decreases from 2.25 mm in case 'L123' to 1.78 mm in both case 'L123_U' and case 'L123_U2' (see Figure 6-34).

When vehicle travels from the ballastless track to the ballasted track, the wheelset moves downwards due to ballast settlement, and the dynamic WRC force therefore decreases. Implementation of USP has reduced the settlement of the ballast layer and therefore mitigate the decrease of WRC force. The minimal value of the dynamic WRC force has been increased from 86.85 kN in case 'L123' to 89.4 kN in case 'L123_U' and 90.6 kN in case 'L123_U2' (static wheel load: 95.6 kN). Nevertheless, the increase of dynamic load at the exit of the transition should be noticed.

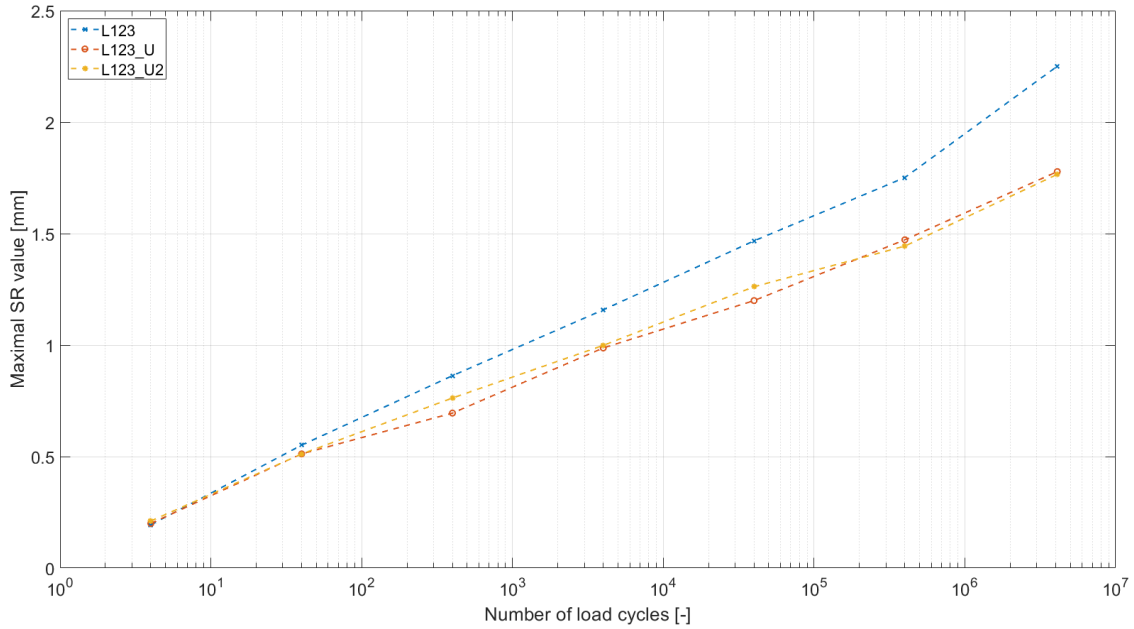

Figure 6-34: Development of maximal SR value of longitudinal level in case'L123', 'L123_U' and 'L123_U2'

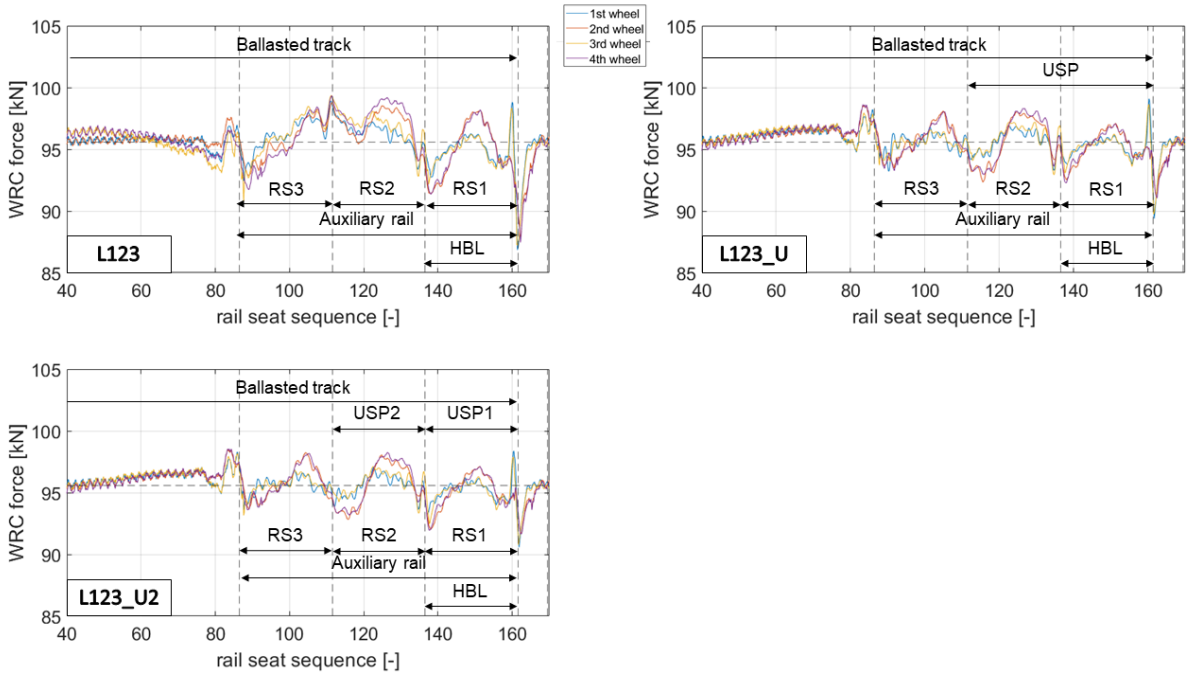

Figure 6-35: Dynamic WRC force after 4.1 million load cycles in case 'L123', 'L123_U' and 'L123_U2', the horizontal line indicates the static wheel load

In this case, the effect of USP can be better understood by statistic evaluation of dynamic WRC force distribution along the whole track section. For this purpose, the coefficient of variation

(CV) of the dynamic WRC load is calculated, which equals to the division of the standard deviation by the mean value. The results are summarised in Table 6-9, from which the improvement brought by the implementation of USP with different bedding modulus can be observed.

Table 6-9: statistic evaluation of the dynamic WRC force in four cases

	Mean [kN]	Standard deviation [kN]	coefficient of variation [%]
Case 'P-300-S-FS'	95.77	3.97	4.14
Case 'P-300-S-L123'	95.62	1.78	1.86
Case 'P-300-S-L123_U'	95.54	1.21	1.27
Case 'P-300-S-SL123_U2'	95.55	1.16	1.22

6.7 Investigation of the influence of the travel direction

Until the previous chapter, the performance of track transition has always been investigated under traffic travelling from the ballastless track to the ballasted track. In this chapter, it is proved that the proposed new design plan is also effective under traffic load in the other direction. For this purpose, the performance of the benchmark design plan and the proposed new design plan 'L123_U2' are compared under following condition:

- Vehicle type: passenger power car
- Travel direction: from the ballasted track to the ballastless track
- Speed: 300 km/h.

As in previous chapters, totally 4.1 million axle loadings corresponding to 80 MGT traffic load are introduced. The calculated dynamic WRC force of the 4 wheelsets after 4.1 million axle loadings is shown in Figure 6-36.

It can be observed that along the benchmark transition, the maximal dynamic WRC force is observed at the boundary between the ballastless track and the 1st subsection, and at the end of HBL within the 1st subsection. The design plan 'L123_U2' has eliminated the extreme values at these positions by spreading it along the whole transition section. Especially, it has led to the increase of dynamic WRC force at the boundary between open track and subsection 3, while the difference of rail seat stiffness is increased from 5 kN/mm in Benchmark plan to 17

kN/mm in plan ‘L123_U2’. Nevertheless, the overall dynamic factor is reduced from 17.7 % in case benchmark to 6.8 % in case ‘L123_U2’. Averaged over the 4 wheelsets, the coefficient of variation of dynamic WRC force is also reduced, from 2.44 in case benchmark to 1.14 to case ‘L123_U2’.

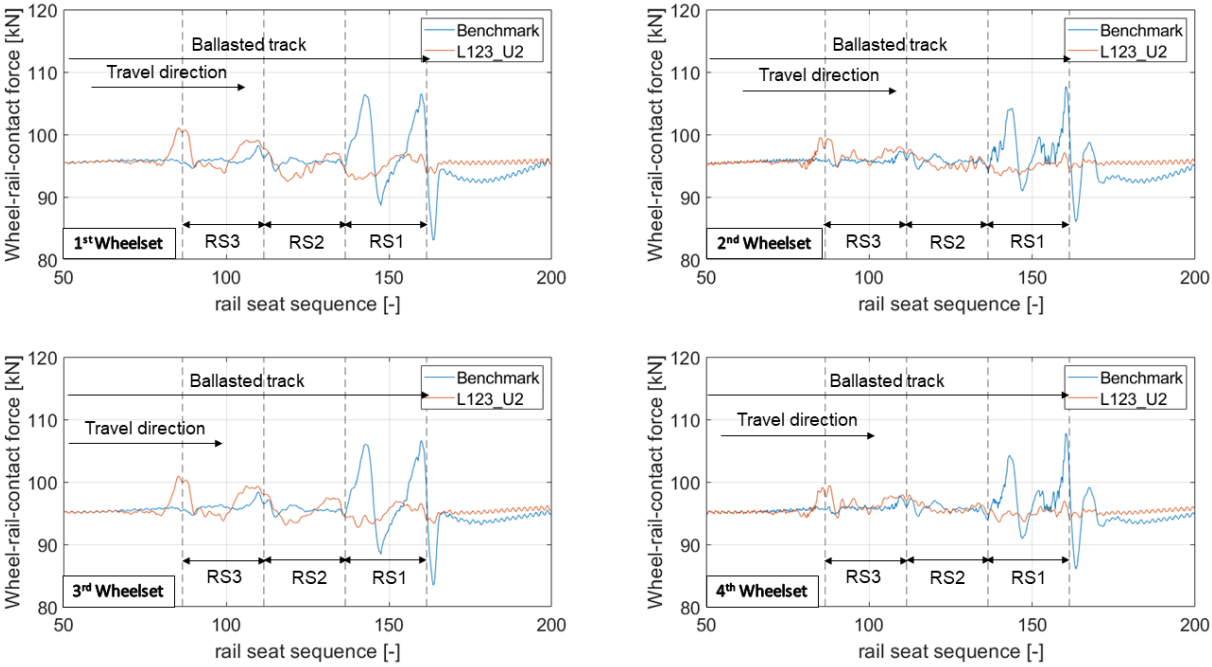

Figure 6-36: Comparison of dynamic WRC force after 4.1 million axle loadings in case benchmark and ‘L123-U2’

The settlement of ballast layer after 4.1 million axle loadings is shown in Figure 6-37. When the track transition is built according to the benchmark plan ‘SL’, the settlement changes insignificantly from the open track to subsection 2. But afterwards, large settlement difference at the end of HBL, and between subsection 1 and the ballastless track can be observed. In comparison, implementation of the design plan ‘L123_U2’ led to more homogenous, quasi-3-step change of ballast settlement. The decrease of settlement difference at the end of HBL and between subsection 1 and the ballastless track explains why the dynamic WRC force at both positions is reduced. But as mentioned above, the enlarged settlement difference at the entrance of the 3rd subsection has also caused the increase of WRC force there.

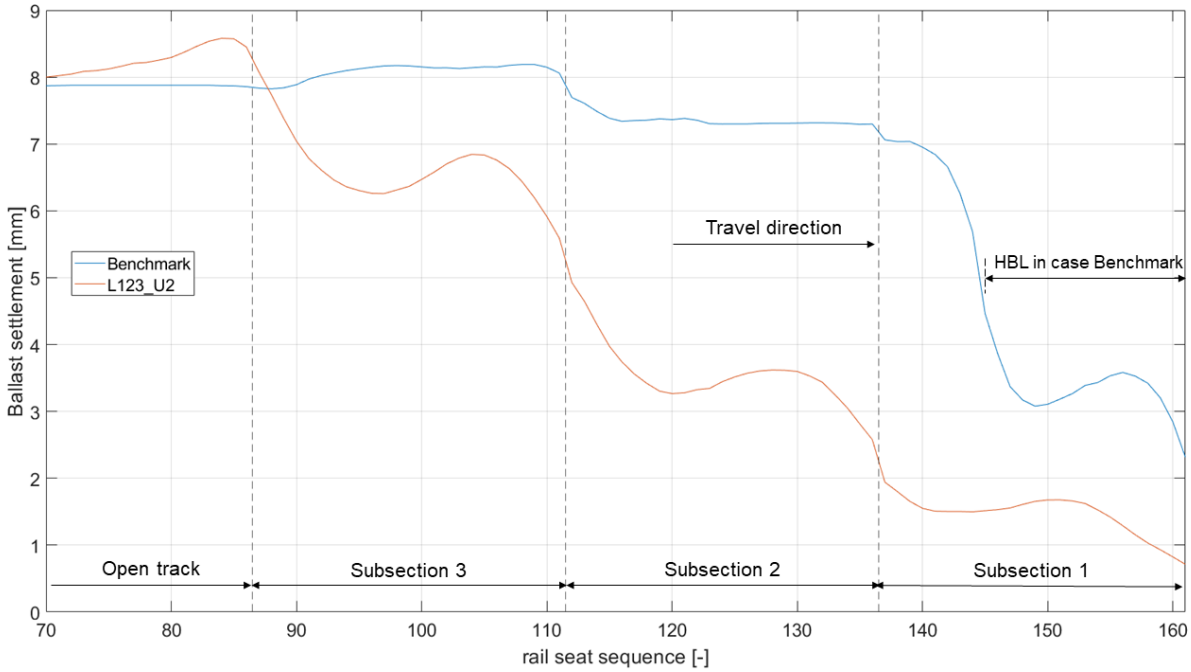

Figure 6-37: Compare of ballast settlement after 4.1 million loading cycles in case Benchmark and 'L123-U2'

Compared to the benchmark transition, the maximal SR-value after 4.1 million axle loadings in case 'L123_U2' is reduced to 1.9 mm from 3.7 mm in case benchmark. In both cases, the maximal under sleeper gap is observed at the boundary between subsection 1 and the ballastless track, but its amplitude is reduced from 1.4 mm in case benchmark to 0.44 mm in case 'L123_U2'. Implementation of design plan 'L123_U2' also shifts the under sleeper gap at the end of HBL to the boundary between the 1st and 2nd subsection, and reduces its amplitude from 0.47 mm to 0.22 mm. Additional under sleeper gap is observed at the end of the transition in case 'L123_U2', whose amplitude is nevertheless small (approximately 0.1 mm).

As conclusion, judging from dynamic vehicle-track-interaction and long-term track geometry deterioration, the advantage of track transition 'L123_U2' over benchmark plan is validated under traffic from the ballasted track to the ballastless track, too.

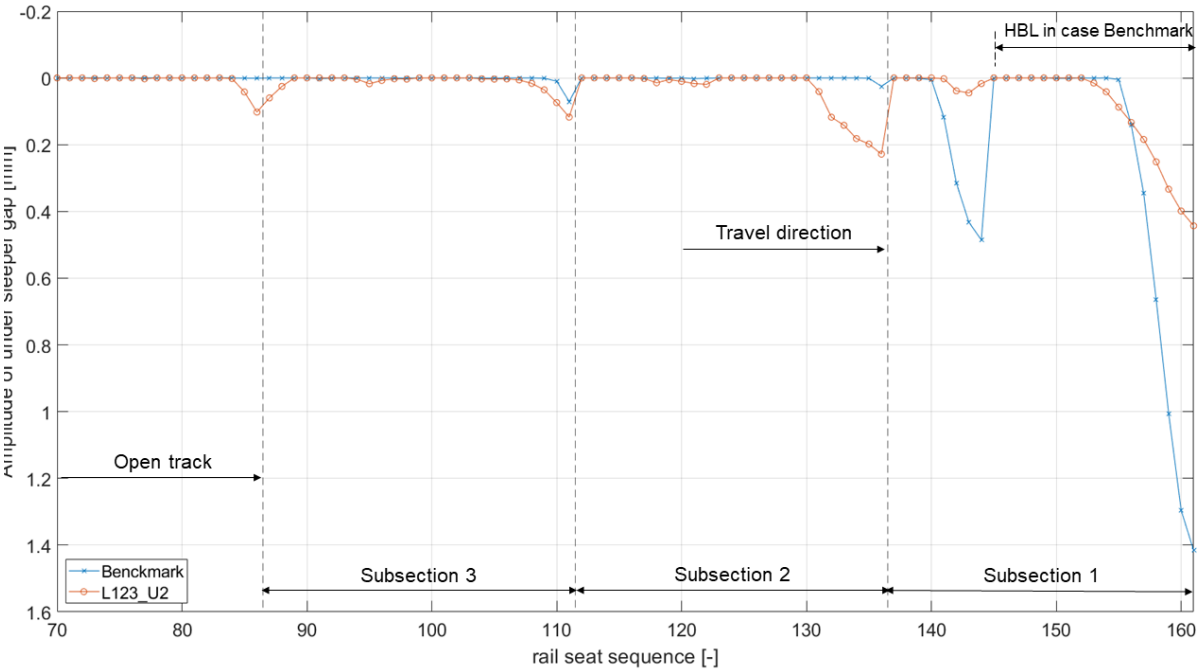

Figure 6-38: Compare of under sleeper gap after 4.1 million loading cycles in case 'benchmark and 'L123-U2'

6.8 Investigation of the influence of transition length

The length of track transition is another factor to be considered during design phase. Without losing generality, its influence is investigated by calculating case 'P-300-S-L123_U2'. Parameter study of the design plan 'L123_U2' with different subsection length shown in Figure 6-39 is performed. Since the aim is only to investigate the relationship between transition length and track performance, 0.4 million instead of 4.1 million axle loadings are introduced to save calculation time. The determined ballast settlement is demonstrated in Figure 6-40.

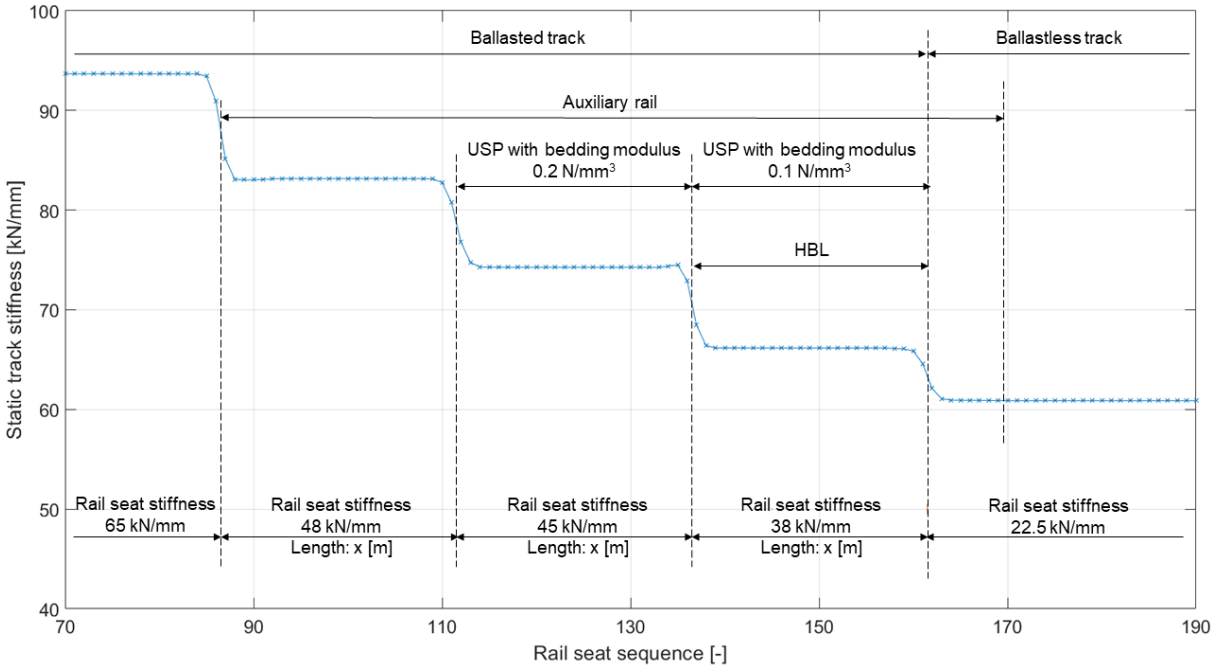

Figure 6-39: Design plan 'L123_U' with varied transition length, x = 3, 6, 9, 12, 15 and 18 [m]

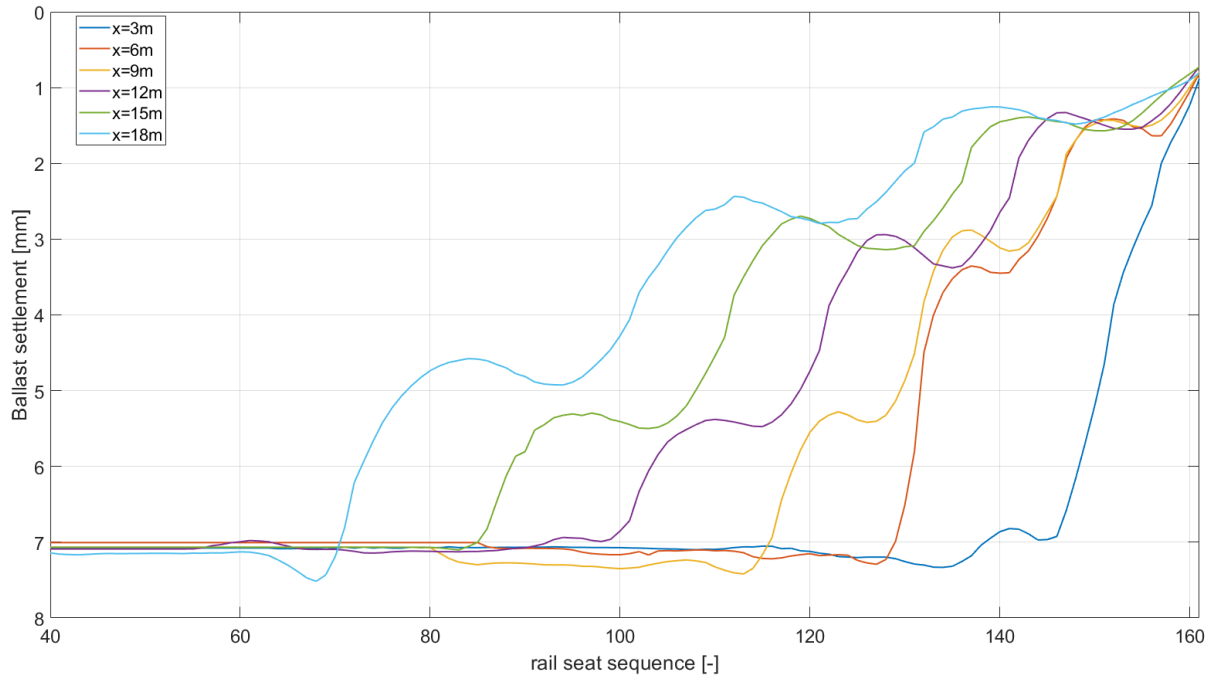

Figure 6-40: Comparison of ballast settlement with different transition length

It can be observed that the ballast settlement increases nearly linearly along the transition when the length of subsection is short, for example x = 3m. With the increase of subsection length, the final ballast settlement becomes more and more "3-step".

It can therefore be inferred that if the step size of track stiffness change between adjacent rail seats are small enough, a continuous transition can be formed. Such a transition can be realised by implementation of subgrade with gradually increasing stiffness, as suggested in (Freudenstein et al., 2015) for bridge for example. However, in this research, the long-term performance of such plans is not investigated, because the implemented settlement law cannot describe the settlement of ballast layer supported by layer with continuously changed bedding modulus. Further laboratory tests on this topic in the future would be of great significance.

Instead, it is turned to the evaluate the short-term performance of such a continuous transition in its final state. By analysing the short-term vehicle-track interaction, requirement of transition length can also be established. For this purpose, it is assumed that a continuous transition solution with the length of L is implemented between a ballastless track and a ballasted track. In the final state, the settlement difference between the ballastless track and the ballasted track is ΔH, and the transition design has successfully generated a continuous settlement pattern in the transition zone (see Figure 6-41). It is implicitly assumed that the final settlement of the ballasted track is not influenced by the length of track transition, which can be valid by Figure 6-40.

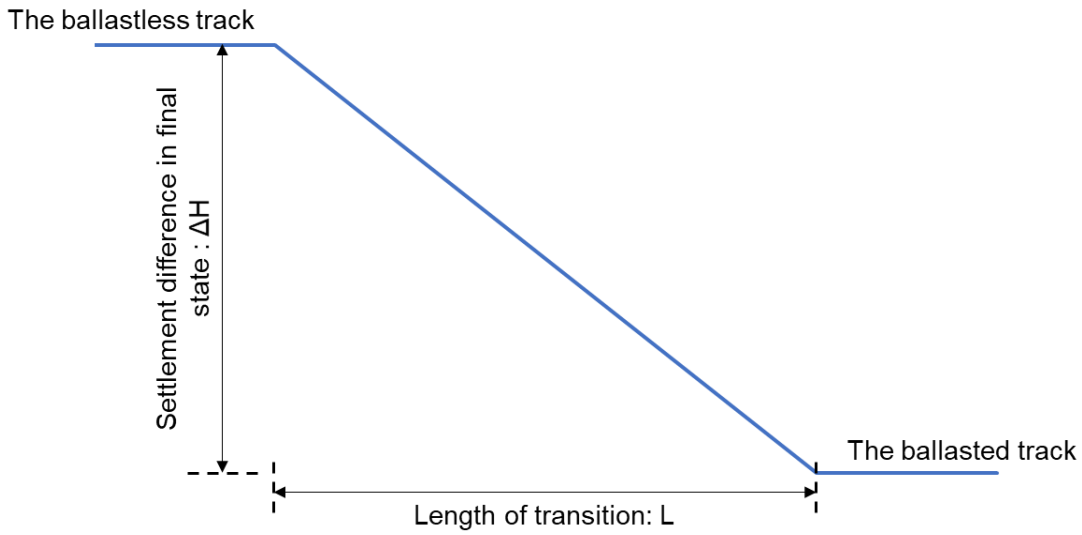

Figure 6-41: the final state of the assumed ideal track transition

In this case, the relationship between speed, the maximal dynamic force and transition length can be determined by numerical simulation using Module I and II of the Matlab program. While it is proved in chapter 5.4 that the influence of speed direction is insignificant here, so the speed direction is set as from the ballastless track to the ballasted track. The results are shown

in Figure 6-42. If the dynamic factor 1.25 is selected as the threshold, the minimum length of track transition under different speed level (300 km/h, 230 km/h, 160 km/h and 100 km/h) and settlement difference (5 mm, 10 mm and 15 mm) can be read from Figure 6-42. The determined minimum length of track transition is summarised in Table 6-10, in case that the maximal permitted dynamic factor is 1.25.

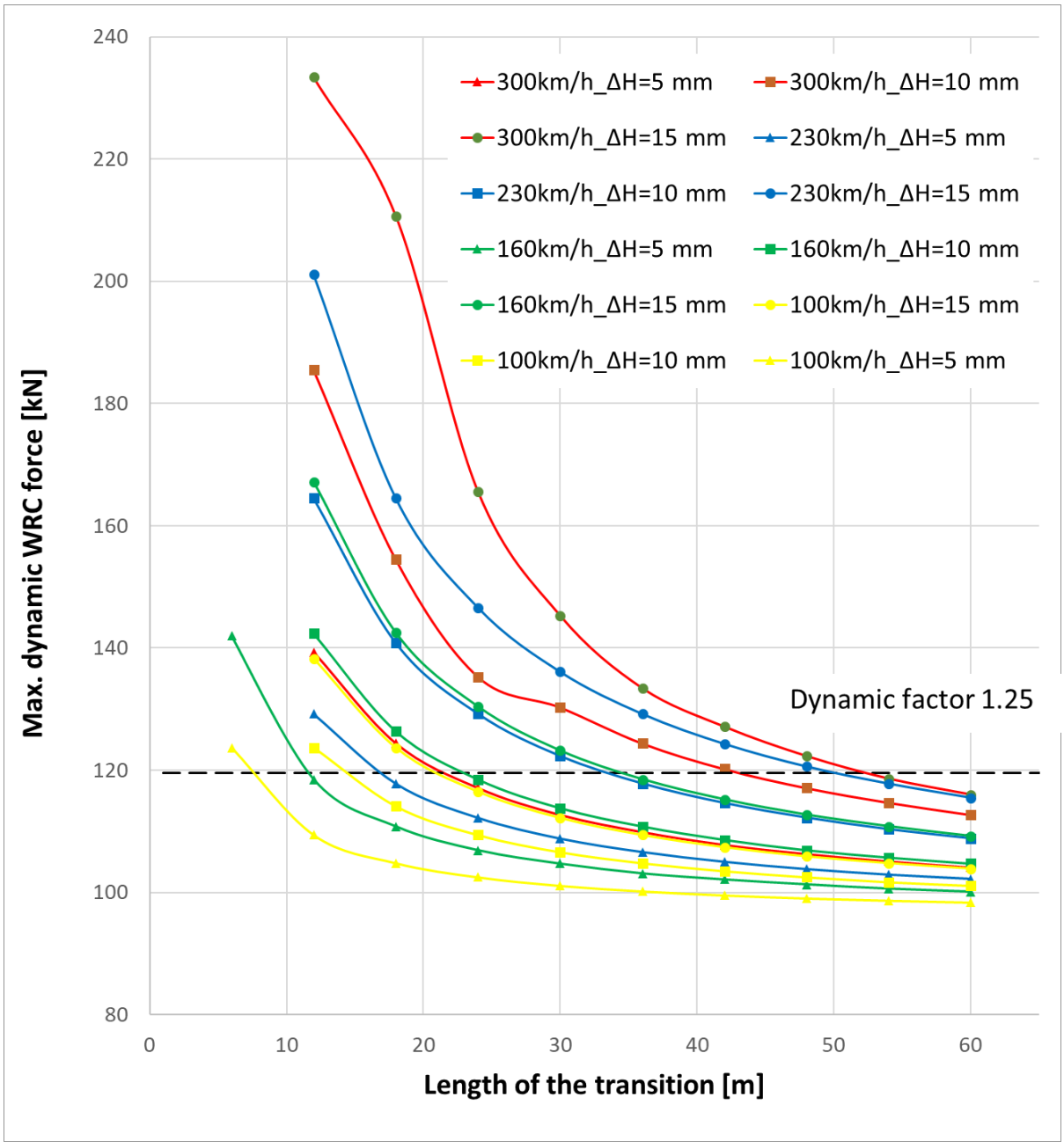

Figure 6-42: Max. dynamic WRC force depending on the length of track transition, speed and settlement difference

Table 6-10: Required minimum length [m] of track transition with given speed, settlement difference, max. dynamic factor 1.25

Speed [km/h]	Settlement difference [mm]	Minimum length [m]
300	5	22
	10	42
	15	52
230	5	17
	10	33
	15	50
160	5	12
	10	23
	15	34
100	5	8
	10	14
	15	21

The results in Table 6-10 are visualized in Figure 6-43 graphically. As comparison, the minimal length of track transition determined according to formular (1) in current standard DIN EN 16432-2:2017-10 (Deutsches Institut für Normung e. V., 2017) is also plotted. It can be observed that the minimal length of track transition derived from the case ΔH = 10 mm is nearly the same as the requirement proposed in the standard. As discussed at the beginning of this chapter, according to practical experience, 10 mm approximately corresponds to the empirical value of the settlement of a ballasted track in good quality in its life cycle (Klotzinger, 2008b). Therefore, it can be concluded that the requirement in current standard is reasonable for normal practical cases, in which the track quality is good. Nevertheless, the calculation results in this research have also demonstrated that the length of the transition should be adjusted according to the expected settlement difference between the ballasted track and the ballastless track to ensure its effect or to avoid unnecessary cost.

It can also be observed that with given settlement difference, the increase of speed will generally require the extension of transition length proportionally under most circumstances. But in critical situation (for example ΔH = 15 mm and speed greater than 230 km/h), increase of speed from 230 km/h to 300 km/h only leads to 4 % increase of the required transition length according to the calculation results. It can therefore be inferred that the length of the transition (50 meter) is already sufficient to reduce the track irregularity to a level that the dynamic effect

is no longer sensitive to the speed. Consequently, further extension of the transition is not necessary.

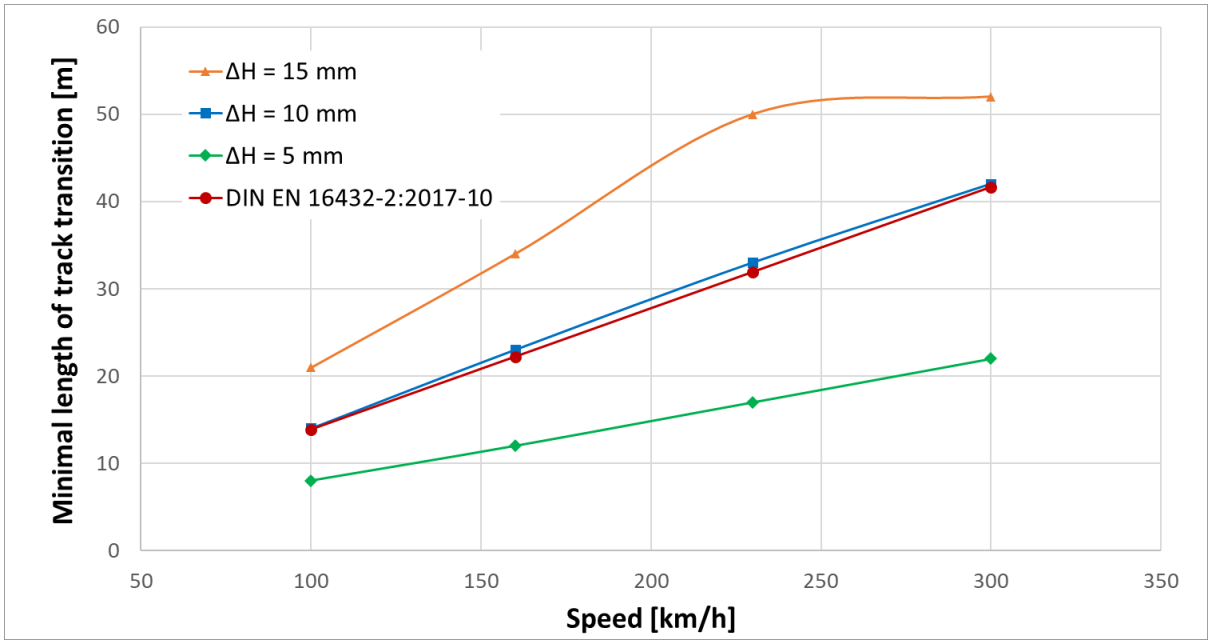

Figure 6-43: Compare calculation results in this research with the requirement in current standard DIN EN 16432-2:2017-10

6.9 Conclusions

In this chapter, the long-term behaviour of the ballasted-ballastless-track-transition is investigated and optimised. Due to the lack of measurement data about the long-term behaviour of track sections with glued ballast, the research here focuses on other countermeasures including extended HBL / flexible pavement, auxiliary rail, modification of rail fastening stiffness, adjustment of rail seat stiffness and implementation of USP. The feasibility to develop a new transition design without glued ballast is investigated.

First, the benchmark design plan (see chapter 6.2) is studied. Development of dynamic WRC force and longitudinal level in the form of SR-value (see Ril 821.2001 (DB Netz AG, 2010)) during 4.1 million axle loadings from a passenger power car travelling from the ballastless track to the ballasted track at the speed of 300 km/h are documented. The maximal dynamic WRC force is observed at the boundary between the ballastless track and the 1st transition subsection, whose amplitude is determined as 132.8 kN, corresponding to a dynamic factor of

38.9%. The maximal SR-value of longitudinal level is 3.8 mm, which is observed at the same position. It lies below the SR_A value 5 mm.

After 4.1 million load cycles, 6 sleepers next to the ballastless track in the ballasted track become unsupported. The maximum amplitude of under sleeper gap there is 1.8 mm. Next to the end of HBL in subsection 1, another 5 under sleeper gaps are found. The maximum amplitude of under sleeper gap there is 0.4 mm.

Starting from the benchmark design plan, optimisation of track transition design is performed progressively. In the end, the design plan 'L123_U2' (see Figure 6-31) is proved the most optimal design plan among all investigated variations. Essential design elements in this plan including:

- HBL / flexible pavement is extended to cover the 1st subsection of the transition.
- The initial tension stiffness of rail fastening system of auxiliary rail is increased.
- Auxiliary rail is mounted along the 1st, 2nd, 3rd subsection of the transition and 5 meters in the ballastless track.
- USP is installed below sleepers in the 1st and 2nd subsection. The bedding modulus of the USP implemented in subsection 1 is 0.10 N/mm^3, and 0.20 N/mm^3 in subsection 2.
- Rail seat stiffness changes in three steps from the ballastless track to the ballasted track. The values are determined based on the principle that the design static deflection should change continuously.

In Table 6-11, its effect on optimizing the long-term performance of track transition is demonstrated.

Table 6-11: Summary of the long-term performance of track transitions of different design, after 80 MGT traffic load, traffic direction from the ballastless track to the ballasted track

Design plan	WRC force		Track geometry	
	dynamic factor	coefficient of variation	max. SR-value	max. under sleeper gap
Benchmark	38.9 %	3.30	3.8 mm	1.8 mm
'L123_U2'	3.9%	1.22	1.8 mm	0.5 mm

Since ballastless track is free of settlement, whereas the settlement of the ballasted track increases with the number of load cycles, under sleeper gap at their boundary is inevitable. Nevertheless, adequate countermeasures can reduce its amplitude. For example, the plan 'L123_U2' helps to reduce the under sleeper gap from 1.8 mm in case benchmark to 0.5 mm.

As demonstrated in Table 6-12, it is proved that the design plan 'L123_U2' can also improve the performance of track transition, when the traffic is in the other direction.

Table 6-12: Summary of the long-term performance of track transitions of different design, after 80 MGT traffic load, traffic direction from the ballasted track to the ballastless track

Design plan	WRC force		Track geometry	
	dynamic factor	coefficient of variation	max. SR-value	max. under sleeper gap
Benchmark	17.7 %	2.44	3.7 mm	1.4 mm
'L123_U2'	6.8%	1.14	1.9 mm	0.4 mm

It is also proved that design track stiffness is an important role in transition design, while increased difference of design track stiffness between two adjacent subsections accelerate the deterioration of track longitudinal level.

Finally, the influence of the length of track transition on its performance is investigated. It is inferred that a section with gradually changed supporting stiffness can provide a continuous transition, but it is not verified, since current model cannot calculate ballast settlement supported by layers with arbitrary supporting bedding modulus. Nevertheless, it is demonstrated how to establish the requirement on minimal length based on the short-term calculation. The calculated results fit well with the requirement in current standard. Based on the calculation results in this research, a more comprehensive instruction for transition design can be achieved.

7. Summary and Conclusions

Railway track transitions refer to the locations where tracks with different designs meet each other. Due to the (potential) discontinuity in track stiffness and track settlement, additional dynamic vehicle-track forces can be activated. Increased maintenance needs (e.g., due to appearance of under-sleeper gaps) and decrease of passenger comfort can be observed.

Analysis of track transition zones requires a comprehensive evaluation of vehicle-track-system behaviour in both short-term and long-term view. For this purpose, a numerical simulation tool has been developed in this research, which consists of four modules as follows:

- the static track equilibrium module with consideration of non-uniform ballast settlement,
- the short-term vehicle-track interaction module to calculate the dynamic vehicle-track interaction forces,
- the ballast settlement module to determine the settlement of ballast based on ballast pressure, number of load cycles, load history and ballast supporting stiffness,
- the evaluation module to assess the behaviour of vehicle-track-system in aspects of maintenance interval indicated by the SR-value according to Ril 821.2001 (DB Netz AG, 2010) and dynamic vehicle-track interaction.

The numerical tool is validated by comparing the calculation results with field measurement results and with commercial software.

Using this numerical tool, the standard design of ballasted-ballastless-track-transition proposed in current standards (BetonKalender 2015 (Freudenstein et al., 2015), DB regulation Ril. 820.2020 (DB Netz AG, 2018) and DIN EN 16432-2:2017-10 (Deutsches Institut für Normung e. V., 2017)) is investigated in both short-term and long-term view. Besides, the feasibility to propose an alternative plan to the standard design plan has also been investigated.

First, the performance of track transition following standard design has been investigated in short-term view. Following conclusions are drawn based on the numerical simulation results:

- The design plan proposed in current standards has successfully smoothed the stiffness discontinuity between the ballasted track and the ballastless track, which is mainly achieved by the implementation of rail pads with adjusted stiffness.
- Auxiliary rail hardly contributes to the static stiffness of new track when the relative deflection between sleeper and auxiliary rail does not exceed the air gap in the fastening system.
- The extended HBL with incompatible length leads to extra stiffness discontinuity.

It is also found that in the calculated cases the vehicle travel direction has nearly no influence on the amplitude of the wheel-rail contact force, but it alters the distribution of the force. The dynamic wheel-rail contact force increases with vehicle speed. The dynamic effect under freight traffic is insignificant in this case due to its low speed.

The largest dynamic factor is determined as 2.6% in case ‘P-300-S-S’, which stands for the calculation case that a passenger power car travels from the ballastless track to the ballasted track at the speed of 300 km/h. As comparison, Liu has determined the dynamic factor of a high-speed ballastless track with excellent quality under operation speed 300 km/h was 11.1%, and the dynamic factor of high-speed ballasted track after one year of service under operation speed 250 km/h was 25.2% (D. Liu, 2015). Consequently, it can be concluded that the standard transition design plan has already reduced the short-term effect caused by track transition to a minor level.

As next step, the design plan is further investigated in long-term view. While there is not enough measurement data about the settlement behaviour of glued ballast section available, the investigation focuses on the effect of other countermeasures including extended HBL/flexible pavement, auxiliary rail, adjustment of rail seat stiffness and rail fastening stiffness, implementation of USP and so on.

The standard design with free ballast is calculated as benchmark. The development of track settlement after 4.1 million axle loadings from a passenger power car travelling from the ballastless track to the ballasted track at the speed of 300 km/h is calculated. The maximal dynamic factor of WRC force after 4.1 million axle loading is determined as 38.9%. The maximal SR-value of longitudinal level is 3.8 mm. Under sleeper gaps with the maximal amplitude of 1.8 mm can be observed between the ballastless track and the 1st subsection.

Afterwards, several variations of the design plan are proposed and investigated. The predicted SR value and dynamic factor prove that the plan 'L123_U2' (see Figure 7-1) is the most optimal design plan among all investigated variations. For traffic from the ballastless track to the ballasted track, implementation of this plan can reduce the dynamic factor from 38.9% in case benchmark to 3.9% and reduce the maximal SR value from 3.8 mm to 1.8 mm after 4.1 million axle loadings. For traffic from the ballasted track to the ballastless track, implementation of the proposed plan can reduce the dynamic factor from 17.7% in case benchmark to 6.8 %. Besides, implementation of the proposed plan can reduce the under sleeper gap from 1.4 mm in case benchmark to 0.4 mm. The maximal SR value is reduced from 3.7 mm to 1.9 mm.

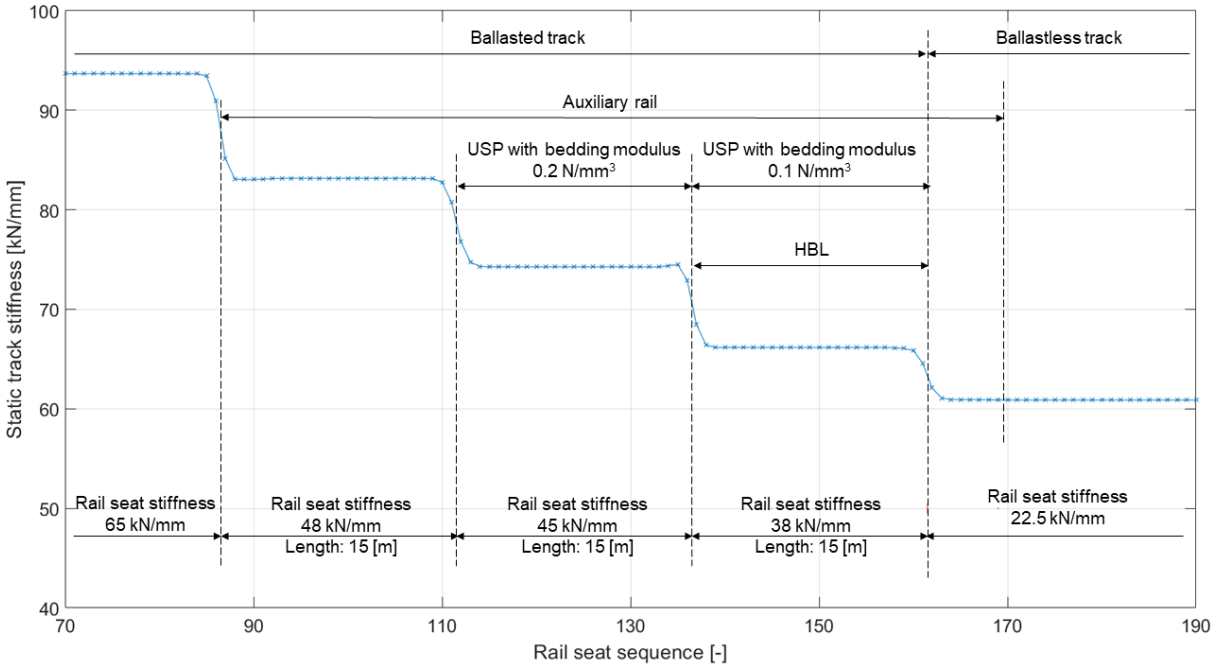

Figure 7-1: Final design plan of the track transition

Features of the finalized design plan 'L123_U2' can be concluded as following:

- HBL / flexible pavement is extended so that its length is the same as the length of the 1st subsection of the transition.
- USP is installed below sleepers in the 1st and 2nd subsection. The bedding modulus of the USP implemented in subsection 1 is 0.10 N/mm³, and 0.20 N/mm³ in subsection 2.
- Auxiliary rail is mounted along the 1st, 2nd, 3rd subsection of the transition and 5 meters in the ballastless track.
- The initial tension stiffness of rail fastening system for auxiliary rail is increased to be same as in the second phase.

- Rail seat stiffness changes in three steps from the ballastless track to the ballasted track. The values are determined based on the principle that the change of design static track deflection should be homogeneous.

Actually, the feature of this design plan can be summarised as gradually changed rail seat stiffness and implementation of connecting beam along the whole section, which is theoretically similar as the track transition solution V-TRAS (Rhomberg Sersa Rail Holding GmbH), which has been proven successful at several ballasted-track-ballastless-track-transitions (Lund & Åswärdh, 2014). It therefore demonstrates the feasibility to design the ballast transition without gluing ballast.

Based on this research, following general understandings of the track transition problem can be summarised:

- **On the influence of track stiffness and track settlement discontinuity**

  Based on the numerical simulation, it can be concluded that both track stiffness discontinuity and track settlement discontinuity should be considered to optimize track transition design. Implementation of auxiliary rail is proved to an effective method to improve the long-term settlement of track transition, although its influence on track stiffness is insignificant.

  The track stiffness difference between the subsections of track transition should be small, while its amplitude is positively related with the deterioration speed of track geometry.

- **Overlap or synchronization of the design elements**

  The final plan in Figure 7-1 generally fits the design principle that the design elements should be overlapped rather than synchronized, i.e., different countermeasures should not end at the same position. One exception is that HBL is extended to 15 m, consequently it ends with the change of rail seat stiffness together at the boundary between the 1st and 2nd subsection. This is initialled to assure the homogenous stiffness distribution within the 1st subsection and facility further optimization process. Another exception is that the auxiliary rail and the 3rd subsection of rail seat stiffness end

together, while numerical simulation has shown that further extension or shortening of auxiliary rail leads to extra dynamic effect.

- **On the length of track transition**

Based on the results of numerical simulation, it is inferred that comparing to the 3-step solution proposed in current standards, gradually changed track stiffness can lead to a continuous transition between the ballasted track and the ballastless track. The current ballast settlement law does not allow the long-term investigation of such a transition. The required minimal length of track transition is alternatively determined by analysing the track transition in its final state. In Table 7-1, the minimal length of such a continuous track transition based on the line operation speed, the settlement difference between the ballasted track and the ballastless track, and the max. permitted dynamic factor (here 1.25) is listed.

Table 7-1: Minimal length [m] of track transition with given speed, settlement difference, max. dynamic factor 1.25

Speed [km/h]	Settlement difference [mm]	Minimal length [m]
300	5	22
	10	42
	15	52
230	5	17
	10	33
	15	50
160	5	12
	10	23
	15	34
100	5	8
	10	14
	15	21

8. Outlook

Due to the restriction of computational resources, several assumptions and simplifications have been made in this research. Following investigations could be performed in further research:

- One common difficulty in investigating track transition problems is that only restricted amount of measurement data is available, for example about the long-term behaviour of track sections with glued ballast. Collecting of more field measurement data in future would be of great benefit.

- Until now, nearly all ballast settlement laws are empirical and descriptive. As a result, these settlement laws fail to exactly describe special mechanism of ballast settlement, such as the influence of ballast particle abrasion, ballast pollution and so on. The implementation of discrete element method (DEM) shed light into this problem. Integration of DEM model into the calculation program could possibly provide a more sophisticated long-term prediction.

- The developed simulation tool can be extended with respect to Life Cycle Costs (LCC). Based on the proposed calculation model here, it is possible to determine the enhanced track life with given interventions. Together with the implementation of costs of implemented interventions, sound advice could be given to infrastructure managers for decision support.

Figure index

Table index

References

Alva-Hurtado, J. E., & Selig, E. T. (1981). Permanent strain behavior of railroad ballast. Paper presented at the Proceedings of the International Conference on Soil Mechanics and Foundation Engineering.

Alves Ribeiro, C., Calçada, R., & Delgado, R. (2018). Calibration and experimental validation of a dynamic model of the train-track system at a culvert transition zone. Structure and Infrastructure Engineering, 14(5), 604-618.

Augustin, S., Gudehus, G., Huber, G., & Schünemann, A. (2003). Numerical model and laboratory tests on settlement of ballast track. In System dynamics and long-term behaviour of railway vehicles, track and subgrade (pp. 317-336): Springer.

Baeßler, M. (2008). Lageveränderungen des Schottergleises durch zyklische und dynamische Beanspruchungen. Dissertation, TU Berlin.

Baeßler, M., & Ruecker, W. (2003). Track settlement due to cyclic loading with low minimum pressure and vibrations. In System dynamics and long-term behaviour of railway vehicles, track and subgrade (pp. 337-356): Springer.

Banimahd, M., Woodward, P. K., Kennedy, J., & Medero, G. M. (2012). Behaviour of train-track interaction in stiffness transitions. Proceedings of the Institution of Civil Engineers-Transport, 165(3), 205-214.

Belytschko, T., Liu, W. K., Moran, B., & Elkhodary, K. (2013). Nonlinear finite elements for continua and structures: John wiley & sons.

Bronsert, J. (2017). Numerische Modellierung der Fahrzeug-Fahrweg-Wechselwirkung an Eisenbahnfahrwegen und ihre Anwendung im Brückenübergangsbereich.

Castillo-Mingorance, J. M., Sol-Sánchez, M., Moreno-Navarro, F., Pérez, V., & del Carmen Rubio-Gámez, M. (2021). High performance bituminous sub-ballast for improving the structural behaviour and durability of railway track substructure. Materials and Structures, 54(3), 1-15.

Chen, K. (2014). Dynamische Simulation eines Gleises unter Berücksichtigung der echtzeitigen Wechselwirkung zwischen Zug und Gleis basierend auf einem kombinierten Ansatz von FEM und MBS. (Master of science). Technical University of Munich

Chen, K., & Lechner, B. (2018). Report on Assessment of Tracks, D2.4, research project DESTination RAIL – Decision Support Tool for Rail Infrastructure Managers.

Choi, J. (2013). Influence of Track Support Stiffness of Ballasted Track on Dynamic Wheel-Rail Forces. Journal of Transportation Engineering, 139(7), 709-718.

Coelho, B. Z., & Hicks, M. A. (2016). Numerical analysis of railway transition zones in soft soil. Proceedings of the Institution of Mechanical Engineers, Part F: Journal of rail and rapid transit, 230(6).

Coelho, B. Z., Hölscher, P., Priest, J., Powrie, W., & Barends, F. (2011). An assessment of transition zone performance. Proceedings of the Institution of Mechanical Engineers Part F-Journal of Rail and Rapid Transit, 225(F2), 129-139.

Dahlberg, T. (2001). Some railroad settlement models—A critical review. Proceedings of the Institution of Mechanical Engineers, Part F: Journal of rail and rapid transit, 215(4), 289-300.

Dahlberg, T. (2010). Railway Track Stiffness Variations - Consequences and Countermeasures. International Journal of Civil Engineering, 8(1), 1-12.

DB Netz AG. (2010). Richtlinie 821.2001: Prüfung der Gleisgeometrie mit Gleismessfahrzeugen.

DB Netz AG. (2018). Richlinie 820.2020: Ausrüstungsstandard Feste Fahrbahn für Gleise und Weichen.

Demharter, K. (1982). Setzungsverhalten des Gleisrostes unter vertikaler Lasteinwirkung. Prüfamt für Bau von Landverkehrswegen, Technischen Universität München.

Deutsche Bahn AG. (2002). Anforderungskatalog zum Bau der Festen Fahrbahn, 4. Auflage. In.

Deutsches Institut für Normung e. V. (2017). DIN EN 16432-2:2017-10. In Bahnanwendungen - Feste Fahrbahn-Systeme - Teil 2: Systementwurf, Teilsysteme und Komponenten; Deutsche Fassung EN 16432-2:2017.

Dietrich, T. (1978). Experimental study of flexible piles in sand cyclically displaced at low frequency.

Diyaljee, V. A. (1987). Effects of Stress History on Ballast Deformation. Journal of geotechnical engineering, 113(8), 909-914.

Eisenmann, J. (1981). Verhaltensfunktion des Schotters, Folgerungen für hohe Fahrgeschwindigkeiten. Eisenbahningenieur.

Eisenmann, J., & Leykauf, G. (2003). Betonfahrbahnen: John Wiley & Sons.

Esveld, C. (2001). Modern railway track.

Fara, A. (2014). Transition Zones for Railway Bridges : A Study of the Sikån Bridge. (Independent thesis Advanced level (degree of Master (Two Years)) Student thesis).

Fendrich, L., & Fengler, W. (2014). Handbuch Eisenbahninfrastruktur: Springer-Verlag.

Freudenstein, S. (2020a). Lecture note of Concrete Pavement System, Technical University of Munich. Technische Universität München.

Freudenstein, S. (2020b). Lecture note of Ergänzungskurs-Verkehrswegebau, Technical University of Munich. Technische Universität München.

Freudenstein, S., Geisler, K., Mölter, T., Mißler, M., & Stolz, C. (2015). Beton Kalender 2015, Sonderdruck, X Feste Fahrbahnen in Betonbauweise. In: Ernst & Sohn.

Fröhling, R. (1997). Deterioration of railway track due to dynamic vehicle loading and spatially varying track stiffness [Thesis]. University of Pretoria, Pretoria, South Africa.

Frohling, R., Scheffel, H., & Ebersöhn, W. (1996). The vertical dynamic response of a rail vehicle caused by track stiffness variations along the track. Vehicle System Dynamics, 25(S1), 175-187.

Giner, I. G., Pita, A. L., Chaves, E. W. V., & Álvarez, A. M. R. (2012). Design of embankment–structure transitions for railway infrastructure. Paper presented at the Proceedings of the Institution of Civil Engineers-Transport.

Gramowski, C. (2013). Gleisseitige Schallemission-Experimentelle Quantifizierung und Bewertung konstruktiver Maßnahmen.

Guerin, N. (1996). Approche expérimentale et numérique du comportement du ballast des voies ferrées. Ecole Nationale des Ponts et Chaussées.

Gundavaram, D., & Hussaini, S. K. K. (2019). Polyurethane-based stabilization of railroad ballast – a critical review. International Journal of Rail Transportation, 7(3), 219-240.

Hawksbee, S., Bezin, Y., & Neves, S. G. M. D. (2018). Dynamic simulation of the V-Tras 'superstructure' transition solution. Paper presented at the The Fourth International Conference on Railway Technology: Research, Development and Maintenance, Sitges, Spain.

Hecke, A. (1998). Effects of future mixed traffic on track deterioration. Report TRITA-FKT, 30.

Henn, W. (1978). Auswirkung von Oberbauform und Betriebsbelastung auf die Veränderung der Gleishöhenlage. Prüfamt für Bau von Landverkehrswegen, Technischen Universität München.

Hettler, A. (1984). Bleibende Setzungen des Schotteroberbaus. Eisenbahn technische Rundschau (ETR), 33(11), 847-853.

Heydari-Noghabi, H., Varandas, J. N., Esmaeili, M., & Zakeri, J. (2017). Investigating the Influence of Auxiliary Rails on Dynamic Behavior of Railway Transition Zone by a 3D

Train-Track Interaction Model. Latin American Journal of Solids and Structures, 14, 2000-2018.

Holtzendorff, K. (2003). Untersuchung des Setzungsverhaltens von Bahnschotter und der Hohllagenentwicklung auf Schotterfahrbahnen.

Holzlöhner, U. (1978). Bleibende Setzung von Fundamenten infolge dynamischer Last.

Huang, H., & Brennecke, B. (2013). Track Stiffness Transition Zone Studied with Three-Dimensional Sandwich Track Model. Transportation Research Record, 2374(1), 136-142.

Hunt, H. E. M. (1997). Settlement of railway track near bridge abutments. Paper presented at the Proceedings of the Institution of Civil Engineers-Transport.

Hyslip, J. P., Li, D., & McDaniel, C. R. (2009). Railway bridge transition case study. Paper presented at the Bearing Capacity of Roads, Railways and Airfields. 8th International Conference (BCR2A'09) University of Illinois, Urbana-Champaign.

Iliev, D. L. (2012). Die horizontale Gleislagestabilität des Schotteroberbaus mit konventionellen und elastisch besohlten Schwellen. Technische Universität München.

Indraratna, B., Sajjad, M. B., Ngo, T., Correia, A. G., & Kelly, R. (2019). Improved performance of ballasted tracks at transition zones: A review of experimental and modelling approaches. Transportation Geotechnics, 21.

Keene, A., Edil, T., Fratta, D., & Tinjum, J. (2013). Modeling the effect of polyurethane stabilization on rail track response. Paper presented at the Geo-Congress 2013: Stability and Performance of Slopes and Embankments III.

Kennedy, J., Woodward, P. K., Medero, G., & Banimahd, M. (2013). Reducing railway track settlement using three-dimensional polyurethane polymer reinforcement of the ballast. Construction and Building Materials, 44, 615-625.

Kerr, A. D., & Bathurst, L. A. (2001). A Method for Upgrading the Performance at Track Transitions for High-Speed Service.

Kerr, A. D., & Moroney, B. E. (1993). Track transition problems and remedies. Bulletin, 742, 267-298.

Klotzinger, E. (2008a). Der Oberbauschotter Teil 1: Anforderungen und Beanspruchung. ETR. Eisenbahntechnische Rundschau(1-2), 34-41.

Klotzinger, E. (2008b). Der Oberbauschotter Teil 2: Qualitätsverlauf und Eingriffsschwellen. ETR. Eisenbahntechnische Rundschau(3), 120-125.

Kumar, N., Suhr, B., Marschnig, S., Dietmaier, P., Marte, C., & Six, K. (2019). Micro-mechanical investigation of railway ballast behavior under cyclic loading in a box test using DEM: effects of elastic layers and ballast types. Granular Matter, 21(4).

Lei, X., & Mao, L. (2004). Dynamic response analyses of vehicle and track coupled system on track transition of conventional high speed railway. Journal of Sound Vibration, 271, 1133-1146.

Lei, X., & Noda, N.-A. (2002). Analyses of dynamic response of vehicle and track coupling system with random irregularity of track vertical profile. Journal of Sound and Vibration, 258(1), 147-165.

Li, D., & Davis, D. (2005). Transition of railroad bridge approaches. Journal of Geotechnical and Geoenvironmental Engineering, 131(11), 1392-1398.

Li, D., Otter, D., & Carr, G. (2010). Railway Bridge Approaches under Heavy Axle Load Traffic: Problems, Causes, and Remedies. Proceedings of the Institution of Mechanical Engineers, Part F: Journal of rail and rapid transit, 224(5), 383-390.

Li, X., Nielsen, J. C. O., & Palsson, B. A. (2014). Simulation of track settlement in railway turnouts. Vehicle System Dynamics, 52, 421-439.

Liu, D. (2015). The influence of track quality to the performance of vehicle-track interaction. München, Technische Universität München, Diss., 2015,

Liu, D., Lechner, B., & Freudenstein, S. (2012). Research Report No. 2949 The influence of track elasticity to the performance of vehicle-track interaction and track settlements (track quality).

Liu, D., Lechner, B., & Freudenstein, S. (2014). Smart Maintenance and Analysis of Rail Infrastructure SMARTRAIL Final report (07/2014), Work package 3.4.

Liu, J., Geisler, K., Lechner, B., & Freudenstein, S. (2012). Forschungsbericht Nr. 2884: Dauerschwingversuch an mit "Solid Seal" verklebten Schotter. Lehrstuhl und Prüfamt für Bau von Landverkehrswegen, Technische Universität München.

Loy, H. (2008). Under sleeper pads: improving track quality while reducing operational costs.

Loy, H., & Augustin, A. (2013). Innovative Schwellenbesohlungen zur Schotterschonung für hochbelastete Strecken. Eisenbahntechnische Rundschau, 12.

Lund, H., & Åswärdh, A. (2014). Transition Zones between Ballasted and Ballast less Tracks. Lund: LTH School of Engineering at Campus Helsingborg, Department of Technology and Society, Lund University.

Mattner, L., & Eisenmann, J. (1990). Messungen am Übergang Fester Fahrbahn/Schotter mit kunststoffverfestigem Schotterbett in Nürnberg-Stein Lehrstuhl und Prüfamt für Bau von Landverkehrswegen, Technische Universität München.

Mauer, L. (1995). An Interactive Track-Train Dynamic Model for Calculation of Track Error Growth. Vehicle System Dynamics, 24(sup1), 209-221.

Namura, A., & Suzuki, T. (2007). Evaluation of countermeasures against differential settlement at track transitions. Quarterly Report of RTRI, 48(3), 176-182.

Newmark, N. M. (1959). A method of computation for structural dynamics.

Nicks, J. E. (2009). The bump at the end of the railway bridge. (DOCTOR OF PHILOSOPHY Dissertation). Texas A&M University,

Paixão, A., Fortunato, E., & Calçada, R. (2015). Design and construction of backfills for railway track transition zones. Proceedings of the Institution of Mechanical Engineers, Part F: Journal of rail and rapid transit, 229(1), 58-70.

Pita, A. L., Teixeira, P. F., & Robuste, F. (2004). High speed and track deterioration: The role of vertical stiffness of the track. Proceedings of the Institution of Mechanical Engineers, Part F: Journal of rail and rapid transit, 218(1), 31-40.

Rapp, S. (2017). Modell zur Identifizierung von punktuellen Instabilitäten am Bahnkörper in konventioneller Schotterbauweise.

Raymond, G. P., & Richard, J. B. (1987). Performance of large-scale model single tie-ballast systems. Transportation Research Record, 1134, 7-14.

Read, D., & Li, D. (2006). Design of track transitions. TCRP Research Results Digest(79).

Rhomberg Sersa Rail Holding GmbH. Universal transition module V-TRAS. Retrieved from http://cdn.rhombergbau.at/bookshelf/vtras-207/files/assets/basic-html/page-1.html

Rump, R. (1997). Warum Feste Fahrbahn. Edition ETR, 8-11.

Sañudo, R., dell'Olio, L., Casado, J. A., Carrascal, I. A., & Diego, S. (2016). Track transitions in railways: A review. Construction and Building Materials, 112, 140-157.

Sasaoka, C. D., & Davis, D. (2005). Implementing track transition solutions for heavy axle load service. Paper presented at the Proceedings, AREMA 2005 Annual Conference, Chicago, IL.

Sato, Y. (1995). Japanese studies on deterioration of ballasted track. Vehicle System Dynamics, 24, 197-208.

Schneider, P., Bolmsvik, R., & Nielsen, J. C. O. (2011). In situ performance of a ballasted railway track with under sleeper pads. Proceedings of the Institution of Mechanical Engineers Part F-Journal of Rail and Rapid Transit, 225(F3), 299-309.

Shan, Y., Shu, Y., & Zhou, S. (2017). Finite-infinite element coupled analysis on the influence of material parameters on the dynamic properties of transition zones. Construction and Building Materials, 148, 548-558.

Shenton, M. (1985). Ballast deformation and track deterioration. Track technology, 253-265.

Soares, D. (2018). Nonlinear dynamic analysis considering explicit and implicit time marching techniques with adaptive time integration parameters. Acta Mechanica, 229(5), 2097-2116.

Sol-Sanchez, M., & D'Angelo, G. (2017). Review of the design and maintenance technologies used to decelerate the deterioration of ballasted railway tracks. Construction and Building Materials, 157, 402-415.

Sol-Sánchez, M., Pirozzolo, L., Moreno-Navarro, F., & Rubio-Gámez, M. C. (2016). A study into the mechanical performance of different configurations for the railway track section: A laboratory approach. Engineering Structures, 119, 13-23.

Sol-Sánchez, M., Thom, N. H., Moreno-Navarro, F., Rubio-Gámez, M. C., & Airey, G. D. (2015). A study into the use of crumb rubber in railway ballast. Construction and Building Materials, 75, 19-24.

Steenbergen, M., & de Jong, E. (2016). Railway track degradation: The contribution of rolling stock. Proceedings of the Institution of Mechanical Engineers Part F-Journal of Rail and Rapid Transit, 230(4), 1164-1171.

Steger, M. V. (2017). Untersuchungen zum Schwingungsverhalten und der daraus resultierenden Beanspruchung von Spannklemmen für Schienenbefestigungen unter Berücksichtigung von hochfrequenten Anregungen. Technische Universität München,

Sun, Q. D., Indraratna, B., & Nimbalkar, S. (2016). Deformation and Degradation Mechanisms of Railway Ballast under High Frequency Cyclic Loading. Journal of Geotechnical and Geoenvironmental Engineering, 142(1).

Teixeira, P. F., López-Pita, A., Casas, C., Bachiller, A., & Robuste, F. (2006). Improvements in high-speed ballasted track design: Benefits of bituminous subballast layers. Transportation Research Record, 1943(1), 43-49.

Tutumluer, E., Stark, T. D., Mishra, D., & Hyslip, J. P. (2012). Investigation and mitigation of differential movement at railway transitions for us high speed passenger rail and joint passenger/freight corridors.

Tutumluer, E., Stark, T. D., Mishra, D., & Hyslip, J. P. (2012). Investigation and mitigation of differential movement at railway transitions for US high speed passenger rail and joint passenger/freight corridors. Paper presented at the 2012 Joint Rail Conference.

Vale, C., & Calçada, R. (2014). A Dynamic Vehicle-Track Interaction Model for Predicting the Track Degradation Process. Journal of Infrastructure Systems, 20(3).

van As, C., & Kearsley, E. (1995). Deterioration of rail track geometry. Journal of the South African Institution of Civil Engineering, 37(1), 1-5.

Varandas, J. N. (2013). Long-term behaviour of railway transitions under dynamic loading application to soft soil sites.

Varandas, J. N., Hölscher, P., & Silva, M. A. G. (2010). A Settlement Model for Ballast at Transition Zones. In B. H. V. Topping, J. M. Adam, F. J. Pallares, R. Bru, & M. L. Romero (Eds.), Proceedings of the Tenth International Conference on Computational Structures Technology (Vol. 93).

Varandas, J. N., Hölscher, P., & Silva, M. A. G. (2011). Dynamic behaviour of railway tracks on transitions zones. Computers & Structures, 89(13-14), 1468-1479.

Varandas, J. N., Hölscher, P., & Silva, M. A. G. (2013). Settlement of ballasted track under traffic loading: Application to transition zones. Proceedings of the Institution of Mechanical Engineers, Part F: Journal of rail and rapid transit, 228(3), 242-259.

Wang, H., & Markine, V. L. (2018). Methodology for the comprehensive analysis of railway transition zones. Computers and Geotechnics, 99, 64-79.

Wang, H., Markine, V. L., Shevtsov, I. Y., & Dollevoet, R. (2015). Analysis of the dynamic behaviour of a railway track in transition zones with differential settlement.

Wolter, C. U. (2013). Rekonstruktion der originalen Gleislageabweichungen aus 3-Punkt-Signalen (Wandersehnenmessverfahren) und Beurteilung hinsichtlich Amplitude, Fehlerwellenlänge sowie Fehlerform: Eurailpress in DVV Media Group.

Zhai, W. (1996). Two simple fast integration methods for large-scale dynamic problems in engineering. International Journal for Numerical Methods in Engineering, 39(24), 4199-4214.

Zhai, W. (2014). 车辆-轨道耦合动力学: 科学出版社.
Zhai, W., & Sun, X. (1994). A Detailed Model for Investigating Vertical Interaction between Railway Vehicle and Track. Vehicle System Dynamics, 23(sup1), 603-615.
Zhai, W., Wang, K., & Cai, C. (2009). Fundamentals of vehicle–track coupled dynamics. Vehicle System Dynamics, 47(11), 1349-1376.
Zhai, W., Wang, K., & Lin, J. H. (2004). Modelling and experiment of railway ballast vibrations. Journal of Sound and Vibration, 270(4-5), 673–683.
Zhang, X., Zhao, C. F., & Zhai, W. (2019). Importance of load frequency in applying cyclic loads to investigate ballast deformation under high-speed train loads. Soil Dynamics and Earthquake Engineering, 120, 28-38.
Zhang, Y. (2000). An integrated rail track degradation model. Queensland University of Technology,
Zhang, Y., Murray, M., & Ferreira, L. (1999). An integrated model for track degradation prediction. Paper presented at the World Transport Research: Selected Proceedings of the 8th World Conference on Transport ResearchWorld Conference on Transport Research Society.

Appendix

Appendix 1: Set up vehicle-track interaction model

The classic passenger coach model shown in Figure 3-1 has following 10 degree of freedoms (DoF):

$$s_v = [u_c \quad \varphi_c \quad u_{t1} \quad \varphi_{t1} \quad u_{t2} \quad \varphi_{t2} \quad u_{w1} \quad u_{w2} \quad u_{w3} \quad u_{w4}]^T \tag{18}$$

with

u_c	: Vertical movement of car body	φ_c	: Pitch motion of car body
u_{t1}, u_{t2}	: Vertical movement of bogies	$\varphi_{t1},\ \varphi_{t2}$	: Pitch motion of bogies
$u_{w1}, u_{w2}, u_{w3}, u_{w4}$	: Vertical movement of wheels		

External force vector could be expressed as:

$$Q_v = \begin{bmatrix} -M_c g \\ 0 \\ -M_t g \\ 0 \\ -M_t g \\ 0 \\ -M_w g + F_{ul1} \\ -M_w g + F_{ul2} \\ -M_w g + F_{ul3} \\ -M_w g + F_{ul4} \end{bmatrix} \tag{19}$$

with

M_c, M_t, M_w	: Mass of car body, bogies and wheels
$F_{ul1}, F_{ul1}, F_{ul1}, F_{ul1}$	: Wheel-rail contact force at 1st to 4th wheel

The generalized mass matrix, damping matrix and stiffness matrix could be expressed as:

$$[M]_v = diag(M_c, J_c, M_b, J_b, M_b, J_b, M_w, M_w, M_w, M_w) \tag{20}$$

$$[\boldsymbol{C}]_v = \begin{bmatrix} 2C_{s2} & 0 & -C_{s2} & 0 & -C_{s2} & 0 & 0 & 0 & 0 & 0 \\ & 2{L_2}^2C_{s2} & -L_2C_{s2} & 0 & L_2C_{s2} & 0 & 0 & 0 & 0 & 0 \\ & & 2C_{s1}+C_{s2} & 0 & 0 & 0 & -C_{s1} & -C_{s1} & 0 & 0 \\ & & & 2{L_1}^2C_{s1} & 0 & 0 & -L_1C_{s1} & L_1C_{s1} & 0 & 0 \\ & & & & 2C_{s1}+C_{s2} & 0 & 0 & 0 & -C_{s1} & -C_{s1} \\ & & & & & 2{L_1}^2C_{s1} & 0 & 0 & -L_1C_{s1} & L_1C_{s1} \\ & & & & & & C_{s1} & 0 & 0 & 0 \\ & & & Symm & & & & C_{s1} & 0 & 0 \\ & & & & & & & & C_{s1} & 0 \\ & & & & & & & & & C_{s1} \end{bmatrix} \quad (21)$$

$$[\boldsymbol{K}]_v = \begin{bmatrix} 2k_{s2} & 0 & -k_{s2} & 0 & -k_{s2} & 0 & 0 & 0 & 0 & 0 \\ & 2{L_2}^2k_{s2} & -L_2k_{s2} & 0 & L_2k_{s2} & 0 & 0 & 0 & 0 & 0 \\ & & 2k_{s1}+k_{s2} & 0 & 0 & 0 & -k_{s1} & -k_{s1} & 0 & 0 \\ & & & 2{L_1}^2k_{s1} & 0 & 0 & -L_1k_{s1} & L_1k_{s1} & 0 & 0 \\ & & & & 2k_{s1}+k_{s2} & 0 & 0 & 0 & -k_{s1} & -k_{s1} \\ & & & & & 2{L_1}^2k_{s1} & 0 & 0 & -L_1k_{s1} & L_1k_{s1} \\ & & & & & & k_{s1} & 0 & 0 & 0 \\ & & & Symm & & & & k_{s1} & 0 & 0 \\ & & & & & & & & k_{s1} & 0 \\ & & & & & & & & & k_{s1} \end{bmatrix} \quad (22)$$

with

J_c, J_b : pitch moment of inertia of car body and bogie

$k_{s1},\ c_{s1}$: stiffness and damping factor of primary suspension

$k_{s2},\ c_{s2}$: stiffness and damping factor of secondary suspension

L_1 : half of the distance between two wheels of the same bogie

L_2 : half of the distance between two bogies

To simulate freight wagon without secondary suspension, the DoFs of wheel should be removed, since they now depended on bogie movement and pitch motion are. For instance, the deflection of wheel 1 could be determined as:

$$u_{w1} = u_{t1} + \varphi_{t1} * L_1 \quad (23)$$

Other parts could be adjusted correspondingly.

In the track model shown in Figure 3-1, rail is represented as Euler-Bernoulli beam. Rail pad is modelled using spring and damper elements. Sleeper is modelled as rigid body, whose flexibility is neglected. Mass and stiffness of ballast layer is determined according to the method proposed in (Zhai, Wang, & Lin, 2004).

Each Euler-Bernoulli beam element has four DoFs: displacement and slopes at two ends, as in (24):

$$s_b^e = [u_{r1} \quad \varphi_{\mathrm{r1}} \quad u_{r2} \quad \varphi_{\mathrm{r2}}]^T \tag{24}$$

with

u_{r1}, u_{r2} : displacement

$\varphi_{r1}, \varphi_{r2}$: slope

Stiffness and mass matrix of Euler-Bernoulli beam element can be expressed as in (25) and (26):

$$[K]_b^e = \frac{EI}{l^3}\begin{bmatrix} 12 & 6l & -12 & 6l \\ 6l & 4l^2 & -6l & 2l^2 \\ -12 & -6l & 12 & -6l \\ 6l & 2l^2 & -6l & 4l^2 \end{bmatrix} \tag{25}$$

$$[M]_b^e = \frac{\rho Al}{420}\begin{bmatrix} 156 & -22l & 54 & 13l \\ & 4l^2 & -13l & -3l^2 \\ & symm & 156 & 22l \\ & & & 4l^2 \end{bmatrix} \tag{26}$$

with

E : E-modulus

I : Inertia moment

l : Element length

ρ : Density

A : Area of cross section

Damping is usually expressed as the linear combination of stiffness and mass matrix as in (27):

$$[C]_b^e = \alpha[M]_b^e + \beta[K]_b^e \tag{27}$$

with

α, β : Rayleigh damping coefficient

Each sleeper and ballast have only DoF of vertical displacement. Taking a unit model consisting of two neighbour rail seats as an example, it has totally 8 DoFs as shown in (28):

$$s_s^e = [u_{ri} \quad \varphi_{\mathrm{ri}} \quad u_{rj} \quad \varphi_{\mathrm{rj}} \quad u_{si} \quad u_{sj} \quad u_{bi} \quad u_{bj}]^T \tag{28}$$

with

u_s, u_b : displacement of sleeper and ballast

The ballast layer is modelled according to (Zhai et al., 2004).

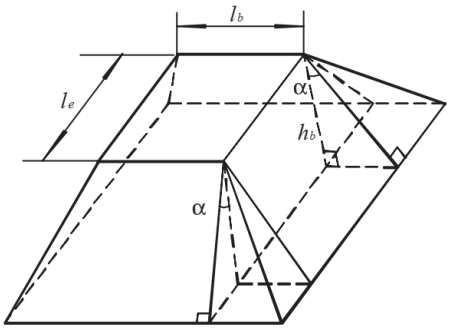

Appendix 1-1: Model of ballast under one rail support point (Zhai et al., 2004)

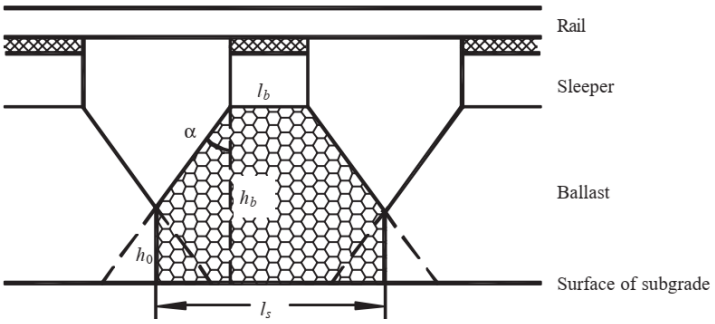

Appendix 1-2:The modified model of ballast (Zhai et al., 2004)

The height of overlapping regions is calculated by

$$h_0 = h_b - \frac{l_s - l_b}{2\tan\alpha} \tag{29}$$

with

l_s : sleeper spacing

The ballast vibrating mass is determined as:

$$M_b' = \rho_b \left[l_e h_b (l_e + h_b \tan\alpha) + l_e \left({h_b}^2 - {h_0}^2 \right) \tan\alpha + \frac{4}{3} \left({h_b}^3 - {h_0}^3 \right) (\tan\alpha)^2 \right], \quad (30)$$

The ballast supporting stiffness is changed into:

$$K_b' = \frac{K_{b1} K_{b2}}{K_{b1} + K_{b2}} \quad (31)$$

with

$$K_{b1} = \frac{2 \tan\alpha \, (l_e - l_b)}{\ln \left(\frac{l_e l_s}{l_b (l_e + l_s - l_b)} \right)} E_b \quad (32)$$

and

$$K_{b2} = \frac{\tan\alpha \, l_s (l_s - l_b + 2l_e + 2h_b \tan\alpha)}{l_b - l_s + 2h_b \tan\alpha} E_b \quad (33)$$

The subgrade stiffness becomes

$$E_f' = l_s (l_e + 2h_b \, tan\,\alpha) E_f \quad (34)$$

where E_f is the K_{30} modulus of subgrade.

In order to model the coupling properties between two neighbouring ballast blocks, shearing springs and shearing dampers are introduced between adjacent ballast massed in the track model.

Stiffness matrix and damping matrix resulting from elastic components could be expressed as:

$$[K]_s^e = \begin{bmatrix} k_{rs} & 0 & 0 & 0 & -k_{rs} & 0 & 0 & 0 \\ 0 & 0 & 0 & 0 & 0 & 0 & 0 & 0 \\ 0 & 0 & k_{rs} & 0 & 0 & -k_{rs} & 0 & 0 \\ 0 & 0 & 0 & 0 & 0 & 0 & 0 & 0 \\ -k_{rs} & 0 & 0 & 0 & k_{rs}+k_{sb} & 0 & -k_{sb} & 0 \\ 0 & 0 & -k_{rs} & 0 & 0 & k_{rs}+k_{sb} & 0 & -k_{sb} \\ 0 & 0 & 0 & 0 & -k_{sb} & 0 & k_{sb}+k_w+k_{bu} & -k_w \\ 0 & 0 & 0 & 0 & 0 & -k_{sb} & -k_w & k_{sb}+k_w+k_{bu} \end{bmatrix} \quad (35)$$

$$[C]_s^e = \begin{bmatrix} c_{rs} & 0 & 0 & 0 & -c_{rs} & 0 & 0 & 0 \\ 0 & 0 & 0 & 0 & 0 & 0 & 0 & 0 \\ 0 & 0 & c_{rs} & 0 & 0 & -c_{rs} & 0 & 0 \\ 0 & 0 & 0 & 0 & 0 & 0 & 0 & 0 \\ -c_{rs} & 0 & 0 & 0 & c_{rs}+c_{sb} & 0 & -c_{sb} & 0 \\ 0 & 0 & -c_{rs} & 0 & 0 & c_{rs}+c_{sb} & 0 & -c_{sb} \\ 0 & 0 & 0 & 0 & -c_{sb} & 0 & c_{sb}+c_w+c_{bu} & -c_w \\ 0 & 0 & 0 & 0 & 0 & -c_{sb} & -c_w & c_{sb}+c_w+c_{bu} \end{bmatrix} \quad (36)$$

The global stiffness matrix could then be formed by combining (25) and (35) with corresponding DoFs. Global damping matrix could be established similarly. Global mass matrix could be assembled by adding the mass of sleeper and ballast into (26).

Ballastless track could be modelled similarly.

Nominal wheel-rail contact force in vertical direction is described using Hertz formula:

$$F_{contact} = \begin{cases} G^{-2/3}(|u_w - u_r - \eta|)^{2/3}, & if(|u_w - u_r - \eta|) < 0, \\ 0 \quad , & if(|u_w - u_r - \eta|) \geq 0 \end{cases} \quad (37)$$

with

u_w : position of wheel

u_r : position of rail

η : rail irregularity at contact point

G is a constant, which could be determined by:

$$G = 4.57 * R^{-0.149} \times 10^{-8} \quad (38)$$

with R as the radius of wheel.

Appendix 2: Newton-Raphson method with linear search

Without loss of generality, the solving process is illustrated using a generalized function:

$$f(x) = p \tag{39}$$

If x_i is an estimation of the solution of (39), expanding (39) using Taylor series about x_i yields:

$$f(x_i + \Delta x) = f(x_i) + \left.\frac{\partial f(x)}{\partial x}\right|_{x_i} (\Delta x)^1 + \frac{1}{2} \times \left.\frac{\partial^2 f}{\partial x^2}\right|_{x_i} (\Delta x)^2 + \cdots \tag{40}$$

If x_i lies near the solution, the higher-order items could be neglected, leading to:

$$f(x_i + \Delta x) \approx f(x_i) + \left.\frac{\partial f(x)}{\partial x}\right|_{x_i} (\Delta x) = p \tag{41}$$

Or

$$R = p - f(x_i) = \left.\frac{\partial f(x)}{\partial x}\right|_{x_i} (\Delta x) \tag{42}$$

with R as the residual force.

A better estimation x_{i+1} is thus given as:

$$x_{i+1} = x_i + \Delta x = x_i + \left(\left.\frac{\partial f(x)}{\partial x}\right|_{x_i}\right)^{-1} R \tag{43}$$

The iteration is terminated, when the residual value is lower than the predefined tolerance or the change of the estimation is less than the predefined tolerance. Convergence of this algorithm is strongly influenced by the starting value. Near the solution, it converges with quadratic rate to the exact solution.

An additional step named line search is inserted before (43) following Literature (Belytschko et al., 2013):

$$minimize\ h(\alpha) = f(x_i + \alpha \cdot \Delta x) \tag{44}$$

The estimation for next step becomes therefore:

$$x_{i+1} = x_i + \alpha_{optimized} \cdot \Delta x \tag{45}$$

with

$\alpha_{optimized}$: step size determined in (44)

Appendix 3: Vehicle and track parameters used in simulation adopted from (Zhai, 2014)

Appendix 3-1: Passenger power car

Notation	Parameter [unit]	Value
M_c	Car body mass [kg]	60840
M_b	Bogie mass [kg]	4680
M_w	Wheelset mass [kg]	1950
I_{cy}	Mass moment of inertia of car body about y axis [kg·m^2]	1.35×10^6
I_{by}	Mass moment of inertia of bogie about y axis [kg·m^2]	4033
K_{ps}	Stiffness coefficient of primary suspension along z axis [N/m]	2.4×10^6
C_{ps}	Damping coefficient of primary suspension along z axis [N·s/m]	3×10^4
K_{ss}	Stiffness coefficient of secondary suspension along z axis [N/m]	8.885×10^5
C_{ss}	Damping coefficient of secondary suspension along z axis [N·s/m]	4.5×10^4
l_c	Semi-longitudinal distance between bogies [m]	5.7
l_t	Semi-longitudinal distance between wheelsets in bogie [m]	1.5
R_0	Wheel radius [m]	0.52

Appendix 3-2: LTF freight wagon

Notation	Parameter [unit]	Value
M_c	Car body mass [kg]	93640
M_b	Bogie mass [kg]	1880
M_w	Wheelset mass [kg]	1150
I_{cy}	Mass moment of inertia of car body about y axis [kg·m^2]	4.41×10^6
I_{by}	Mass moment of inertia of bogie about y axis [kg·m^2]	1560
K_{ps}	Stiffness coefficient of primary suspension along z axis [N/m]	1.3×10^7
C_{ps}	Damping coefficient of primary suspension along z axis [N·s/m]	9×10^4
K_{ss}	Stiffness coefficient of secondary suspension along z axis [N/m]	6.2×10^6
C_{ss}	Damping coefficient of secondary suspension along z axis [N·s/m]	1×10^5
l_c	Semi-longitudinal distance between bogies [m]	4.05
l_t	Semi-longitudinal distance between wheelsets in bogie [m]	0.9
R_0	Wheel radius [m]	0.42

Appendix 3-3: Ballasted track parameters

Notation	Parameter [unit]	Value
E	Young's modulus of rail material [N/m^2]	2.1×10^{11}
ρ	Density of rail material [kg/m^3]	7850
A	Area of rail cross section [m^2]	7.67×10^{-3}
I_z	Rail second moment of area about z axis [m^4]	3.04×10^{-5}
M_r	rail mass per unit length [kg/m]	60.21
K_{rs}	fastener stiffness in vertical direction [N/m]	6.5×10^7
C_{rs}	fastener damping in vertical direction [N·s/m]	7.5×10^4
M_s	half sleeper mass [kg]	140
l_s	Sleeper spacing [m]	0.60
l_e	Effective support length of half sleeper [m]	1.04
l_b	Sleeper width [m]	0.285
ρ_b	Ballast density [kg/m^3]	1.8×10^3
E_b	Young's modulus of ballast [N/m^2]	1.2×10^8
C_b	Ballast damping [N·s/m]	5.88×10^4
K_w	Ballast shear stiffness [N/m]	7.84×10^7
C_w	Ballast shear damping [N·s/m]	8.0×10^4
α	Ballast stress distribution angle [°]	35
h_b	Ballast thickness [m]	0.35
E_f	Subgrade bedding modulus [N/m^3]	1.0×10^8
C_f	Subgrade damping [N·s/m]	3.115×10^4
E_{sbm}	Bedding modulus of sub ballast mat [N/m^3]	5.0×10^7